

The Scientific Case of ELI Nuclear Physics Bucharest-Magurele, Romania

The ELI-Nuclear Physics Experiment working group

April 10, 2010

Editors:

Dietrich Habs, Martin Groß, Peter G. Thirolf, Matthias Zepf

Authors

P. Böni¹², D. Bucurescu¹¹, Gh. Cata-Danil¹¹, B. Dietz⁵, N. Elkina³, A. Fedotov¹⁰, H. Gies⁴, M. Groß³, D. Habs^{3,8}, C. Harvey¹⁶, R. Hajima², T. Hayakawa¹, T. Heinzl¹⁶, A. Henig^{3,8}, R. Hörlein^{3,8}, Ch. Hugenschmidt¹², A. Ilderton¹⁶, C. Ivan¹¹, D. Kiefer^{3,8}, W. Ma^{6,8}, N. Marginean¹¹, M. Naumova⁶, F. Negoita¹¹, G. Paulus⁴, N. Pietralla⁵, H. Ruhl³, D. Savran⁵, K. Schreckenbach¹², J. Schreiber⁸, R. Schützhold¹⁵, T. Shizuma², K. Sonnabend⁵, X.Q. Yan^{8,14}, P.G. Thirolf³, H.A. Weidenmüller⁹, N.V. Zamfir¹¹, M. Zepf¹³.

Affiliations

¹ Advanced Photon Research Center, JAEA, Kizugawa, Kyoto, Japan

² Advanced Photon Research Center, JAEA, Tokai, Ibaraki, Japan

³ Fakultät für Physik, Ludwig-Maximilians-Universität München, Munich, Germany

⁴ Friedrich Schiller Universität, Jena, Germany

⁵ Institut für Kernphysik, TU Darmstadt, Darmstadt, Germany

⁶ Institute of Physics, CAS, Beijing, P.R. China

⁷ Laboratoire d'Optique Appliquée, UMR 7639 ENSTA, Palaiseau, France

⁸ Max-Planck Institute of Quantum Optics, Garching, Germany

⁹ Max-Planck Institut für Kernphysik, D-69029 Heidelberg, Germany

¹⁰ Moscow Engineering Physics Institute, Moscow, Russia

¹¹ National Institute for Physics and Nuclear Engineering, Bucharest-Maurele, Romania

¹² Physik-Department E21, Technische Universität München, Garching, Germany

¹³ Queen's University, Belfast, Northern Ireland, UK

¹⁴ State Key Lab of Nuclear Physics and Technology, Peking University, Beijing, P.R. China

¹⁵ Universität Duisburg-Essen, Duisburg, Germany

¹⁶ University of Plymouth, Plymouth, PL4 8AA, UK

Contents

1	Foreword	3
2	Executive Summary	4
2.1	Basic Objectives	4
2.2	History of the Project	5
2.3	The Scientific Case of ELI-Nuclear Physics	6
2.4	Principles of Planning, Layout and Performance Goals of the Facility	9
2.5	Requirements by the Experiments for the High-power Laser and the γ/e^- Facility	9
2.6	Cost, Schedule and Personnel	10
3	Introduction	11
4	Stand-alone APOLLON Experiments	11
4.1	A Laser-Accelerated Th Beam is used to produce Neutron-Rich Nuclei around the $N = 126$ Waiting Point of the r -Process via the Fission-Fusion Reaction Mechanism	11
4.2	From Radiation Pressure Acceleration (RPA) and Laser-Driven Ion Pistons to Direct Laser Acceleration of Protons at Intensities up to $10^{24}\text{W}/\text{cm}^2$	14
4.3	Deceleration of Very Dense Electron and Ion Beams	17
4.4	A Relativistic Ultra-thin Electron Sheet used as a Relativistic Mirror for the Production of Brilliant, Intense Coherent γ -Rays	19
4.5	Nuclear Techniques for Characterization of Laser-induced Radiations	22
5	APOLLON Laser + γ/e^- Beam	27
5.1	Pair Creation from the Vacuum	27
5.1.1	Catalysis of Schwinger Pair Production. (Gies)	27
5.1.2	Pair Production (Heinzl)	31
5.1.3	Self-field effects and vacuum stability in strong external fields (Ruhl)	33
5.2	The Real Part of the Index of Refraction of the Vacuum in high Fields: Vacuum Birefringence	39
5.3	Compton Scattering and Radiation Reaction of a Single Electron at High Intensities	43
5.4	Nuclear Lifetime Measurements by Streaking Conversion Electrons with a Laser Field.	51
6	Stand-alone γ/e^- Facility for Nuclear Spectroscopy	55
6.1	Measuring Narrow Doorway States, embedded in Regions of High Level Density in the First Nuclear Minimum, which are identified by specific (γ, f) , (γ, α) , (γ, p) , (γ, n) Reactions and allow to map out the Nuclear Potential Landscape	55
6.2	Precision Tests of Fluctuating Quantities in Nuclear Physics of Highly Excited Nuclear Levels in Comparison to Random-Matrix-Theory and Quantum Chaos	56
6.3	High Resolution Inelastic Electron Scattering (e, e')	59
6.4	Nuclear Transitions and Parity-violating Meson-Nucleon Coupling	60
6.5	The Pygmy Dipole Resonance (PDR) of deformed nuclei	62
6.6	Fine-structure of Photo-response above the Particle Threshold	64
6.7	Nuclear Resonance Fluorescence on Rare Isotopes and Isomers	65
6.8	Multiple Nuclear Excitons	66

7	Stand-alone γ/e^- Facility for Astrophysics	69
7.1	Neutron Capture Cross Section of s-Process Branching Nuclei with Inverse Reactions	69
7.2	Measurements of (γ, p) and (γ, α) Reaction Cross Sections for p-Process Nucleosynthesis	71
8	Stand-alone γ Facility for Applications	73
8.1	Industrial Applications for the Management of Nuclear Materials	73
8.2	High Resolution, high Intensity X-Ray Beam	74
8.3	Extremely BR Illiant N eutron-Source produced via the (γ, n) Reaction without Moderation (BRIN)	75
8.4	An Intense BR Illiant P ositron-Source produced via the (γ, e^+e^-) Reaction (BRIP)	77
9	Industry Relevant Developments at ELI-NP	78
10	Layout, Principles of Panning and Performance Goals of the Complete ELI-NP Facility	79
11	Questions and Comments	86

1 Foreword

This report contains a comprehensive description of the new international research infrastructure, the Extreme Light Infrastructure - Nuclear Physics facility (ELI-NP), emphasizing the physics which can be addressed with it. The report has been prepared from contributions by many people from various laboratories throughout the world. Their contributions have been merged by a group of editors. This report at the same time demonstrates that ELI-NP can count on a large international user community. Here the extreme light infrastructure consisting of two components: a very high intensity laser system and a very short wavelength brilliant, intense γ beam. With this report we demonstrate our deep conviction that this infrastructure will create a new European laboratory with a broad range of science covering new nuclear physics, astrophysics, fundamental high field physics as well as applications in radioactive waste management, material science and life sciences.

For the realization of ELI-NP we envisage the following two principles as guideline:

- 1) a staged realization of ELI-NP
- 2) a flexible design of the ELI-NP facility.

The first principle allows for a sequential buildup of the facility according to the available resources. For example, the first stage may target only the most basic physics topics and the basic facility components that need to be started immediately. Thus the starting version may cover the period from 2011 - 2015. The second stage might start from 2016 for five years, including more ambitious programs. Subsequently the third stage might start from 2021 for ten years. This stage might include the most ambitious and far reaching projects as well as the ones that are yet to be discovered by the preceding investigations till 2020.

When we take such a staged approach, it occurs to us that we need to build the first stage facility in such a way as to accommodate the future growth of the above. Thus some of the ambitious experiments should be allowed, though they might not come in immediately, without too much of modification of the basic floor plan. For this we ought to adopt a flexible design philosophy.

2 Executive Summary

2.1 Basic Objectives

ELI will be the only European and International Centre for high-level research on ultra-high intensity laser, laser-matter interaction and secondary sources with unparalleled possibilities. Its pulse peak power and briefness will go beyond the current state-of-the-art by several orders of magnitude. Because of its unique properties, this multidisciplinary facility will provide magnificent new opportunities to study the fundamental processes unfolded during light-matter interaction.

ELI will create a platform, where Extreme Light applications for the benefit of society will be dynamically promoted. In its mission ELI will practice a vigorous technology transfer to European SMEs and large firms. High on ELI agenda will be the training of aspiring scientists and engineers in the numerous disciplines associated with the Extreme Light.

The ELI project, a collaboration of 13 European countries, will comprise four pillars:

- High Energy Beam Science devoted to the development and usage of dedicated beam lines with ultra short pulses of high energy radiation and particles reaching almost the speed of light (100 GeV).
This part of ELI will be realized in Prague (Czech Republic)
- Attosecond Laser Science designed to conduct temporal investigation of electron dynamics in atoms, molecules, plasmas and solids at attosecond scale (10^{-18}) sec.
Szeged (Hungary) will host the short pulse pillar of ELI.
- Laser-based Nuclear Physics:
The third site in Magurele (near Bucharest/Romania) will focus on laser-based nuclear physics. While atomic processes are well suited to the visible or near visible laser radiation, as a third pillar ELI-NP will generate radiation and particle beams with much higher energies, brilliances suited to studies of nuclear and fundamental processes.
- Ultra High Field Science that will explore relativistic laser-matter interaction in an energy range where totally new phenomena like radiation dominated interaction become dominant.
The decision on the location of the technologically most challenging pillar will be taken in 2012 after validation of the technology.

For ELI-NP it is foreseen to install three arms of the APOLLON laser, each with a power of 10 PW. A highly brilliant γ beam will be generated via the laser interaction with a brilliant bunched electron beam. Thus ELI-NP will allow either combined experiments between the high-power laser and the γ beam or stand-alone experiments.

2.2 History of the Project

γ beams: Tagger, bremsstrahlung source, Linear Compton Back-scattering (LCS), synchrotron light sources

Table 1: Planned Linear Compton Back-scattering Sources

	VELOCI- RAPTOR (LLNL)[1]	γ ERL high-flux [2]	γ ERL high-brilliance [2]	γ storage ring [3]
max. e energy	250 MeV	1 GeV	1 GeV	1 GeV
max. γ energy	2.2 MeV	19 MeV	19 MeV	19 MeV
e-energy spread (FWHM)		$9 \cdot 10^{-4}$	$9 \cdot 10^{-4}$	$\approx 2 \cdot 10^{-2}$
γ -energy spread (FWHM)	10^{-3}	$8 \cdot 10^{-3}$	$2 \cdot 10^{-3}$	$(4-10) \cdot 10^{-2}$
total flux(ph/s)	10^{10}	$5 \cdot 10^{13}$	$1 \cdot 10^{13}$	10^{13}
pulse repetition	120 Hz	10 MHz	100 MHz	50-200 MHz
pulse duration	2 ps	3 ps	3 ps	? ps
collision spot size	? μm	15 μm	10 μm	70 μm
peak brilliance ph/(mm ² mrad ² s0.1%)	$4 \cdot 10^{21}$	$7 \cdot 10^{19}$	$6 \cdot 10^{22}$	10^{16}
ave. brilliance ph/(mm ² mrad ² s0.1%)	10^{11}	$3 \cdot 10^{15}$	$3 \cdot 10^{19}$	$5 \cdot 10^{12}$

References

- [1] Ch. Barty, private communication (2010).
- [2] R. Hajima and N. Nishimori, private communication (2010).
- [3] Extrapolation to high γ energy; THOMX, Conceptual Design Report; A. Variola et al., LAL/RT 09/28, Dec 2009.

2.3 The Scientific Case of ELI-Nuclear Physics

For ELI-NP two new central instruments are planned:

1. A very high intensity laser, where three 10 PW Apollon lasers are coherently added to the high intensity of $10^{24}\text{W}/\text{cm}^2$ or electrical fields of $2 \cdot 10^{15}\text{V}/\text{m}$.
2. A very intense, brilliant γ beam ($E_\gamma \leq 19\text{ MeV}$), which is obtained by incoherent Compton back scattering of direct laser light or laser light from a super cavity off a very brilliant, intense, classical electron beam ($E_e \leq 800\text{ MeV}$). There are many γ beam lines, but in contrast to synchrotrons mostly one user will be supplied at a time, due to the very different requirements.

The γ beam will have unique properties in world wide comparison and opens new possibilities for high resolution spectroscopy at higher nuclear excitation energies. They will lead to a better understanding of nuclear structure at higher excitation energies with many doorway states, their damping widths, and chaotic behaviour, but also new fluctuating properties in the time and energy domain. The detailed investigation of the pygmy dipole resonance above and below the particle threshold is very essential for nucleosynthesis in astrophysics. In ion acceleration the high power laser allows to produce 10^{15} times more dense ion beams than achievable with classical acceleration. The cascaded fission-fusion reaction mechanism can then be used to produce very neutron-rich heavy nuclei for the first time. These nuclei allow to investigate the $N = 126$ waiting point of the r -process in nucleosynthesis. With this type of new laser acceleration mechanism very significant contributions to one of the fundamental problems of astrophysics, the production of the heavy elements beyond iron in the universe can be addressed. According to a recent report by the National Research Council of the National Academy of Science (USA), the origin of the heaviest elements remains one of the 11 greatest unanswered questions of modern physics [1]. The γ beam also opens many new possibilities for applications. The γ beam itself can be used to map the isotope distributions of radioactive waste remotely via Nuclear Resonance Fluorescence (NRF) of radioactive waste [4]. At lower energies around 100 keV the high resolution of the beam is very important for protein structural analysis. In addition we want to produce low energy, brilliant, intense neutron beams and low energy, brilliant, intense positron beams, which open new fields in material science and life sciences. The possibility to study the same target with these very different brilliant beams will be unique and advance science much faster.

The high power laser allows for intensities of up to $10^{24}\text{W}/\text{cm}^2$. Here very interesting synergies are achievable with the γ beam and the brilliant high energy electron beam to study new fundamental processes in high field QED. When the γ beam is injected into the focus of the high intensity laser, which in this special case consists of a standing E -field of two focused lasers, the most recent nonperturbative QED calculations predict that one can observe already at $10^{24}\text{ W}/\text{cm}^2$ the catalytic pair creation from the vacuum [2]. If confirmed, this would constitute a very basic non-perturbative textbook QED result. Also the radiation damping theory could be tested very accurately with the very brilliant electron beam injected into the laser focus. Here reflected high-energy γ quanta and cascades of e^+e^- pairs could be studied as a function of the γ factor of the electron beam and the laser field strength. While the predictions for radiation damping will probably be correct in the perturbative regime, the different theoretical approximations can be tested very sensitively for nonlinear radiation damping. On the other hand, the central questions of high-field QED for the ultra-relativistic laser-plasma interaction

Table 2: Overview of the main areas of the scientific case of ELI-NP

Science Case of ELI-NP	
Basic Science	Applications
Fundamental physics of perturbative and non-perturbative high-field QED: – pair creation, high energy γ rays, birefringence of the quantum vacuum	Developing nuclear resonance fluorescence (NRF) for radioactive waste management: – ^{235}U , ^{239}Pu , minor actinides, neutron poisoning
High-resolution nuclear spectroscopy: (γ, γ') , (γ, n) , (γ, p) , (γ, α) , (e, e') , $(e, e'\gamma)$, (γ, f) – chaotic properties of nuclear states, nuclear potential landscape, parity-violating meson-nucleon coupling, pygmy dipole resonance	Brilliant γ , X , n , e^+ , e^- micro beams in material science and life science: – (γ, n) reaction at threshold for low energy neutrons, (γ, e^+e^-) reaction at 2-3 MeV for cold positrons
Astrophysics of the r-, s-, p-processes in nucleosynthesis: – masses of waiting point nuclei, pygmy resonance	Developing techniques of laser acceleration and of a brilliant γ beam for nuclear physics: – relativistic mirrors

with $I \geq 10^{24}$ W/cm² including all new corresponding applications will be subject of the 4th pillar of ELI on ultra-high fields.

In this project we want to use a very high intensity laser and a very brilliant, intense γ beam to achieve major progress in nuclear physics and its associated fields like the element synthesis in astrophysics and many new applications or even to observe in fundamental physics the first catalysed pair creation from the quantum vacuum.

However, we should first place the laser developments into the right perspective. Typical nuclear excitation energies are of the order of 100 keV – 1 MeV and typical nuclear radii are below 10 fm. Thus relevant electrical field strengths in a nucleus, which change the dynamics, are of the order of 100 keV/(e·10 fm)= 10^{19} V/m and as such much beyond the Sauter field strength for pair creation from the vacuum of $1.3 \cdot 10^{18}$ V/m [3]. Since fields beyond the Sauter field cause cascades of e^+e^- pairs and limit the field to the Sauter field, it is impossible to reach laser fields which directly influence the internal dynamics of nuclei significantly.

The second instrument, the intense, brilliant γ beam, is envisaged to provide a photon flux of $I = 10^{13}/[\text{s} (100 \mu\text{m})^2]$, or – introducing the maximum Breit-Wigner cross section λ^2/π for 5 MeV γ quanta of $(\approx 100 \text{ fm})^2$ – a flux of $10^{-5}/[\text{s} (100 \text{ fm})^2]$, thus demonstrating the limitations by the presently achievable photon flux, where e.g. pump-probe experiments will remain impossible. The reflecting relativistic mirror probably will work at larger wave length. However it is a high risk that the reflecting relativistic mirror with 10^{16} photons per shot and $(\mu\text{m})^2$ will also be realized for MeV energies. If so, double excitation and pump-probe experiments in nuclear physics would become possible for the first time. The main achievements with the γ beam facility probably will occur with high resolution at higher nuclear excitation energies. Thus the nuclear physics experiments have to be carefully designed and it has to be considered that the success of lasers in atomic physics cannot simply be duplicated in nuclear physics due to the

very different scales and dimensions.

Amongst other goals, the envisaged new nuclear physics spectroscopy aims at a much better understanding of highly excited chaotic nuclear resonances, while up to now nuclear physics – due to the facilities – focused more on various lower lying vibrational and rotational nuclear states with more periodic nuclear motion. Also the transition from period to chaotic motion is of large interest. Though the basic ideas of a compound nuclear state were already formulated by N. Bohr in 1936 [5], now we have a much more detailed theory of these states within the framework of random-matrix theory [6] and conceptual pictures like quantum chaos. Due to the new experimental possibilities within ELI-NP, new theoretical predictions for experiments are introduced [7]. One example: A nuclear state excited by a γ pulse below the particle threshold is predicted to decay exponentially in time via γ quanta, while a state above the particle threshold shows a different decay law resulting from folding an exponential function with a power law. To verify these new decay laws in the attosecond and zeptosecond time range will be quite an experimental challenge, however, at the same time it would constitute an essential confirmation of random matrix theory. In the energy domain other known properties of compound nuclear states like Ericson fluctuations [10] or changes of the Weisskopf width [11] will be studied in a systematic way. If double excitations become possible with the relativistic mirror γ beam, the excited state can be treated with random-matrix theory similar to the double giant dipole excitation [8]. Here the new laser based measuring technologies will start a much better understanding of these high lying states and will lead to a reincarnation of nuclear physics, where the MeV photon pulses with much shorter wavelength and much shorter pulse duration will lead to an improved insight into compound nuclear states and quantum chaos.

In the field of basic nuclear physics, a better theoretical understanding of compound nuclear resonances in comparison with much improved experiments will also lead to better models for the element synthesis in astrophysics.

On a deeper level nuclear physics is described by QCD and their effective theories like chiral symmetry breaking and the condensate structure of low-energy QCD [9]. Here close lying resonances or the newly planned parity violating experiments at high excitation energies are a typical example, where we want to determine the parity-violating effective couplings between Z_0 and π, ρ and ω mesons.

Compared to former γ facilities, the much improved bandwidth is decisive for the new γ beam facility. Several experiments, like the parity violation experiment, only become possible due to this much better bandwidth (projects 6.1, 6.2, 8.2 and 8.3). The large majority of γ beam experiments will profit proportionally from the better bandwidth, because the widths of the studied nuclear levels are significantly smaller than the width of the beam. Thus the ratio of 'good' γ quanta within the nuclear linewidth compared to the 'bad' γ quanta outside, which undergo Compton scattering and cause background in the detectors, will be significantly improved.

This compilation of the main projects does not reflect a weighting of the political, socio-economical or scientific importance of the projects:

The project to develop techniques for remote characterization of radioactive waste via NRF will gain large importance for society in Europe. The unsolved problems of long-term storage of radioactive waste from reactors, while having to deal with large amounts of old, insufficiently characterized radioactive waste requires a precise isotopic characterization in the first place. It may even turn out that a detailed in-situ characterization of partially used reactor fuel elements may result in producing more usable energy in reactors for the same amount of radioactive waste.

References

- [1] E. Haseltine, <http://discovermagazine.com/2002/feb/cover>
- [2] G. V. Dunne, H. Gies and R. Schützhold, Phys. Rev. D **80**, 111301 (2009) [arXiv:0908.0948 [hep-ph]].
- [3] F. Sauter, “Über das Verhalten eines Elektrons im homogenen elektrischen Feld nach der relativistischen Theorie Diracs,” Z. Phys. **69**, 742 (1931).
- [4] R. Hajima et al., NIM **A 608**, S57 (2009).
- [5] N. Bohr, Nature **137**, 344 (1936).
- [6] H.A. Weidenmüller and G.T. Mitchell, *Random matrices and chaos in nuclear Physics:Nuclear structure*, Rev. Mod. Phys. **81**, 539 (2009).
G.E. Michell, A. Richter and H.A. Weidenmüller, *Random Matrices and Chaos in Nuclear Physics: Nuclear Reactions*, arXiv:1001.2411v1[nucl-th]14 jan 2010.
- [7] H.A. Weidenmüller and B. Dietz, *Photonuclear Reactions induced by Intense Short Laser pulses*, to be published (2010).
- [8] J.Z. Gu and H.A. Weidenmüller, Nucl. Phys. **A 690**, 382 (2001).
- [9] P. Finelli et al., Nucl. Phys. **A 735**, 449 (2004).
N. Kaiser and W.Weise, Nucl. Phys. **836**, 256 (2010).
J.W. Holt et al., Phys. Rev. **C 81**, 024002 (2010).
N. Kaiser; arXiv 1003.1143 (2010).
- [10] T. Ericson, Phys. Rev. Lett. **5**, 430 (1960).
- [11] N. Bohr and J.A. Wheeler, Phys. Rev **56**, 426 (1939).
A. Feshbach, C.E. Porter and V.F. Weisskopf, Phys. Rev. **96**, 448 (1954).

2.4 Principles of Planning, Layout and Performance Goals of the Facility

- Starting version
- provisions for future upgrades of the facility:
 - for buildings
 - for experiments

2.5 Requirements by the Experiments for the High-power Laser and the γ/e^- Facility

Properties of APOLLON laser, properties of γ -beam facility. Three classes of experiments can be envisaged for ELI-NP:

- i) stand-alone experiments with the high-power APOLLON laser,
- ii) combined experiments of the APOLLON laser and the γ -beam facility,

iii) stand-alone use of the γ -beam facility.

accelerator based γ sources; HI γ S [1]

Combined experiments require matched beams with respect to repetition rate, focus dimensions, pulse duration, etc.

New areas of research will be opened up in fundamental physics, nuclear physics, astrophysics, relativistic laser-plasma interaction and many new possibilities open up in applications of brilliant X-rays and γ -rays, neutrons and positrons.

However, a high resolution γ facility would also be of interest in the 100 keV energy range for protein structure analysis and e.g. XAFS environmental studies. With higher resolution even the study of superconductivity (a typical neutron domain) could be included into the research portfolio of ELI-NP.

References

[1] H.R. Weller et al., Prog. in Part. and Nucl. Phys. **62** , 257 (2009).

[2] W.J. Brown et al., Phys. Rev. ST AB **7**, 060702 (2004).

2.6 Cost, Schedule and Personnel

3 Introduction

For ELI-NP the extreme light is realized in a twofold way: by very high optical laser intensities of APOLLON and by the very short wavelength beams with very high brilliance. This combination allows for three types of experiments: stand-alone APOLLON experiments, stand-alone γ beam experiments and combined experiments of both facilities. Here the low repetition rate (1/min) of the high power laser requires the same low repetition rate for the γ beam in combined experiments. While the stand-alone γ beam will be used with typically 100 MHz the low repetition mode requires few very intense γ pulses.

4 Stand-alone APOLLON Experiments

With the APOLLON laser we do not plan to interact with nuclear dynamics directly, but we use the laser for ion acceleration or to produce relativistic electron mirrors by laser acceleration followed by a coherent reflection of a second laser beam in order to generate very brilliant X-ray or γ beams. We plan to use these beams later to produce exotic nuclei or to perform new γ spectroscopy experiments in the energy or time domain.

4.1 A Laser-Accelerated Th Beam is used to produce Neutron-Rich Nuclei around the $N = 126$ Waiting Point of the r -Process via the Fission-Fusion Reaction Mechanism

D. Habs¹ and P.G. Thirolf¹

¹ *Ludwig Maximilians University, Munich (Germany)*

According to a recent report by the National Research Council of the National Academy of Science (USA), the origin of the heaviest elements remains one of the 11 greatest unanswered questions of modern physics [1]. While the lower path of the r -process for the production of heavy elements is well explored, the nuclei around the $N = 126$ waiting point critically determine this element production mechanism, and at present basically nothing is known about these nuclei. We propose to produce neutron-rich nuclei in the range of the astrophysical r -process (the rapid neutron-capture process) around the waiting point $N = 126$ [2, 3, 4] by fissioning a dense thorium ion bunch with about 10 MeV/u in a 1 mm thick thorium target, where the light fission fragments of the beam fuse with the light fission fragments of the target. Via laser Radiation Pressure Acceleration (RPA) [10, 11] we are able to produce very efficiently bunches of solid state density of ^{232}Th with about 10 MeV/u, which pass through a Th foil and desintegrate into light and heavy fission fragments. The expected strongly reduced stopping power for these very dense ion bunches helps to obtain intense fission fragment beams. The high density of the bunch and the target furthermore leads to a reasonable fusion yield. In contrast to classical radioactive beam facilities, where intense, low density radioactive beams of one isotope are merged with stable targets, we here study the fusion between neutron-rich short-lived target-like nuclei and neutron-rich, short-lived projectile-like nuclei. Since each of these mass distributions consists of a multitude of isotopes, we exploit the fluctuations in neutron number of both target and beam fragment to reach more neutron-rich nuclei. Also the neutron transfer before the first fission reaction will increase the fluctuations in neutron number of the light fission fragments. The new acceleration scheme allows to reach this so far unexplored region of neutron-rich nuclei with

importance to nuclear physics and astrophysics. One expects for the 30 PW APOLLON laser with 600 J about 10^{12} accelerated thorium ions with a $9 \mu\text{m}$ beam diameter, 30 nm bunch length and 0.1 Hz repetition rate. This should result in about $3 \cdot 10^6$ ions/shot of fused neutron-rich nuclei with masses close to $A = 180 - 190$. In a velocity filter the other species with $A \approx 232$, $A \approx 140$ and $A \approx 100$ can be separated from the beam-like nuclei of interest with $A = 180 - 190$. Since the yield of very neutron-rich fusion products grows strongly nonlinearly with laser energy, a final use of several coincident APOLLON lasers could be very advantageous, especially since the detection of the new ms-isotopes should be rather straightforward.

Radiation Pressure Acceleration (RPA) with solid state density ion bunches, which are about 10^{15} times more dense than classically accelerated ion bunches, allows for a high probability that generated fission products fuse again, when the thorium beam strikes a second close Th target. The fission fragments have a $1/\sin(\Theta)$ angular distribution and thus are predominantly emitted in beam direction and stay within the cylinder volume defined by the small spot diameter of the first Th target. In this two-step reaction neutron-rich light fission fragments of the beam fuse with neutron-rich light fission fragments of the target and we can reach more neutron-rich nuclei than with classical radioactive beams only. The produced beam of new radioactive nuclei will be analyzed with a classical ‘‘SHIP’’-like velocity filter[7], where the technical optimization is well known and one gets a very good suppression of background for nearly symmetric fusion reactions. The small repetition rate of the 30 PW APOLLON lasers of about 0.02 Hz with very short production pulses is stretched by the β -decay half-lives of the produced nuclei to counting rates acceptable to nuclear detectors. Very neutron-rich nuclei still have small production cross sections, because weakly bound neutrons ($B_N \geq 3 \text{ MeV}$) are evaporated easily. It is important that the hindrance of fusion for nearly symmetric systems (break-down of fusion) only sets in for projectile and target masses heavier than 100 u [8, 9]. Thus for the fusion of light fission fragments we expect an unhindered fusion evaporation process. The velocity filter has to suppress the many fused nuclei close to the valley of stability. Here we want to look specifically for nuclei close to the waiting point at $N = 126$ of the r -process, which is decisive for the astrophysical production of heavy elements and was not accessible until now. We estimate sufficient rates for these interesting nuclei. We envision having behind the velocity filter a gas stopping cell for the preparation of the ions [10] prior to their injection into a Penning trap [11], where nuclear masses can be measured with high accuracy, thus giving access to nuclear binding energies.

References

- [1] E. Haseltine, <http://discovermagazine.com/2002/feb/cover>
- [2] K.L. Kratz et al., Prog. in Part. and Nucl. Phys. **59**, 147 (2007).
- [3] M. Arnould, S. Griely, K. Takahashi, Phys. Rep. **450**, 97 (2007).
- [4] I.V Panov and H.-Th. Janka, Astr. Astroph. **494**, 829 (2009).
- [5] A. Henig et al., Phys. Rev. Lett. **103**, 245003 (2009).
- [6] T. Tajima, D. Habs, X. Yan, *Laser Acceleration of Ions for Radiation Therapy*, RAST **2**, 221 (2009).

- [7] G. Münzenberg et al., Nucl. Instr. Meth. **161**, 65 (1979).
- [8] A.B. Quint et al., Z. Phys. **A 346**, 119 (1993).
- [9] W. Morawek et al., Z. Phys. **A 341**, 75 (1991).
- [10] J.B. Neumayr et al., Nucl. Instr. Meth. **B244**, 489 (2006).
- [11] M. Block et al., Nature **463**, 785 (2010).

4.2 From Radiation Pressure Acceleration (RPA) and Laser-Driven Ion Pistons to Direct Laser Acceleration of Protons at Intensities up to $10^{24}\text{W}/\text{cm}^2$

D. Habs¹, A. Henig¹, J. Schreiber¹, R. Hörlein¹, X.Q. Yan² and M. Zepf³

¹ *Ludwig Maximilians University, Munich (Germany)*

² *State Key Lab of Nuclear Physics and Technology, Peking University, Beijing, (P.R. China)*

³ *Queen's University Belfast, Northern Ireland (UK)*

Since the pioneering work that was carried out 10 years ago [1, 2, 3, 4], the generation of highly energetic ion beams from laser-plasma interactions has been investigated in much detail in the regime of target normal sheath acceleration (TNSA) [5]. Creation of ion beams with small longitudinal and transverse emittance and energies extending up to tens of MeV fueled visions of compact, laser-driven ion sources for applications such as ion beam therapy of tumors, fast ignition inertial confinement fusion or the generation of neutron-rich nuclei. However, new pathways are of crucial importance to push the current limits of laser-generated ion beams further towards parameters necessary for those applications.

To overcome the limitations of TNSA, a novel mechanism which is referred to as Radiation Pressure Acceleration (RPA) was proposed [6, 7, 8, 9]. Here, much thinner foil targets of only nanometers are used so that the laser transfers energy to all electrons located within the focal volume. While for TNSA the accelerating electric field that is generated by hot electrons is stationary and ion acceleration is spatially separated from laser absorption into electrons, in RPA a localized longitudinal field enhancement is present that co-propagates with the ions as the accompanying laser pulse pushes the electrons forward. By changing the laser polarization to circular, electron heating and expansion are efficiently suppressed, resulting in a phase-stable acceleration that is dominated by the laser radiation pressure and is maintained for an extended time. Thus, the whole target is accelerated ballistically as a quasi-neutral, dense plasma bunch like a light sail. Just recently, this novel acceleration process has been observed for the first time in an experiment at intensities of $5 \times 10^{19} \text{ W}/\text{cm}^2$ [10, 11] and pulse energies below 1 J, generating a peaked spectrum of C^{6+} ions. Compared to quasi-monoenergetic ion beam generation within the TNSA regime [12], a more than 40 times increase in conversion efficiency was achieved.

A large number of theoretical studies lately predicted further improvement of the ion beam characteristics in terms of conversion efficiency as well as peak energy and monochromaticity when significantly higher laser pulse energies and intensities are used [13, 14, 15, 16, 17]. In particular, it is expected that the RPA process progresses much more stably when ions reach relativistic velocities already in the initial hole-boring phase before the whole target is set in motion (i.e., before the light sail stage). At intensities around $10^{23} \text{ W}/\text{cm}^2$ simulations show that protons become relativistic within one half-cycle of the laser pulse and acceleration by the laser radiation pressure is dominant even for linear polarization in what is referred to as the laser-piston regime [18, 19]. Here, the target can be viewed as a relativistic plasma mirror with Lorentz factor γ being propelled by the reflected laser and the laser-to-ion conversion efficiency $\eta = 1 - 1/(4\gamma^2)$ approaches unity in the ultrarelativistic limit.

In all ion acceleration mechanisms discussed so far, the laser energy was not directly transferred to ions but mediated by electrons instead. For even higher laser intensities of $\sim 5 \times 10^{24} \text{ W}/\text{cm}^2$ at a wavelength of $1 \mu\text{m}$, protons can be driven to relativistic velocities directly by the laser field. This regime of direct ion acceleration has not been studied in simulations so far since the new phenomenon of radiation damping strongly changes the laser-plasma interaction and is also

expected to occur at 10^{24} W/cm², hence preventing the straightforward application of existing PIC codes [20, 21]. Basically all theories of radiation damping suffer from more or less severe intrinsic inconsistencies [22] and only by comparison with experiment the proper theory can be established (see project 5.3: Radiation Damping at 10^{24} W/cm²).

Employing the APOLLON laser unprecedented intensities on the order of 10^{24} W/cm² become available for experiments, allowing for improved RPA and for the first time study of the laser-piston regime as well as direct proton acceleration. According to theory, mono-energetic solid density ion bunches are expected at laser-to-ion conversion efficiencies approaching unity. Such a novel compact ion source could serve a wealth of experiments and applications, with an example being given by the production of neutron-rich nuclei around the N=126 waiting point as described in project 4.1.

References

- [1] E. L. Clark et al., Phys. Rev. Lett. **85**(8), 1654–1657 (2000).
- [2] A. Maksimchuk et al., Phys. Rev. Lett. **84**(18), 4108–4111 (2000).
- [3] R. A. Snavely et al., Phys. Rev. Lett. **85**(14), 2945–2948 (2000).
- [4] S. P. Hatchett et al., Phys. Plas. **7**(5), 2076–2082 (2000).
- [5] S.C. Wilks et al., Phys. Plasma **8**, 542 (2001).
- [6] A. Macchi et al., Phys. Rev. Lett. **94**(16), 165003 (2005).
- [7] O. Klimo et al., Phys. Rev. ST Accel. Beams **11**, 031301 (2008)
- [8] A.P.L. Robinson et al., New J. of Phys. **10**, 013021 (2008).
- [9] X. Q. Yan et al., Phys. Rev. Lett. **100**(13), 135003–4 (2008).
- [10] A. Henig et al., Phys. Rev. Lett. **103**, 245003 (2009).
- [11] T. Tajima, D. Habs, X. Yan, *Laser Acceleration of Ions for Radiation Therapy*, RAST **2**, 221 (2009).
- [12] B. M. Hegelich et al., Nature, **439**, 441–444 (2006).
- [13] X. Q. Yan et al., Phys. Rev. Lett., **103**(13), 135001 (2009).
- [14] B. Qiao et al., Phys. Rev. Lett. **102**, 145002 (2009).
- [15] A.P.L. Robinson et al., Plasma Phys. Control Fusion **51**, 024004 (2009).
- [16] A. Macchi et al., Phys. Rev. Lett. **103**, 085003 (2009).
- [17] A. Macchi et al., *Radiation pressure acceleration of ultrathin foils*, New J. Phys. (2010), in press.
- [18] T. Esirkepov et al., Phys. Rev. Lett. **92**, 175003 (2004).

- [19] F. Pegoraro and S.V. Bulanov, Phys. Rev. Lett. **99**, 065002 (2007).
- [20] T. Schlegel et al., Phys. Plas., **16**, 083103 (2009).
- [21] M. Chen et al., *Radiation reaction effects on ion acceleration on laser foil acceleration*, arXiv:0909.5144v1(2009).
- [22] I.V. Sokolov, JETP **109**, 207 (2009).

4.3 Deceleration of Very Dense Electron and Ion Beams

D. Habs¹, A. Henig¹, J. Schreiber¹, R. Hörlein¹, W. Ma² and M. Zepf³

¹ *Ludwig Maximilians University, Munich (Germany)*

² *Institute of Physics, CAS, Beijing, (P.R. China)*

³ *Queen's University Belfast, Northern Ireland (UK)*

In nuclear physics the Bethe-Bloch formula [2] is used to calculate the atomic stopping of energetic individual electrons [1] by ionization and atomic excitation:

$$-\left[\frac{dE}{dx}\right]_I = K \cdot z^2 \frac{Z}{A} \frac{1}{\beta^2} \left[\frac{1}{2} \ln \frac{2m_e c^2 \beta^2 \gamma^2 T_{\max}}{I^2} - \beta^2 - \frac{\delta}{2} \right] \quad (1)$$

and ions:

$$-\frac{dE}{dx} = 4\pi n_e \frac{Z_{\text{eff}}^2 e^4}{m_e v^2 (4\pi\epsilon_0)^2} \left[\ln \left(\frac{2m_e v^2}{I(1-\beta^2)} \right) - \beta^2 \right] \quad (2)$$

where I is the ionization potential, n_e the density of the electrons, m_e the mass of the electron, v is the ion velocity, $\beta = v/c$, T_{\max} is the maximum kinetic energy which can be imparted to a single electron in a single collision, and Z_{eff} is the effective charge of the ions.

For relativistic electrons the other important energy loss is bremsstrahlung with:

$$-\left[\frac{dE}{dx}\right]_R = (4\pi n_e / (m_e c^2)) \frac{Z}{137\pi} (\gamma - 1) \ln(183Z^{-1/3}) \quad (3)$$

The approximate ratio of the two loss processes [2] is:

$$\left[\frac{dE}{dx}\right]_I / \left[\frac{dE}{dx}\right]_R = EZ / 1600 mc^2 \quad (4)$$

Thus radiation loss is dominant for high energy electrons e.g. $E \geq 100$ MeV and $Z=10$. If, however (see below), the atomic stopping becomes orders of magnitude larger by collective effects, the radiation loss can be neglected.

For laser acceleration the electron and ion bunch densities reach solid state densities, which are about 15 orders of magnitude larger compared to beams from classical accelerators. Here collective effects become important. One can decompose the Bethe-Bloch equation according to Ref. [3] into a first contribution describing binary collisions and a second term describing long range collective contributions:

$$-\frac{dE}{dx} = 4\pi n_e \frac{Z_{\text{eff}}^2 e^4}{m_e v^2 (4\pi\epsilon_0)^2} \left[\ln(m_e v^2 / e^2 k_D) + \ln(k_D v / \omega_p) \right] \quad (5)$$

Here k_D is the Debye wave number and ω_p is the plasma frequency of the electrons. Similar to bubble acceleration [4] but now with opposite phase for deceleration a strong collective field is built up by the blown-out electrons that decelerates them much faster than the processes that take effect for individual charged particles. Typical electric fields E are:

$$E = m_e \omega_p \cdot v \cdot \frac{n_b}{n_e e} \quad (6)$$

where n_b is the charge density of the bunch. In Ref. [6] we discuss this mechanism of collective deceleration of a dense particle bunch in a thin plasma, where the particle bunch fits into part of the plasma oscillation and is decelerated $10^5 - 10^6$ stronger than predicted by the classical Bethe-Bloch equation [2] due to the strong collective wakefield. For ion deceleration we want to use targets with suitable low density. These new laws of deceleration and stopping of charged particles have to be established to use them later in experiments in an optimum way.

We may also discuss the opposite effect with a strongly reduced atomic stopping power that occurs when sending an energetic, solid state density ion bunch into a solid target. For this target the plasma wavelength ($\lambda_p \approx 1$ nm) is much smaller than the ion bunch length (≈ 100 nm) and collective acceleration and deceleration effects cancel each other. Only the binary collisions are important. Hence, we may consider the dense ion bunch as consisting of 300 layers with \AA distances. Here the first layers of the bunch will attract the electrons from the target and – like a snow plough – will take up the decelerating electron momenta. The predominant part of the ion bunch is screened from electrons and we expect a $\approx 10^2$ fold reduction in stopping power. The electron density n_e is strongly reduced in the channel because many electrons are driven out by the ion bunch and the laser. Again all these effects have to be studied in detail.

References

- [1] Particle Data Group, Phys. Rev. **D 66**, 010001 (2002).
- [2] S. Segre, *Nuclei and Particles*, 2nd edition, W.A. Benjamin, RA, London (1977)
- [3] S. Ichimaru, *Basic Principles of Plasma Physics: A Statistical Approach*, Benjamin, Reading, MA (1973).
- [4] A. Pukhov and J. Meyer-ter-Vehn; Appl. Phys. **B74**, 355 (2002).
- [5] H.-C. Wu et al., *Collective Deceleration*, arXiv:0909.1530v1 [physics.plasm-ph] (2010).

4.4 A Relativistic Ultra-thin Electron Sheet used as a Relativistic Mirror for the Production of Brilliant, Intense Coherent γ -Rays

D. Habs^{1,2}, D. Kiefer^{1,2}, R. Hörlein^{1,2} and X.Q. Yan^{2,3}

¹ *Ludwig Maximilians University, Munich (Germany)*

² *Max-Planck Institute of Quantum Optics, Garching (Germany)*

² *State Key Lab of Nuclear Physics and Technology, Peking University, Beijing, (P.R. China)*

In Ref. [1] we have proposed the use of an intense laser to drive a very dense electron sheet out of an ultra-thin Diamond-Like-Carbon (DLC) foil. The sheet then surfs on the half-wave of the laser pulse and gains a relativistic energy characterized by $\gamma = 1/\sqrt{1-\beta^2}$ with the total velocity $\beta = v/c$. We also introduce $\gamma_x = 1/\sqrt{1-\beta_x^2}$ with the velocity $\beta_x = v_x/c$ normal to the electron sheet. This relativistic electron mirror is expected to allow the reflection of a second laser beam for very brilliant, very intense, coherent X ray and γ beams with many unique applications.

Kulagin et al. [2, 3] showed that the produced flat electron sheet stays together for some μm , having energies of $\gamma \approx a$, where a is the dimensionless laser intensity parameter. This γ is different from the $\gamma = 1 + a^2/2$ calculated for a single electron, which probably is too high for a dense electron sheet. We have experimentally observed this production of electron sheets for the first time at the Trident laser in Los Alamos for 500 fs laser pulses [4] and also at the laser of the Max Born Institute in Berlin with their 35 fs laser pulses [5].

If one would reflect optical photons of energy $E_0 = 1$ eV normally from this electron sheet with an energy characterized by γ_x , one naively would expect to obtain reflected γ photons of energy $E_\gamma = 4 \cdot \gamma_x^2 \cdot E_0$. However, Wu et al. [6, 7] showed that the electron sheet also acquires a transverse velocity component v_x from the transverse laser E-field. Only later the $\vec{v} \times \vec{B}$ force leads to the dominant forward acceleration. The transverse velocity causes a much smaller Doppler boost of the reflected γ photons of $E_\gamma = 4 \cdot \gamma_x^2 \cdot E_0 = 2 \cdot \gamma \cdot E_0$, where γ is the total γ . However, recently Wu et al. [8] showed that one should place a second foil of about 2 times the skin depth (15 nm) in a 1-2 μm distance behind the first target foil, where the accelerating laser pulse is reflected. The reflected laser pulse completely cancels the transverse velocity component v_x , but basically leaves the longitudinal velocity component unchanged. In this way the originally expected full Doppler boost of the γ photons with $E_\gamma = 4 \cdot \gamma^2 E_0$ is recovered. While the preliminary simulations of Wu et al., [8] are very impressive more realistic ultrathin foils with much larger n_e/n_c for 1nm foils are required. The present simulations correspond to independent individual electrons, while then collective effects like expansion of the foil become important.

We invented a special target design with ultra-thin DLC foils and a very low-density carbon nanotube target as a spacer inbetween, in order to realize such a target for a perfectly reflecting electron sheet. The dense electron sheet then traverses the reflector target and shortly behind the reflector is bombarded with the second laser pulse (split off from the APOLLON laser with wavelength λ_0) to produce the γ photons with $\lambda_\gamma = \lambda_0/4\gamma^2$. The thickness d of the electron sheet determines up to which γ energy a coherent reflection occurs. In the inner rest frame of the electron sheet the photons have the wavelength $\lambda_i = \lambda_0/2\gamma$ before reflection. The requirement is $\lambda_i/2 \leq d$. Possibly the electron sheet is compressed during acceleration and also by the interaction with the reflected laser, reducing the thickness d . If we use $d = 1$ nm and $\lambda_0 = 1$ μm and $\gamma = 250$, we obtain reflected γ -photons of ≈ 250 keV. These γ pulses would be coherent and would have a pulse length of a few zeptoseconds. Since we will have about $N \approx 10^9 - 10^{10}$ coherently reflecting electrons, the reflected amplitude is increased by N . If we assume a spot

diameter of the reflected laser pulse of $3 \mu\text{m}$, we obtain a large reflectivity (1%) and expect $\approx 10^{16} \gamma/\text{shot}$ with $(6 \mu\text{m})^2$, $(\approx 5 \text{ mrad})^2$, 10^{-20} s and 0.1 % BW. Thus a rough estimate of the peak brilliance is $10^{39}/[\text{s} (\text{mm mrad})^2 0.1 \text{ \% BW}]$. With the APOLLON laser we easily can realize $a = 250$, but require in addition a very high contrast of 10^{16} for the survival of ultrathin foils during the prepulse. In this context careful experimental studies have to be performed aiming to characterize potential effects of reflectivity modifications by distortions of the reflecting mirror foil during the laser interaction.

In Ref. [9] we showed that a much larger reflecting force should occur, since the transition from the Lorentz force to the radiation damping force is strongly enhanced. While the Lorentz force scales with charge e , the radiation damping force or Landau-Lifshitz term scales with $(\frac{2}{3} \frac{e^3}{mc^3})$ [10] and thus if N electrons act coherently, the Lorentz force is proportional to N , while the Landau-Lifshitz force scales with N^2 and thus one obtains an acceleration due to radiation damping which is N fold enhanced. Thus 10^2 larger γ -energies may be reflected, reaching energies in the 25 MeV range. Here the ensemble of all electrons reflects like one macro-particle, which then takes up the recoil momentum as a whole. The electron sheet is trapped between the potential of the strongly reflecting laser and the Coulomb potential of the more backward layers of the electron sheet. This binding together of the electrons to a macroparticle is essential to result in a Mössbauer-like reflection scenario. If the Landau-Lifshitz force becomes dominant and higher order terms of the Landau-Lifshitz expansion series become important, even higher orders of N become relevant.

If these coherent intense γ pulses become available, many proposed experiments of ELI-NP with the incoherent γ beam like pair creation from the vacuum or excited multiple nuclear excitons will give orders of magnitude better results. Furthermore pump-probe experiments with two consecutive excitations of nuclei will become possible, which open a new field of studying highly excited states described by random matrix theory [6].

References

- [1] D. Habs et al., Appl. Phys. **B 93**, 349 (2008).
- [2] V.V. Kulagin et al., Phys. Rev. Lett. **99**, 124801 (2007).
- [3] V.V. Kulagin et al., Phys. Rev. **E 80**, 016404 (2009).
- [4] D. Kiefer et al., Eur. Phys. J. **D 55**, 427 (2009).
- [5] D. Kiefer et al., to be published.
- [6] H.-C. Wu and J. Meyer-ter-Vehn., Eur. Phys. J. **D 55**, 443 (2009).
- [7] J. Meyer-ter-Vehn and H.-C. Wu, Eur. Phys. J. **D 55**, 433 (2009).
- [8] H.-C. Wu et al., *Laser-like X-Ray Sources Based on Optical Reflection from Relativistic Electron Mirror*, arXiv:1003.1739v2 (2010).
- [9] D. Habs et al., *Proposed studies of radiation damping in laser interaction with an ultra-thin coherently reflecting electron sheet, regarded as a macro-particle*, Brasov Conference, AIP (2009).

- [10] L.D. Landau and E.M. Lifschitz; *Klassische Feldtheorie*, Volume 2, chapter 76, Verlag Harri Deutsch, 1992.
- [11] J.Z. Gu and H.A. Weidenmüller, Nucl. Phys. **A 690**, 382 (2001).

4.5 Nuclear Techniques for Characterization of Laser-induced Radiations

D. Bucurescu¹, GH. Cata-Danil¹, C. Ivan¹, N. Marginean¹, F. Negolta¹, and N.V. Zamfir¹
¹ *National Institute for Physics and Nuclear Engineering, Bucharest-Magurele (Romania)*

General overview During the last decade it was experimentally proved that when a high-intensity laser beam hits a target it induces ionization and acceleration processes. Consequently, several kinds of radiations were observed following the irradiation: accelerated electrons, protons and ions arising from the primary ionization and acceleration process, but also neutrons and a very intense gamma flux generated in secondary processes as bremsstrahlung and nuclear reactions. The investigation of laser-based acceleration process and of the radiations generated in this way evolves very fast and there is a stringent need to collect experimental data in a systematic way in order to understand and properly evaluate the potential use of high-intensity lasers for nuclear physics experiments and applications. We briefly outline several characteristics of the laser-induced radiations as known in the present:

- Large particle and photon fluxes are produced in a very short (below 1 picosecond) time interval.
- Several kinds of radiations are generated in primary and secondary processes: electrons, protons, heavy ions, X and gamma rays. Each of these is distributed in a specific energy range, strongly depending on the irradiated target and on the power of the laser source.
- The emittance is different for different radiation types, i. e. electrons are better focused and protons or heavier ions have a relatively broad angular distribution.

According to the processes that lead to the generation of these radiations, one can classify them as follows:

Radiations arising from primary processes: These are accelerated **electrons, protons and heavier ions**, with energies and angular distributions strongly depending on the acceleration scheme, irradiation geometry and target characteristics. The well established acceleration scheme at laser intensities up to 10^{20} W/cm² is the so-called *Target Normal Sheath Acceleration* e. g. [?], when the electrons are pushed out from the target, form a negative charge cloud and the ions from the target are accelerated by the electrostatic potential created in this way. TNSA is low-efficiency accelerating mechanism, where the maximum ion energy scales with the square root of the laser intensity. Recently another acceleration mechanism was experimentally evidenced, the *Radiation Pressure Acceleration* [2]. When a nanometer-thick foil is irradiated with circular polarized high intensity laser pulse appears a cold compression of electron sheet followed by the acceleration of ions in the rectified dipole field created between electrons and ions. In this way are created macroscopically neutral bunches of ions and electrons traveling at the same speed. This RPA mechanism is more efficient than TNSA and scales linearly with the laser intensity. At laser intensities of 10^{24} W/cm² and higher, the H and He nuclei are expected to enter the relativistic regime, when they will be accelerated directly by the laser as the electrons for laser intensities greater than 10^{18} W/cm². The electron energies obtained in the present are up to several hundreds of MeV, while for heavy ions are about several MeV/nucleon and are expected to increase with one-two orders of magnitude at ~ 10 PW, 10^{24} W/cm² lasers.

Radiations from secondary processes: Following the interaction of accelerated electrons with matter an intense flux of bremsstrahlung photons is produced. This brilliant gamma flux might further produce photonuclear reactions. In addition, depending on their energy, the nuclei accelerated from the primary target might produce nuclear reactions. All these lead to the emission of a large variety of secondary radiations: neutrons, charged particles and gamma rays.

Taking into account the high instantaneous flux and the relatively low repetition rate specific to the present high-intensity lasers, the well-established event-counting and coincidence techniques from nuclear spectroscopy are very difficult to be applied directly. Instead, simple nuclear spectroscopy techniques as analysis of activated samples or Thomson spectrometers coupled with CR-39 plastic track detectors were used until now. These techniques are not real-time and provide information about the investigated radiation field in minutes or even hours after the irradiation. Recently several experiments e.g. [?] were performed using a microchannel plate (MCP) with phosphorous screen, which provides almost real-time response as track detector. A systematic and efficient investigation of laser-induced radiations requires further optimization of currently used diagnosis techniques and further development of new methods. In nuclear spectroscopy the high-resolution experiments are performed in an event-by-event mode, which means recording into so-called "events" the radiations detected in a time window typically ranging from nanoseconds to microseconds. Obviously the "prompt flash" of radiation produced by a high-power laser beam hitting a target would be recorded as one event, if the detectors were not already overloaded by the intense radiation flux. The event-by-event way to measure is based on accumulating statistics; therefore using it in combination with the low repetition rate of the high power lasers constitutes a challenge for the nuclear spectroscopy technology of present days. The solution is to use state-of-art high granularity detectors, in which case every single detector element will see a reduced flux of radiation and will be active even during the "prompt flash". The granularity might compensate partially also the low repetition rate since there are many elements detecting coincident radiations, and sensible statistics can be obtained in a reasonable amount of time. Several high-granularity detection systems and associated digital electronics are presently used and some others are under development. The scope is to use them to the high intensity and radioactive beam facilities under construction. One example is the European AGATA project, which develops a state-of-art highly segmented HPGe gamma detectors array to be used in sites like FAIR/GSI (Germany) or SPIRAL2/GANIL (France). There is a striking similarity between the experimental conditions expected at FAIR and the ones encountered in working with laser-induced radiations, since in both cases there is a "prompt flash" the detection system must stand, then recover and continue to measure. Thus many ongoing developments in nuclear radiation detector technology will find immediate use in spectroscopic studies with laser-induced radiations.

Spectroscopy of accelerated heavy ions

The main characteristics needed for the understanding of the laser-induced ion acceleration are energy, charge-state and angular distributions as well as their absolute number per pulse. As stated before direct event-counting methods typical for nuclear spectroscopy are very difficult to apply for the detection of the prompt radiation produced by the laser pulse. Thus several alternative techniques must be used, in parallel with an intense R&D activity for the development of faster response, high-resolution spectroscopic methods suitable for the spectroscopy of laser-induced radiations. Presently, for the spectroscopy of laser-accelerated ions several experimental techniques are suitable for use and further development.

Activation techniques: basically consist in placing a stack of thin foils in front of the beam, to be activated by the beam particles. The radioactivity of each foil is measured individually after irradiation, in this way the incident beam intensity can be estimated. The beam energy distribution might be estimated using threshold reactions or from the de-convolution of the number of final reaction products in each foil when the beam energy dependence of the cross section of reaction in which they were produced is reliably known. The activation method is mostly suited for proton beams, where the reactions cross-sections are better known and have well-defined threshold behavior. This method might be further refined using low-background, high-efficiency HPGe spectrometer stations. Besides the optimized shielding for low-background counting, the HPGe detectors can have BGO anti-Compton shields which will reject the Compton scattering background and will improve the peak-to-total ratio, thus the spectrometer sensitivity. The "response time" of the method can be increased using in parallel several counting stations. Low-granularity angular distributions can also be obtained if an array of foil stacks is used; in this case the radioactivity per foil will be lower and very efficient counting spectrometers must be used.

Thomson spectrometers: are compact devices using a configuration with parallel static electric and magnetic fields to deviate ions on a parabolic trajectory according to the mass-over-charge ratio and energy. With Thomson spectrometers one can measure the charge-state and energy distributions of the accelerated ions, on the limits defined by the acceptance of the spectrometer and the sensitivity of the detection system. The Thomson spectrometer is normally used coupled with CR-39 plastic track detectors, thus the "response time" of this detection system is long. Being compact devices, arrays of Thomson spectrometers can be used to increase the granularity and to cover a larger solid angle. With proper collimation a Thomson spectrometer might be used for preselecting ions with defined A/q ratio or energy range, which can be further analyzed by large-acceptance magnetic spectrometers with a faster response time for the focal plane detectors.

Scintillation-based techniques with digital image recording: few experimental solutions were already investigated, i.e. the coupling of a Multi-Channel Plate with a phosphorus screen at the exit from an Thomson spectrometer and digital acquisition of the image obtained during the irradiation with heavy ions. An interesting development came very recently from RAL(UK), when the image obtained on very fast plastic scintillator foils at irradiation with laser-accelerated protons was recorded with gated CCD cameras, avoiding in this way the signals by electrons or X-rays [4]. With this detection device were obtained relatively precise angular distributions of protons integrated over several energy ranges defined by the thickness of the scintillation foil. The scintillator-gated CCD camera detection has almost instant response time and can be used continuously for many successive laser shots, being thus a very promising technique.

De-convolution of the pulse shape (proposed development): with a very fast plastic scintillator coupled with a fast phototube one can obtain a well-defined detector signal for one charged particle, signal with few nanoseconds width. When the detector is irradiated with a bunch of ions the output signal can be recorded with a (triggered) high-frequency digitizer. If the temporal dispersion of the ion bunch is larger than the standard one-particle signal width the output signal will have a pulse shape function of the distribution of the ion bunch in time. This temporal dispersion can be obtained with time-of-flight techniques. In this way it will be possible to obtain an estimate of the velocity distribution of the ions inside the bunch from the de-convolution of the digitally recorded pulse shape. The energy distribution of the ions can be thus obtained. This kind of detector is appropriate for the construction of medium granularity arrays with small

individual elements, and can provide also information about the angular distribution of the ions. The saturation effects, which might appear when the scintillator is irradiated with high dose, must be taken into account when the detector is designed. Moreover, special geometries with light guides should be investigated in order to prevent the accelerated electrons travelling faster than the ion beam to enter directly in the phototube.

Dispersion magnetic spectrometers with large momentum acceptance and relatively small coverage of the solid angle might become a powerful tool to investigate the energy, charge-state and angular distributions of the ions. The magnetic spectrometer design can be similar to that of existing large-acceptance heavy-ion spectrometers like VAMOS or PRISMA: one quadrupole element to enhance collection followed by a large magnetic dipole for dispersion and a large (1 m) focal plane detection area. The particular conditions for the laser-accelerated ions prevent the use of any start detectors and ion-by-ion counting, thus a small entrance opening of the spectrometer is required and the "start" signal for the time-of-flight must be given by the laser pulse. In the focal plane special detectors should be designed, since more than one ion per pulse will be detected. Digital recording of a scintillation image might be a possibility, with the limitation that the time-of-flight information will be lost. A more suitable solution, which needs technical developments, is based on fast scintillators and de-convolution of digital signals idea described above. A high granularity focal-plane array of fast scintillators can be constructed at reasonable price. With this focal plane detector the "stop" signal for the time-of-flight can be obtained with good resolution, therefore the velocity distribution of the ions will be measured with higher precision. In order to simplify the image obtained in the focal plane, devices like the Thomson spectrometer or a Wien velocity filter might be used.

Spectroscopy of accelerated electrons

Similar with protons and heavier ions, the parameters that must be measured for accelerated electrons are energy and angular distributions as well as the beam intensity. However, not having to deal with charge-state distribution simplifies the design of electron spectrometers, and the small mass respect to protons allows more compact solutions. Although the techniques used for detection of laser-accelerated electrons are relatively well established, further developments might significantly improve them as well.

Characteristic X-ray tracers, based on the observation of K α lines (typically of Cu) focused in crystals are a powerful tool to measure the angular distribution of electrons with high resolution [5]. This method is however limited, and cannot provide the energy distribution for the electron beam.

Thomson spectrometers can be used for electrons as well, with the advantages and disadvantages mentioned in the previous section. With these devices one can obtain the energy distribution with moderate resolution and also the beam intensity.

Scintillation foils with triggered CCD camera might be used to detect the angular distribution. As for the X-ray tracers, the information obtained about energy distribution is rather limited. Magnetic spectrometers based on dispersion are very efficient for measuring the energy distribution of the electrons with high resolution. Typically, in the focal plane are placed track detectors or a phosphor screen imaged on a CCD camera. A possible use of fast scintillators in the focal plane would give also the time-of-flight of the electrons and might further improve the quality of energy measurements.

References

- [1] S.C. Wilks et al., *Phys. Plasmas* **8**, 542 (2001).
- [2] A. Henig et al., *Phys. Rev. Lett.* **103**, 245009, (2009).
- [3] H. Schwoerer et al., *Nature* **439**, 445 (2006).
- [4] J.S. Green et al., *CFL Ann. Rep. 2008/2009*, p. 311.
- [5] B. Ramakrishna et al., *CLF Ann. Rep. 2008/2009*, p. 34.

5 APOLLON Laser + γ/e^- Beam

5.1 Pair Creation from the Vacuum

In this field several theoretical groups discuss the exciting catalytic pair decay of the vacuum in a laser focus and a beam of high energy γ quanta. The tremendous increase in catalytic pair creation by about 35 orders of magnitude when going from 10 MeV to 100 MeV γ quanta shows that we should produce a γ beam up to 100 MeV by using surface harmonic for the linear Compton backscattering. The 10. harmonic compared to the first harmonic has a $\approx 10^3$ times reduced yield, but is overwhelmed by the factor of $\approx 10^{35}$ for pair production. Thus high flux, very high energy γ with small emittance have to be optimized. For ERL's besides the high brilliance and high flux option also an ultrafast fs option exists, which should be used here to match the pulse structure of the APOLLON laser. Thus the smaller single shot laser for the γ ray generation first produces high harmonics, which then are Doppler boosted in energy via the relativistic electron bunch. Apparently for the very high energy γ -quanta ≈ 100 MeV one quantum produces many e^+e^- pairs in the APOLLON laser focus and we can study this production in detail as a function of the energy of the γ quanta and the intensity in the laser focus and will not have counting rate problems. Even measurements at 10^{23} W/cm² become possible.

Once such an electron-positron pair is produced, it may be possible that these electrons and positrons get accelerated in the laser focus that much, that cascades of pairs develop, which drastically change the signal for detection of pair creation by cascading. If on the other hand a single electron can induce such cascades of pairs, one has to be more concerned about background reactions e.g. from imperfect vacuum conditions, and optimizing the vacuum in the laser focus will become a serious experimental issue. Thus finally it may even be advantageous to perform catalytic pair creation under conditions, where a single slow electron cannot induce these cascades of pairs – the sparking of the vacuum – to suppress contributions from insufficient vacuum conditions. While A.R. Bell and J.G. Kirk [15] predict cascades of pairs already for 10^{24} W/cm², Ruhl et al. in dedicated numerical simulations expect this only for higher intensities. It may be a large advantage if the focused laser or the high energy γ beam do not produce cascades of positron electron pairs from a single slow electron or positrons but the pair creation only shows up in their joint action.

5.1.1 Catalysis of Schwinger Pair Production. (Gies)

R. Schützhold¹, H. Gies², G. Paulus², D. Habs³, M. Gross³ and P.G. Thirolf³

¹ *University Duisburg-Essen,, Duisburg (Germany),*

² *Friedrich Schiller Universität, Jena (Germany),*

³ *Ludwig Maximilians University, Munich (Germany)*

Future high-power lasers will provide electromagnetic fields of unprecedented intensity, allowing for a new experimental window into the largely unexplored domain of nonperturbative quantum electrodynamics (QED). This has implications not just for QED, but also for fundamental issues in quantum field theory, as well as nuclear, atomic, plasma, gravitational and astro-physics. Whereas there are impressive confirmations of the precision of perturbative QED, we know very little about the nonperturbative regime of QED, arising in ultra-strong external fields.

The long-standing spectacular prediction of spontaneous decay of the vacuum in terms of Schwinger pair production, i.e., production of electron-positron pairs, in strong electric fields exists already since the early days of quantum field theory [1, 2, 3]. Based on constant-field calculations, this break-down of the vacuum is expected to occur near a critical field strength $E \sim E_{cr} = m^2 c^3 / (e \hbar) \simeq 1.3 \times 10^{16} \text{V/cm}$, which is still orders of magnitude beyond upcoming future laser capacities.

Recent new theoretical ideas suggest that lasers such as those planned for ELI may be able to reach this elusive and exponentially suppressed nonperturbative regime. The Schwinger mechanism can be *dynamically assisted* [8] by superimposing a strong electric field with a weak but rapidly varying field. Thereby, it is possible to enhance significantly the pair creation rate, as the effective spectral gap between the electron states and the Dirac sea, i.e., the relativistic tunneling barrier, is decreased. A realistic experimental scenario is given by a new catalysis mechanism for Schwinger pair production [9], where a strongly focused optical laser pulse in a purely electric standing wave mode is superimposed by a plane-wave γ -ray probe beam. This superposition leads to a dramatic enhancement of the expected yield of e^+e^- pairs, and brings the vacuum pair production effect significantly closer to the observable regime.

Figure 1 shows the number of pairs produced by an incident high-energy photon, traversing a strong electric field of 1μ length, as a function of incoming photon frequency ω during one day of operation. The strong field is assumed to be produced in a standing-wave mode of a focussed laser beam at an intensity of $I = 10^{24} \text{W/cm}^2$. The two curves correspond to two sets of parameters: 10^{13} high-energy photons per pulse with 1 shot per minute repetition rate (blue curve), and 10^{15} high-energy photons per pulse with 100 kHz repetition rate (purple curve). We observe that the threshold of 1 pair per day is crossed right near $\omega \simeq 10 \dots 20 \text{MeV}$. Beyond this threshold, i.e. for higher photon frequency or higher field strength, pair production increases exponentially as is characteristic for a nonperturbative phenomenon.

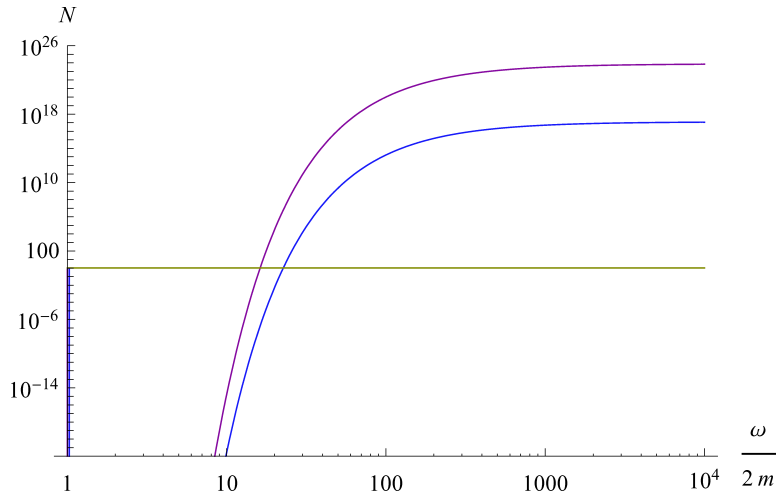


Figure 1: Number of pairs produced by an incident high-energy photon of frequency ω , traversing a strong electric field of 1μ length, during one day of operation. The strong field corresponds to a laser intensity of $I = 10^{24} \text{W/cm}^2$. Parameter sets: 10^{13} high-energy photons per pulse with 1 shot per minute repetition rate (blue curve), and 10^{15} high-energy photons per pulse with 100 kHz repetition rate (purple curve).

This prediction has been confirmed with very different theoretical methods [10, 7, 7], pointing towards a close conceptual connection between Schwinger pair production, Hawking radiation of black holes and the decay of metastable strings. Alternative scenarios involving various laser components colliding with a relativistic nucleus have also been developed [9]. Further suggestions in the literature even point to the possibility that the number of produced pairs might be enhanced by an avalanche process in a strong laser field above $I = 10^{24} \text{W/cm}^2$ [15]. The proposal of a catalyzed Schwinger mechanism on the one hand introduces a strong amplification mechanism for pair production by a tunnel barrier suppression, but on the other hand fully preserves the nonperturbative character of the Schwinger mechanism. Its experimental discovery has the potential to open up an entirely new domain in the parameter space of quantum field theories, with the prospect of further fundamental discoveries as well as practical applications.

The index of refraction of the vacuum in high fields consists of an imaginary absorptive part describing the e^+e^- production and a dispersive part. For the dispersive part the birefringence of the vacuum has been discussed, when a linearly polarized probe beam traverses the focus of a very high power laser. The simple formulas for the small turning of the polarisation vector of Ref. [11] only is true when the $\omega_p \ll m_e$, however it is clear that MeV γ rays with energies in the range of more than twice the electron rest mass are much more adequate to probe specific problems close to real e^+e^- pair creation. There a more complex dependence with anomalous dispersion are expected. Also the assisted pair creation with a high power laser and an intense γ leads to a strong reduction of the threshold from the Sauter limit of 10^{29}W/cm^2 [14]. Compared to the estimated effect, where γ intensities of 10^8ph/s were assumed, the new γ -beam facility allows for much larger intensities and it appears possible to see some positrons per day in combination with the APOLLON laser.

The requirements on the incoherent γ beam in these two experiments are different, but also indicate the requirements for other experiments which intend to use the very high fields in the focus of APOLLON. For an optimized positron production we just require the most intense γ beam and do not critically care about the energy spread. We have to reflect a part of an APOLLON laser from the intense electron bunch. However, we have to realize an excellent timing between APOLLON and the electron accelerator (50 fs) and have to go for very short pulses (50 fs). Perhaps we could even produce a converging e-bunch in a way that the γ beam is focused into the focus of APOLLON. In the second study of the quantum vacuum we want to measure the birefringence of the vacuum by the small turn of the linear polarisation of the γ beam, which we can measure very sensitively using NRF. Thus here we need a γ beam with a rather good energy resolution and we have to observe the modification of the pronounced minimum in the angular distribution of the $0^+ \rightarrow 1^- \rightarrow 0^+$ cascade.

References

- [1] F. Sauter, “Über das Verhalten eines Elektrons im homogenen elektrischen Feld nach der relativistischen Theorie Diracs,” *Z. Phys.* **69**, 742 (1931).
- [2] W. Heisenberg and H. Euler, “Consequences of Dirac’s Theory of Positrons”, *Z. Phys.* **98**, 714 (1936); English translation at arXiv:physics/0605038.
- [3] J. Schwinger, “On gauge invariance and vacuum polarization”, *Phys. Rev.* **82** (1951) 664.

- [4] R. Schützhold, H. Gies and G. Dunne, Phys. Rev. Lett. **101**, 130404 (2008) [arXiv:0807.0754 [hep-th]].
- [5] G. V. Dunne, H. Gies and R. Schützhold, Phys. Rev. D **80**, 111301 (2009) [arXiv:0908.0948 [hep-ph]].
- [6] A. Monin and M. B. Voloshin, Phys. Rev. D **81**, 025001 (2010) [arXiv:0910.4762 [hep-th]].
- [7] A. Monin and M. B. Voloshin, arXiv:1001.3354 [hep-th].
- [8] V. N. Baier and V. M. Katkov, arXiv:0912.5250 [hep-ph].
- [9] A. Di Piazza, E. Lotstedt, A. I. Milstein and C. H. Keitel, Phys. Rev. Lett. **103**, 170403 (2009) [arXiv:0906.0726 [hep-ph]].
- [10] A. R. Bell and J. G. Kirk, Phys. Rev. Lett. **101**, 200403 (2008); J. G. Kirk, A. R. Bell and I. Arka, arXiv:0905.0987 [hep-ph].
- [11] T. Heinzl et al., Opt. Comm. **267**, 318 (2006).
- [12] W. Tsai and T. Erber, Phys. Rev. **D 12** , 1132 (1975).
- [13] W. Tsai and T. Erber, Phys. Rev. **D 10**, 492 (1974).
- [14] R. Schützhold, H. Gies and G. Dunne, Phys. Rev. Lett. **101**,130404 (2008)
- [15] G.V. Dunne, H. Gies and R. Schützhold, Phys. Rev **D 80**, 111301(R) (2009).

5.1.2 Pair Production (Heinzl)

C. Harvey¹, A. Ilderton¹ and T. Heinzl¹

¹ *University of Plymouth, Plymouth, PL4 8AA (UK)*

The vacuum becomes unstable against pair production in the presence of a homogeneous electric field, exceeding Sauter's critical value $E_S = m^2/e \simeq 1.3 \times 10^{18}$ V/m [3]. In a field of this magnitude the energy acquired by an electron traversing a Compton wavelength equals its rest mass, hence $\epsilon = eE/m^2 = 1$ (in a given frame). Schwinger was the first to calculate the pair creation rate $W_{e^+e^-}$ by evaluating the imaginary part on the left-hand side of Fig. 2 resulting in his famous exponential suppression factor, $W_{e^+e^-} \sim e^{-\pi/\epsilon}$ [4]. He also pointed out that a

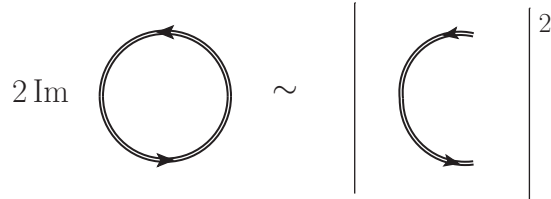


Figure 2: Total probability for vacuum pair production.

Lorentz and gauge invariant analysis should not be based on electric and magnetic field strengths (\vec{E} and \vec{B} , respectively) but rather on the invariant field strength bilinears,

$$\mathcal{S} \equiv -\frac{1}{4}F_{\mu\nu}F^{\mu\nu}, \quad \mathcal{P} \equiv -\frac{1}{4}F_{\mu\nu}\tilde{F}^{\mu\nu}, \quad (7)$$

where $\tilde{F}^{\mu\nu}$ is the dual field strength. From $\mathcal{S} = (E^2 - B^2)/2$ and $\mathcal{P} = \vec{E} \cdot \vec{B}$ it is clear that the purely electric case corresponds to $\mathcal{P} = 0$, $\mathcal{S} > 0$.

A purely magnetic field ($\mathcal{P} = 0$, $\mathcal{S} < 0$), on the other hand, cannot produce pairs from the vacuum as it does not transfer energy to charged particles, real or virtual. As a result, the vacuum bubble of Fig. 2 is always real in this case. One thus needs external (probe) photons which can convert their energy, ω' , into pairs (see [5] for an early review). The basic diagram is then a vacuum polarisation loop as shown in Fig. 3. The loop diagram on the left-hand

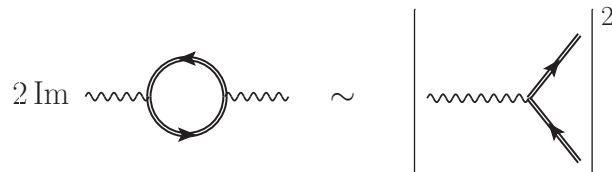


Figure 3: Total probability for photon induced pair production.

side represents the polarization tensor $\Pi^{\mu\nu}$ and was first calculated long ago by Toll [1]. As already stated there, pair creation by magnetic photon conversion is a threshold process which requires a probe photon energy ω' such that $\nu' = \omega'/m > 2$. Only above this threshold does $\Pi^{\mu\nu}$ develop an imaginary part which defines a photon absorption coefficient. In addition, this

coefficient displays a saw-tooth pattern when ν' is in resonance with the Landau levels. This has recently been reanalyzed in more depth in [6]. Replacing the constant magnetic by a constant electric field yields a nonvanishing answer as well, however, without a resonance structure (but possibly harmonic peaks), so the pair rate is a smooth function of energy. Still, the situation is intricate and depends sensitively on the relative size of ν' and ϵ_0 compared to each other and to unity. Baier and Katkov have very recently given a comprehensive overview for pair creation in a constant electric field [7]. Generically, one finds that there is no threshold behaviour in this case but rather exponential suppression. For the parameter ranges of interest here the relevant result of [7] is

$$W_{e^+e^-} \sim e^{-[\pi(1+\nu'^2/4)-2\nu']/\epsilon}, \quad \epsilon \ll \nu' \ll \epsilon^{-1/3}. \quad (8)$$

This yields the Schwinger exponent when $\nu' \rightarrow 0$ and recovers the findings of [8, 9, 10] when $\nu' = O(1)$. Note that the external photon *reduces* the exponential suppression.

In a laser beam one obviously has both electric and magnetic fields, \vec{E} and \vec{B} . Adopting a plane wave model (or its long wavelength limit, crossed fields) \vec{E} and \vec{B} are orthogonal and of equal magnitude ($\mathcal{S} = \mathcal{P} = 0$). The parameter ϵ is then defined in terms of the r.m.s. field in the lab system. Again, the constant (i.e., crossed) field case has been studied by Toll [1]. He realized that the imaginary part of $\Pi^{\mu\nu}$ in this case only depends on the product $\epsilon\nu'$ and that there is exponential suppression of the pair creation rate, $W_{e^+e^-} \sim \exp(-4/3\epsilon\nu')$ for $\epsilon\nu' \ll 1$. Note that this behaviour is nonperturbative in $\epsilon\nu'$, cf. the discussion in [2]. Vacuum pair creation in a plane wave is impossible as, in a sense, the magnetic field cancels the “pair creativity” of the electric field. In a standing wave of counter-propagating laser beams for which $\mathcal{S} > 0$ (i.e., E dominates over B) the presence of the magnetic field still reduces pair creation by approximately an order of magnitude [11].

The above considerations clearly show that pair creation in external fields depends sensitively on the details of these ambient fields. ELI is in the unique position to study most of the possible configurations, namely (i) null-fields ($\mathcal{S} \simeq 0 \simeq \mathcal{P}$), (ii) the electric case ($\mathcal{S} > 0$) and (iii) the magnetic case ($\mathcal{S} < 0$). The electric case should yield the largest pair creation rates, both for vacuum and stimulated or assisted scenarios. (Note that the vacuum contribution will always be present in the total rate.) In addition, one may enhance pair creation signals by having the laser propagate in an under-dense plasma [15, 16] or by using a multiple beam configuration [14]. In both cases, the intensity threshold may come down to about $I_{24} = 10^{24}$ W/cm².

References

- [1] J. Toll, (1952), PhD thesis, Princeton, 1952.
- [2] T. Heinzl and O. Schröder, J. Phys. **A39**, 11623 (2006), hep-th/0605130.
- [3] F. Sauter, Z. Phys. **69**, 742 (1931).
- [4] J. S. Schwinger, Phys. Rev. **82**, 664 (1951).
- [5] T. Erber, Rev. Mod. Phys. **38**, 626 (1966).
- [6] V. N. Baier and V. M. Katkov, Phys. Rev. D **75**, 073009 (2007) [arXiv:hep-ph/0701119].
- [7] V. N. Baier and V. M. Katkov, arXiv:0912.5250 [Unknown].

- [8] R. Schutzhold, H. Gies and G. Dunne, Phys. Rev. Lett. **101**, 130404 (2008) [arXiv:0807.0754 [hep-th]].
- [9] G. V. Dunne, H. Gies and R. Schützhold, Phys. Rev. D **80**, 111301 (2009) [arXiv:0908.0948 [hep-ph]].
- [10] A. Monin and M. B. Voloshin, Phys. Rev. D **81**, 025001 (2010) [arXiv:0910.4762 [Unknown]].
- [11] M. Ruf, G. R. Mocken, C. Müller, K. Z. Hatsagortsyan and C. H. Keitel, Phys. Rev. Lett. **102**, 080402 (2009) [arXiv:0810.4047 [physics.atom-ph]].
- [12] A. R. Bell and J. G. Kirk, Phys. Rev. Lett. **101**, 200403 (2008).
- [13] J. G. Kirk, A. R. Bell and I. Arka, PPCF **51**, 085008 (2009), arXiv:0905.0987 [hep-ph].
- [14] S. S. Bulanov, V. D. Mur, N. B. Narozhny, J. Nees and V. S. Popov, arXiv:1003.2623 [Unknown].

5.1.3 Self-field effects and vacuum stability in strong external fields (Ruhl)

H. Ruhl¹, N. Elkina¹ and A. Fedotov¹

¹ *Department of Physics, LMU Munich, 80333 Munich (Germany)*

Vacuum breakdown Field assisted vacuum breakdown is likely to be important at intensities envisioned at ELI. We consider a scenario where a single slow electron is initially present in a very intense electromagnetic field. In the context of those strong external fields the latter electron is capable of emitting photons at enhanced rates, which in turn seed e^+e^- -pairs. The process leads to a multiplication effect and sets in about two orders of magnitude in the external field earlier than the production of a pair from photons only.

The quantum efficiency parameter In order to observe the emission of a photon in the context of a strong electromagnetic field it is necessary to maximize the external electric field at the location of an electron or positron. Calculations done by Nikishov and Ritus identify the quantum efficiency parameter for the emission of radiation from charges

$$\chi_e = \frac{e\hbar}{m^3c^4} \sqrt{-(F^{\mu\nu}p_\nu)^2} = \frac{\gamma}{E_s} \sqrt{\left(\vec{E} + \vec{v} \times \vec{B}\right)^2 - \left(\frac{\vec{v} \cdot \vec{E}}{c}\right)^2}, \quad (9)$$

where

$$\gamma = \sqrt{1 + \frac{\vec{p}^2}{m^2c^2}}, \quad \vec{v} = \frac{c\vec{p}}{\sqrt{m^2c^2 + \vec{p}^2}}, \quad E_s = \frac{m^2c^3}{e\hbar} = 1.32 \cdot 10^{18} \frac{V}{m} \quad (10)$$

that has to be as large as possible. The parameter χ_e can be calculated for simple situations neglecting hard photon emission. If a circularly polarized standing wave is assumed to be present at the position of an electron, where $\vec{B} = 0$ holds, the equations of motion of an electron initially at rest in the field of the latter are

$$\frac{d\vec{p}}{dt} = -e\vec{E}, \quad \vec{p}(0) = 0, \quad (11)$$

where

$$\vec{E}(t) = E_0 \begin{pmatrix} \cos \omega t \\ \sin \omega t \end{pmatrix}. \quad (12)$$

The solutions for $\vec{p}(t)$ is

$$\vec{p}(t) = -\frac{e E_0}{\omega} \begin{pmatrix} \sin \omega t \\ 1 - \cos \omega t \end{pmatrix} \quad (13)$$

and for $\vec{v}(t)$

$$\vec{v}(t) = -\frac{e E_0^2}{m \omega \gamma(t)} \begin{pmatrix} \sin \omega t \\ 1 - \cos \omega t \end{pmatrix}, \quad (14)$$

where $\gamma(t)$ is

$$\gamma(t) = \sqrt{1 + 4 a^2 \sin^2 \frac{\omega t}{2}}, \quad a = \frac{e E_0}{m \omega c}. \quad (15)$$

Now $\chi_e(t)$ can be calculated to be

$$\chi_e(t) = \frac{E_0}{E_s} \sqrt{1 + 4 a^2 \sin^2 \frac{\omega t}{2} - a^2 \sin^2 \frac{\omega t}{2}} = \frac{a \hbar \omega}{m c^2} \sqrt{1 + 4 a^2 \sin^4 \frac{\omega t}{2}}, \quad (16)$$

where

$$\frac{\hbar}{m c^2} = 1.288 \cdot 10^{-21} \text{ sec}. \quad (17)$$

Figure 4 shows $\chi_e(t)$ neglecting the emission of hard photons.

Hard photon emission and pair production If hard photon emission is included $\chi_e(t)$ has to be computed numerically since the momentum of the emitting electron changes in the course of hard photon emission. We make the following assumptions

$$\vec{k} = \frac{\vec{p}}{p} \frac{\omega}{c}, \quad \vec{p}' = \frac{\vec{p}}{p} \sqrt{\left(\sqrt{m^2 c^2 + p^2} - \frac{\hbar \omega}{c}\right)^2 - m^2 c^2}, \quad p > 0, \quad \theta \approx \frac{1}{2\gamma}, \quad (18)$$

where \vec{k} is the photon wave vector, \vec{p}' is the post-emission electron vector, and θ is the angle between emitting electron and emitted photon. Figure 5 shows $\chi_e(t)$ with hard photon emission included. Due to hard photon emission the parameter $\chi_e(t)$ is essentially prevented from becoming large. The red line in the figure shows the case without photon emission. The blue lines give $\chi_e(t)$ with photon emission included. Since pairs are generated at arbitrary phase of the external field (blue lines at later times) their quantum efficiency parameters $\chi_e(t)$ can become very large (be above the red line). A similar parameter holds for the production of a e^+e^- -pair from a photon

$$\chi_\gamma = \frac{e \hbar^2}{m^3 c^4} \sqrt{-(F^{\mu\nu} k_\nu)^2} = \frac{\hbar \omega}{m c^2} \frac{1}{E_s} \sqrt{\left(\vec{E} + \frac{c \vec{k}}{k_0} \times \vec{B}\right)^2 - \left(\frac{\vec{k} \cdot \vec{E}}{k_0}\right)^2}, \quad (19)$$

where $k_0 = \omega/c$ and \vec{k} is obtained from Eqn. (18).

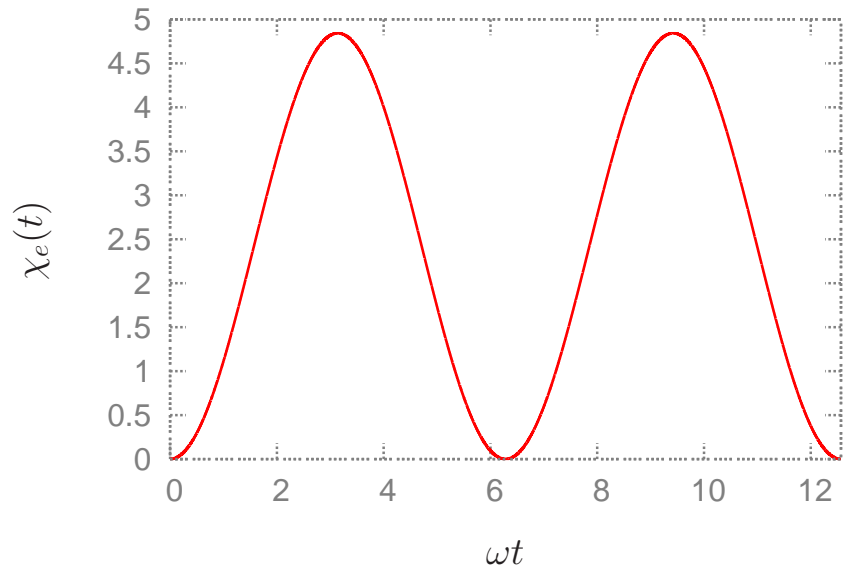


Figure 4: The parameter $\chi_e(t)$ for a circular polarized electric field at $a = 1000$ and $\omega = 1.88 \cdot 10^{15} \text{ s}^{-1}$.

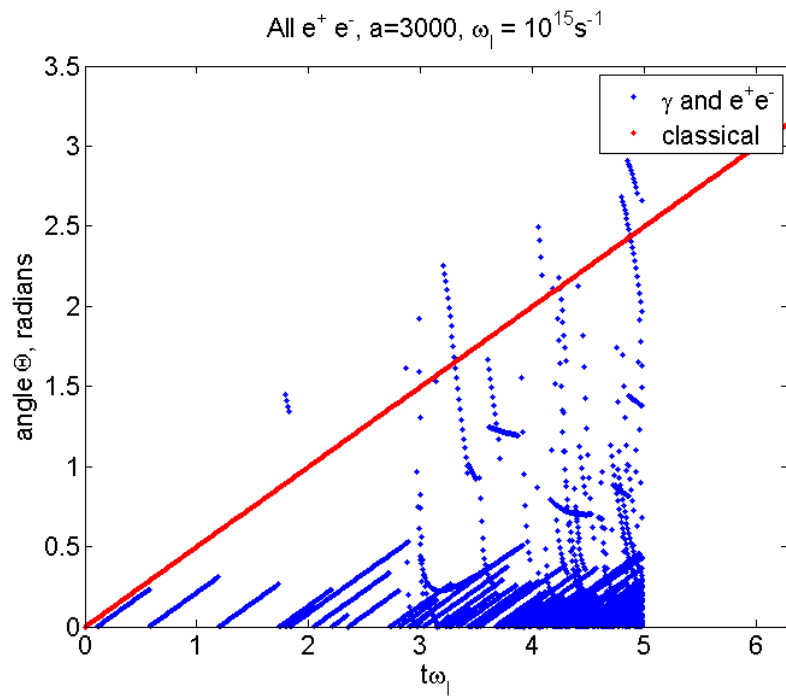
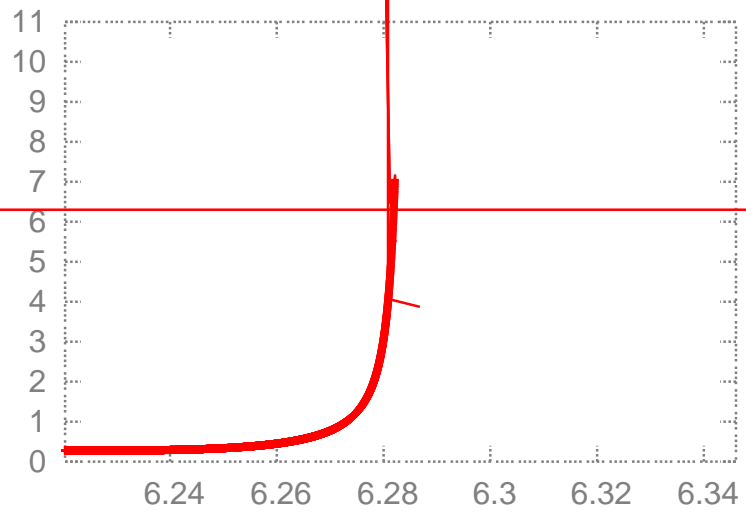


Figure 5: The parameter $\chi_e(t)$ from numerical computation including hard photon emission at $a = 3000$ and $\omega = 10^{15} \text{ s}^{-1}$.



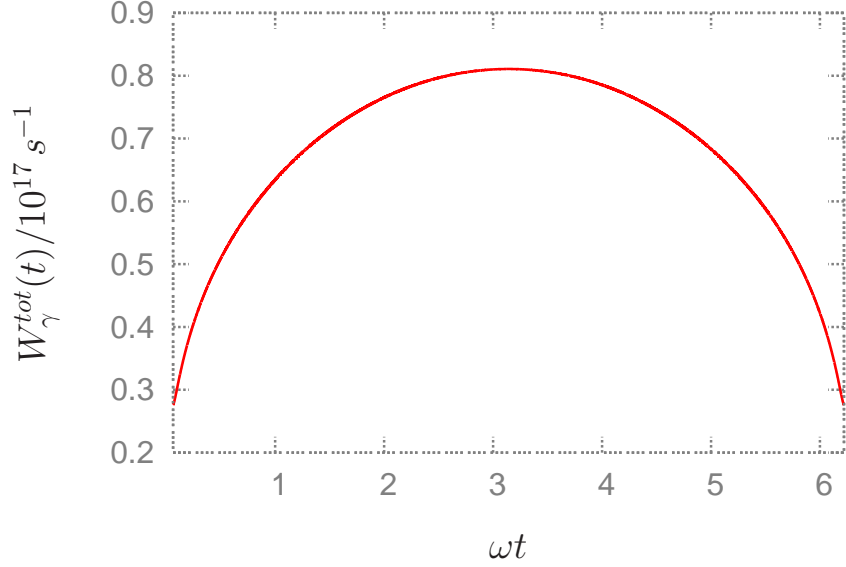


Figure 7: The total transition rate $W_\gamma^{tot}(t)$ for a circular polarized electric field at $a = 1000$ and $\omega = 1.88 \cdot 10^{15} \text{ s}^{-1}$.

time and length scales on which the electron accelerates and hence can enlarge $\chi_e(t)$. Yet other length and time scales are given by

$$l_{free} = \frac{c}{t_{free}}, \quad \int_0^{t_{free}} d\tau W_{\gamma, e^+e^-}^{tot}(\tau) \approx 1. \quad (23)$$

Those are the time and length scales between two events.

Transport equations Neglecting higher order effects as annihilation of pairs and classical radiation reaction effects the system consisting of electrons, positrons, and radiation can be described by transport equations of the following kind

$$\begin{aligned} & \left(\partial_t + \vec{v} \cdot \partial_{\vec{x}} - e \left(\vec{E} + \vec{v} \times \vec{B} \right) \cdot \partial_{\vec{p}} \right) f_{\pm}(\vec{x}, \vec{p}, t) \\ &= \int_{\omega > \omega_0} d^3k W_\gamma^{\vec{E}, \vec{B}}(\vec{k}, \vec{p} + \vec{k}) f_{\pm}(\vec{x}, \vec{p} + \vec{k}, t) - f_{\pm}(\vec{x}, \vec{p}, t) \int d^3k_{\omega > \omega_0} W_\gamma^{\vec{E}, \vec{B}}(\vec{k}, \vec{p}) \\ &+ \int_{\omega > \omega_0} d^3k W_{e^+e^-}^{\vec{E}, \vec{B}}(\vec{k}, \vec{p}) f_\gamma(\vec{x}, \vec{k}, t) \end{aligned} \quad (24)$$

$$\begin{aligned} & \left(\partial_t + \frac{\partial \omega}{\partial \vec{k}} \cdot \partial_{\vec{x}} \right) f_\gamma(\vec{x}, \vec{k}, t) \\ &= \int d^3p W_\gamma^{\vec{E}, \vec{B}}(\vec{k}, \vec{p}) [f_+(\vec{x}, \vec{p}, t) + f_-(\vec{x}, \vec{p}, t)] \\ &- f_\gamma(\vec{x}, \vec{k}, t) \int d^3p W_{e^+e^-}^{\vec{E}, \vec{B}}(\vec{k}, \vec{p}), \end{aligned} \quad (25)$$

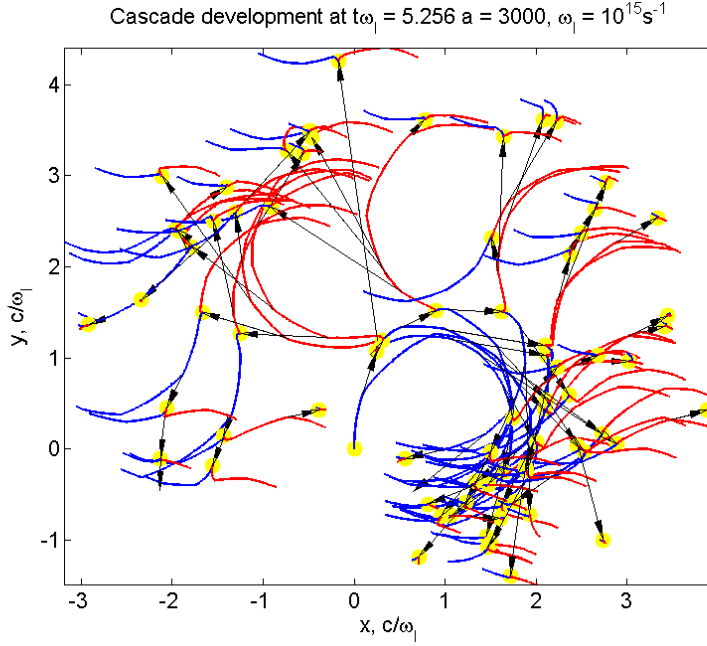


Figure 8: The $\gamma e^+ e^-$ -cascade for a circular polarized electric field at $a = 3000$ and $\omega = 10^{15} \text{ s}^{-1}$.

which for $\omega < \omega_0$ have to be coupled to Maxwell's equations with the current

$$\vec{j}(\vec{x}, t) = e \int d^3 p \vec{v} [f_+(\vec{x}, \vec{p}, t) - f_-(\vec{x}, \vec{p}, t)] . \quad (26)$$

It has to be made sure that radiation contained in \vec{E} , \vec{B} , and f_γ will not lead to double counting of radiation, hence the $\omega < \omega_0$ threshold.

Pair production Simple analytical estimates yield

μ	I	$\frac{W}{\text{cm}^2}$	N_\pm
0.1	$3 \cdot 10^{23}$		non
1.0	$3 \cdot 10^{25}$		$\approx 10^4$
2.0	$1.2 \cdot 10^{26}$		$\approx 10^{10}$

where the production rates depends on a parameter $\mu = E_0/\alpha E_s$. The simulations, however, show that pair creation is over-estimated by the analytical model but still strong. We obtain a linear growth with time for various amplitudes a . Figure 8 shows the distribution of hard photons (black arrows), electrons (red lines), and positrons (blue lines) after one full cycle of the external fields. The yellow dots indicate pair creation events. Figure 9 shows a logarithmic plot of the number of electrons and positrons as a function of time. The growth rate that can be inferred is $\Gamma \approx 10^{16} \text{ s}^{-1}$ for $a = 3000$ and $\omega = 10^{15} \text{ s}^{-1}$. In conclusion, a novel numerical code has been presented that is capable of calculating the effects of vacuum instability. Starting from a single initial electron a cascade consisting of radiation, electrons and positrons is obtained with a growth rate of about $\Gamma \approx 10^{16} \text{ s}^{-1}$ at $a = 3000$ and $\omega = 10^{15} \text{ s}^{-1}$. With growing a the laser energy distributed over electrons, positrons and hard photons shifts. At large a radiation is suppressed in favor of matter.

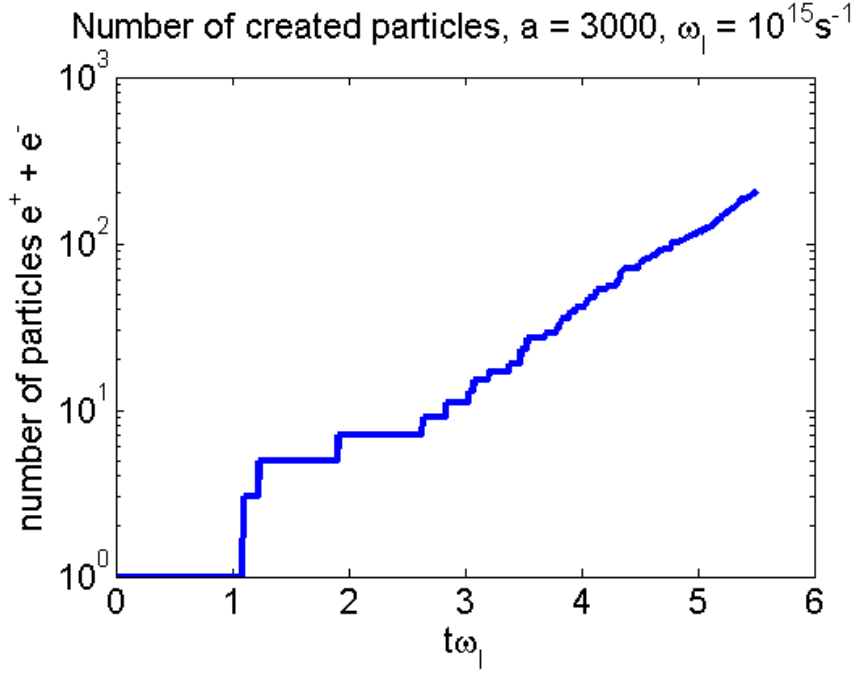


Figure 9: The total number of electrons and positrons as a function of time for a circular polarized electric field at $a = 3000$ and $\omega = 10^{15} \text{ s}^{-1}$.

5.2 The Real Part of the Index of Refraction of the Vacuum in high Fields: Vacuum Birefringence

The study of vacuum birefringence will be more difficult than the detection of the imaginary part of the vacuum refraction index with pair creation, because the signal is more difficult to detect. For catalytic pair creation we can use a broad band γ beam, for the polarisation measurement of multi MeV γ quanta we want to use NRF, which requires a very narrow band width γ beam with much smaller intensities. While the theory for the imaginary part of the refraction index has been extended to high MeV quanta and shows a very strong increase of pair production with energy (≈ 35 orders of magnitude from 10 MeV to 100 MeV) a similar extension for the real part of the refraction index is still lacking. For higher energies a transition from anomalous dispersion to normal dispersion reduced the changes in the real part of the refraction index. However, the Kramer-Kronig dispersion relation will help to predict the real part of the refraction index from the known inaginary part. Naively one expects a similar large increase for the real part of the index of refraction (causing birefringence) from the Kramer-Kronig relation in comparison to the imaginary part, but this has to we predicted carefully. Thus probably also the real part of the index of refraction of the vacuum becomes nicely measurable for multi MeV γ quanta using NRF for detection of the polarisation.

Vacuum Birefringence C. Harvey¹, A. Ilderton¹ and T. Heinzl¹
¹ *University of Plymouth, Plymouth, PL4 8AA (UK)*

In ultra-high laser fields the vacuum shows a changed index of refraction, where the imaginary part corresponds to the electron positron pair creation (discussed in the preceding proposal)

and the real part results in a birefringence for light traversing the laser focus. Both quantities are related by a Kramers-Kronig relation [1] to the same integral of the polarisation tensor. Thus again we learn something about nonperturbative QED, however the measurement of the birefringence appears more difficult and the production of positron electron pairs for the imaginary part is a very unique signature.

Instead of probing the laser beam with electrons one may alternatively use probe photons (with four-momentum k' and frequency ω'). Thus, we may trade p for k' which in particle physics jargon amounts to ‘crossing’. The nonlinear Compton process (32) then gets replaced by nonlinear Breit-Wheeler pair production, $n\gamma + \gamma' \rightarrow e^+ + e^-$, as recently reanalysed in [2]. Obviously, this introduces a new parameter which replaces ν_0 , namely

$$z_0 \equiv \frac{k \cdot k'}{m^2} = \frac{2\omega\omega'}{m^2} = 2\nu\nu', \quad (27)$$

with the second identity valid for a head on collision which will henceforth be assumed. With the probe being photons there is no rest frame so that in this section frame dependent quantities are generically evaluated in the lab frame. Physically, $z_0 = 2$ represents the (linear) pair creation threshold in units of the electron mass m while the nonlinear threshold is given by $z_0^* = (1+a_0^2)z_0$. However, even below threshold a probe photon feels the presence of the external laser field as its propagation properties change due to enhanced vacuum polarisation. The most striking consequence is a change in the ambient refractive index leading to vacuum birefringence as first discussed in Toll’s thesis [1]. The polarized vacuum acts as a medium with preferred directions dictated by the external fields which we assume to be generated by a high-power laser of frequency ω . Accordingly, there are two different refractive indices for electromagnetic probe beams of different polarization states. These are

$$n_{\pm} = 1 + \frac{\alpha\epsilon^2}{45\pi} \left\{ 11 \pm 3 + O(\epsilon^2\nu'^2) \right\} \left\{ 1 + O(\alpha\epsilon^2) \right\}, \quad (28)$$

to the lowest order in (dimensionless) laser intensity $\epsilon^2 \equiv E^2/E_S^2 = (a_0\nu)^2$ and probe frequency ν' . Note the frequency dependence in terms of the product $\epsilon\nu'$ which is essentially due to Lorentz invariance¹. Adopting an optimal value of $a_0 \simeq 5 \times 10^2$ corresponding to an intensity of 10^{24} W/cm² and an X-ray probe of $\omega' = 500$ keV, one may achieve values as high as $\epsilon \simeq 10^{-3}$ and $\nu' \simeq 10^0$.

The experimental proposal [5] is to send a linearly polarized probe beam of sufficiently large frequency ω' into a high-intensity region of extension d generated by one laser beam (or two counter-propagating laser beams) and measure the ellipticity signal, $\delta^2 \sim \nu'^2(n_+ - n_-)^2$ caused by a phase retardation of one of the polarization directions, see Fig. 10.

To the leading order in probe frequency ν' and intensity parameter a_0^2 , assuming a laser photon energy $\omega = 1$ eV, one finds a signal of size

$$\delta^2 = 1.1 \times 10^{-17} \left(\frac{d}{\mu\text{m}} a_0^2 \nu' \right)^2 \quad (29)$$

which grows quadratically with the dimensionless parameters ν' and a_0^2 as well as the spot size d (taken to be the Rayleigh length). For ELI one expects a maximal value of $\delta^2 \simeq 10^{-4}$,

¹This may be seen upon introducing the invariant $\kappa \equiv e\sqrt{(F^{\mu\nu}k'_\nu)^2}/m^3 = 2\epsilon\nu'$ which replaces ϵ_0 from (41), cf. Footnote 2.

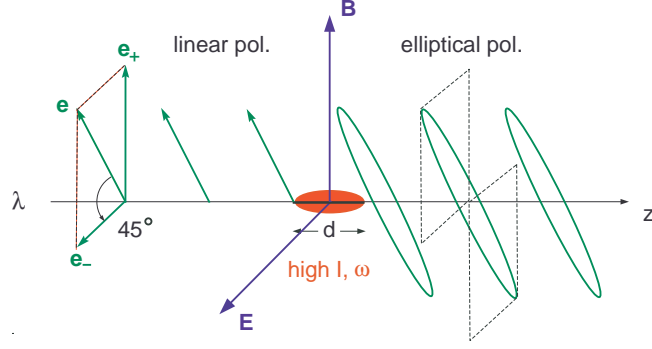


Figure 10: Schematic experimental setup to measure vacuum birefringence via an ellipticity signal.

assuming $\nu' = 10^0$, $a_0 = 5 \times 10^2$ and $d = 10 \mu\text{m}$. γ ray polarimetry via NRF should be sensitive to ellipticities of about 10^{-4} . So one indeed requires intensities in the upper range of ELI specifications (10^{24} W/cm^2). However, the situation changes if one could produce polarized photon beams of MeV energies. Then the signal should increase significantly (with an expansion in $\epsilon\nu' = O(1)$ no longer possible). In this case one becomes sensitive to the frequency dependence of the refractive indices in a regime where a Kramers-Kronig relation is expected between real and imaginary parts, the presence of the latter being tied to anomalous dispersion, $\partial n/\partial\nu' < 0$ [2]. This would be an alternative signal for vacuum pair production [?], see Fig. 11.

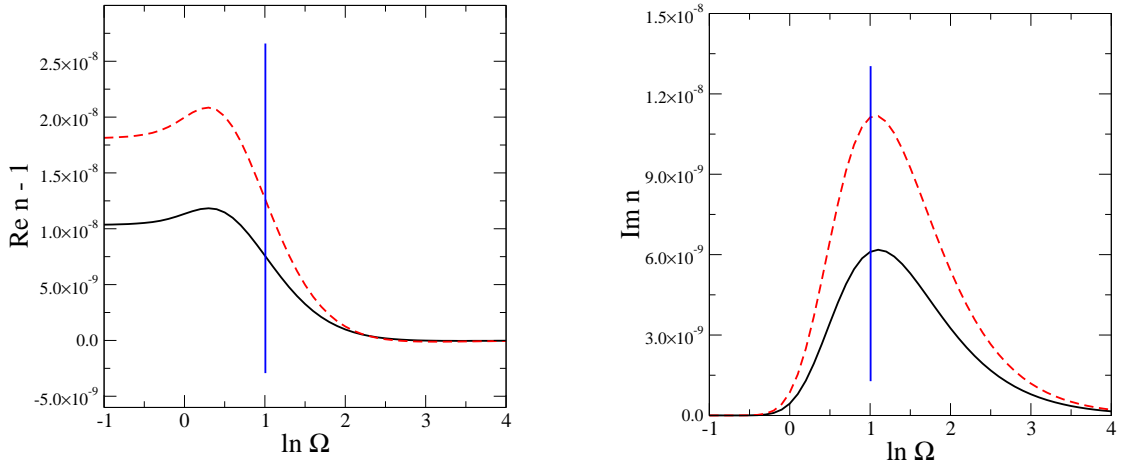


Figure 11: Real and imaginary parts of the QED refractive indices as a function of $\ln \Omega \equiv \ln \epsilon\nu'$. Dashed line: n_+ , full line: n_- , vertical line: $\ln \Omega = 1$, achieved for photons backscattered off 3 GeV electrons.

References

- [1] J.D. Jackson; *Classical Electrodynamics*, Third edit., John Wiley, chapt 7.10 (2001).

- [2] T. Heinzl, A. Ilderton and M. Marklund, arXiv:1002.4018.
- [3] J. Toll, (1952), PhD thesis, Princeton, 1952.
- [4] T. Heinzl and A. Ilderton, Opt. Commun. **282**, 1879 (2009), arXiv:0807.1841.
- [5] T. Heinzl *et al.*, Opt. Commun. **267**, 318 (2006), hep-ph/0601076.
- [6] T. Heinzl and O. Schröder, J. Phys. **A39**, 11623 (2006), hep-th/0605130.
- [7] T. Heinzl and A. Ilderton, Eur. Phys. J. D **55**, 359 (2009) [arXiv:0811.1960 [hep-ph]].

5.3 Compton Scattering and Radiation Reaction of a Single Electron at High Intensities

We want to explore the interaction of a relativistic electron with a focused laser beam for increasing focused intensities. With increasing intensity, characterized by the laser amplitude a , the Compton scattering becomes nonlinear and the dressed electron acquires an increased dressed mass $m_* = m \cdot \sqrt{1 + a^2}$, results in a decreasing energy of the back-scattered photons. At further increased intensities close to 10^{24}W/cm^2 the new radiation damping force becomes dominant, leading to a much stronger deceleration of the electron with the strong emission of high energy γ quanta. We want to compare the measurements to extensive theoretical predictions, to determine the best description of these nonlinear high field QED processes.

Compton Scattering and Radiation Damping for increasing Laser Intensities T. Heinzl¹, N.M. Naumova² D. Habs³, and P. G. Thirolf³

¹ *University of Plymouth, Plymouth PL4 8AA, (UK),*

² *Laboratoire d'Optique Appliquée, UMR 7639 ENSTA, Palaiseau (France)* ³ *Ludwig Maximilians University, Munich (Germany)*

The process in question is the collision of an electron and a high intensity laser beam, such that a photon γ' is scattered out of the beam. The relevant physical parameters are the laser frequency, ω , the electron energy measured in terms of their gamma factor, $\gamma = E_{\text{el}}/m$, and the dimensionless laser amplitude,

$$a_0 = \frac{eE}{m\omega} . \quad (30)$$

This represents the energy gain of an electron (charge $-e$, mass m) traversing a laser wavelength, $\lambda = \lambda/2\pi = 1/\omega$, in an r.m.s. field E , in units of the electron rest energy, m (employing natural units, $\hbar = 1 = c$). Thus, when a_0 is of order unity, the electron quiver motion becomes relativistic. It is useful to rewrite (30) in terms of laser intensity I and wavelength λ ,

$$a_0 = 6 \times 10^2 \sqrt{I/I_{24}} \lambda/\mu\text{m} , \quad (31)$$

where $I_{24} \equiv 10^{24} \text{W/cm}^2$ is the intensity envisioned for the Romanian ELI subproject.

Using the theory of quantum electrodynamics (QED) nonlinear Compton scattering has been analysed already in the early sixties (soon after the invention of the laser) treating the laser field as an infinite plane wave [2, 3, 4, 5]. In this case, one can utilise an exact solution of the Dirac equation going back to Volkov which provides a quantum description of the quivering electron. In QED jargon, such an electron is said to be ‘dressed’ by the background field and may be depicted as shown on the left-hand side of Fig. 12 which, when expanded in the number of laser photons involved, becomes a sum of diagrams of the type shown on the right-hand side representing the processes

$$e + n\gamma_L \rightarrow e' + \gamma' . \quad (32)$$

Here, the electron absorbs an arbitrary number n of laser photons γ_L of energy $\omega \simeq 1 \text{ eV}$ before emitting a single photon γ' of energy ω' .

Note that the tree-level diagrams involved have a classical limit which is a good description of the process when the electron mass m is the dominant energy scale [6]. This classical limit

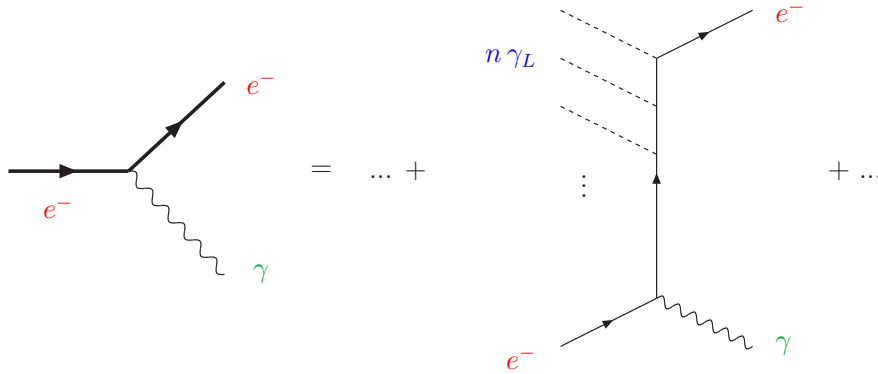


Figure 12: Feynman diagrams for nonlinear Compton scattering.

is referred to as Thomson scattering. It is valid as long as the following frame independent inequality holds,

$$\nu_0 \equiv \frac{k \cdot p}{m^2} \ll 1, \quad (33)$$

where k and p are the asymptotic four-momenta of laser photons and electrons, respectively. In the electron rest frame one has $\nu_0 = \hbar\omega_0/mc^2$ (temporarily reinstating \hbar and c). In terms of lab quantities, this implies $\gamma \ll m/2\omega \simeq 10^5 \dots 10^6$, in agreement with the folklore that the Thomson scattering is the a low-energy limit. With an energy recovery linac producing electrons in the GeV range γ will be of order 10^3 so that one is starting to move away from the Thomson (towards the Compton) regime. In any case, it is important to stress that, unlike say pair creation, the processes (32) are not suppressed by any threshold effects. Thus, one can study intensity effects at arbitrarily low centre-of-mass energies both for photons and electrons. This is quite a unique feature of nonlinear Thomson/Compton scattering and singles out this process from a particle physics point of view.

In Fig. 13 we show the photon emission rates as a function of the emitted photon frequency, ω' . The central peak corresponds to the first harmonic ($n = 1$) located at scattered frequency $\omega'_1 \simeq 4\gamma^2\omega/a_0^2 \simeq 10^2$ eV. Note that this is substantially *red-shifted* from the linear Compton edge, $4\gamma^2\omega \simeq 25$ MeV. The side maxima to the right of the global maximum correspond to higher harmonics, $\omega'_n \simeq n\omega'_1$. In the lab frame, for the parameter values chosen, there is still some energy transfer from electrons to the scattered photons, hence the blue-shift $\omega \rightarrow \omega'_n > \omega$. In an astrophysical context such a process is referred to as ‘inverse Compton scattering’. This is to be contrasted with ‘normal’ Compton scattering (Compton’s original experiment) where the electrons are at rest in the lab and one observes a red-shift of the photon frequency, $\omega' < \omega$. The inverse Thomson/Compton up-shift is now being routinely used to create γ beams, for instance at Lawrence Livermore National Laboratory, where the T-Rex facility is the world’s highest peak brightness MeV γ source.

The details of nonlinear Compton scattering have recently been reviewed in [7] with an emphasis on lab frame signatures, treating the laser as an infinite plane wave. In this case the red-shift of the linear Compton edge may be understood in terms of the electron mass shift,

$$m_* = m \sqrt{1 + a_0^2}, \quad (34)$$

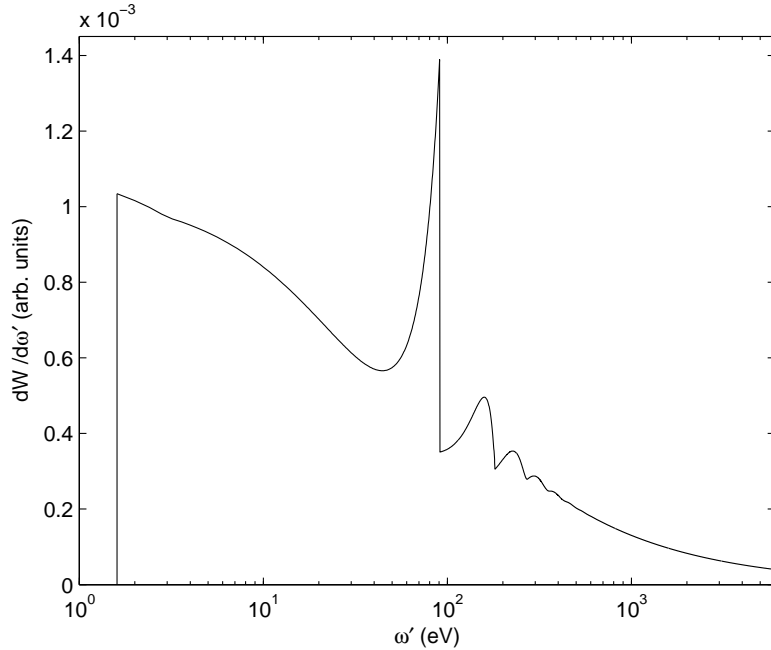


Figure 13: Nonlinear Compton spectrum for ELI parameters (intensity parameter $a_0 = 500$, laser energy $\omega = 1.5$ eV and electron energy $E_{\text{el}} = 1$ GeV).

which may be interpreted as being due to an averaging over the electron quiver motion. This adds an intensity dependent, longitudinal contribution to the electron four-momentum p resulting in the *quasi-momentum*

$$q = p + \frac{a_0^2 m^2}{2k \cdot p} k. \quad (35)$$

Using the fact the photons are massless ($k^2 = 0$), it is easy to see that $q^2 = m_*^2$. Thus, as the electron ‘gains weight’ ($m \rightarrow m_*$) it will recoil less, reducing the energy transfer to the final state photon, hence the red-shift in the maximum photon energy², see Fig. 13. The associated spectra are characterised by momentum conservation using electron *quasi-momenta*, i.e. $q + nk = q' + k'$, with the momenta in one-to-one correspondence with the particles of (32). Among other things, this conservation law determines the spectral ranges, in particular its minimum and maximum values, or ‘Compton edges’ [7].

In the lab frame there is an interesting interplay between laser intensity and electron energy. We have seen that backscattering off high-energy electrons ($\gamma \gg 1$) produces a blue-shift (‘inverse’ Compton). On the other hand, high intensity ($a_0 \gg 1$) produces a red-shift, hence works in the opposite direction. It turns out that there is exact balance in the centre-of-mass frame of the Volkov electrons and the n laser photons, that is when $4\gamma^2/a_0^2 \simeq 1$ [7]. This can obviously be achieved by fine-tuning γ and a_0 : for 1 GeV electrons the associated a_0 is about $2\gamma \simeq 4 \times 10^3$. Hence, for a_0 of this order or larger one expects an overall red-shift, $\omega' < \omega$, as the Volkov electron has become so heavy that it appears almost ‘static’ from the photons’ point of view.

²Therefore, if one is interested in a large energy up-shift, e.g. to produce γ rays, one should rather use low intensity beams ($a_0 < 1$) to scatter off from the electrons.

On the other hand, assuming the ELI value $a_0 \simeq 500$, one would just need 100 MeV electrons to test this interesting spectral regime. Fig. 14 gives an idea of how sensitively the spectra depend on the magnitude of a_0 choosing $\gamma = 100$ so that the critical $a_0 \simeq 200$.

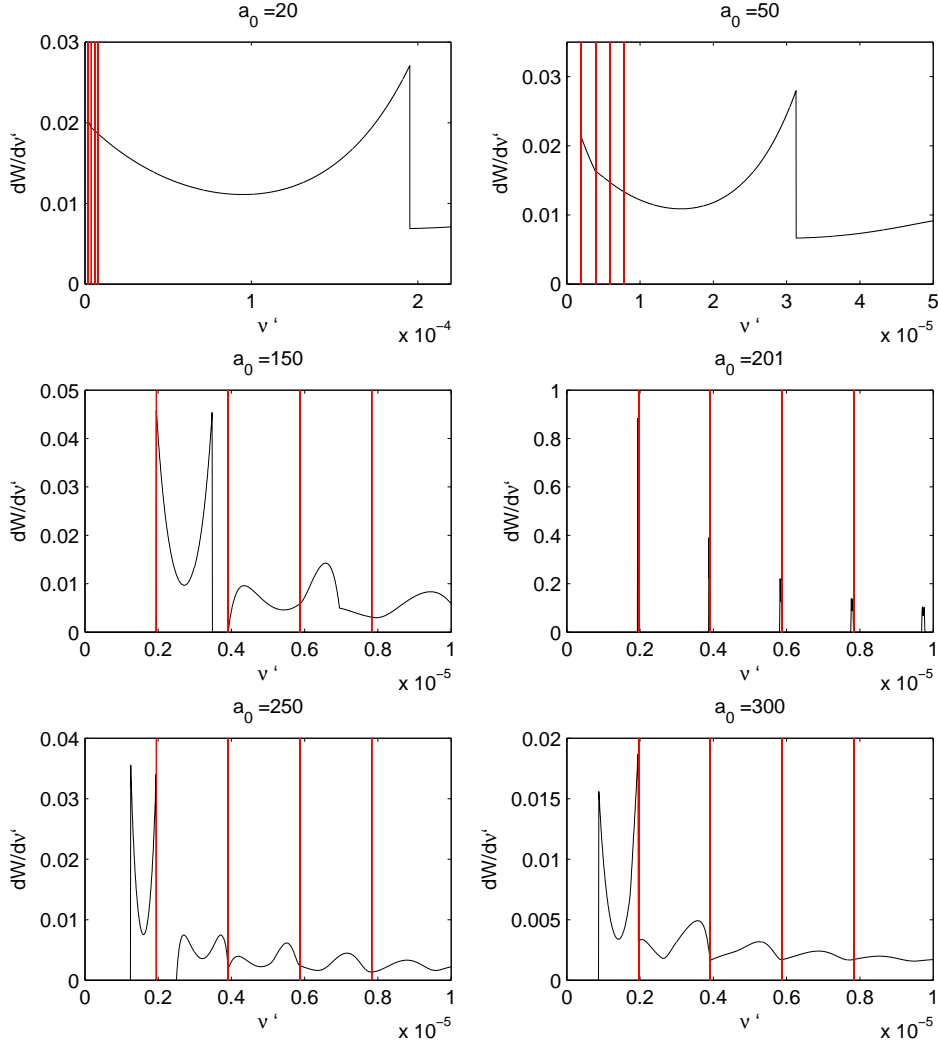


Figure 14: Photon emission spectra as a function of $\nu' = \omega'/m$ for different values of a_0 , $\gamma = 100$ and incoming frequency $\nu = \omega/m = 2 \times 10^{-6}$ assuming a head on collision of the incoming particles. The vertical (red) lines correspond to frequencies $n\nu$ [7].

As stated above, the critical value of $a_0 \simeq 2\gamma$ defines an intensity dependent centre-of-mass frame where the total momentum vanishes,

$$\vec{P} \equiv \vec{q} + n\vec{k} = \vec{p} + \left(\frac{a_0^2 m^2}{2k \cdot p} + n \right) \vec{k} = 0. \quad (36)$$

As $k \cdot p > 0$ this obviously requires that \vec{p} and \vec{k} are anti-parallel (head-on collision). Again, note the explicit dependence on the laser strength parameter a_0 .

It is important to stress that the electron mass shift, though predicted long ago [8, 5], has never been directly confirmed in an experiment as intensities have been too small until recently. Non-linear Compton scattering (32) has been observed and analysed in the SLAC E-144 experiment [9] using 47 GeV electrons from the SLAC beam and a Terawatt laser with $a_0 \simeq 0.4$. This was a high energy ($\gamma \simeq 10^5$) and low intensity ($a_0 < 1$) experiment (hence deep in the ‘inverse’ Compton regime). Photon spectra were not recorded and hence no red-shift was observed [9]. ELI should rectify this omission by recording detailed photon spectra in the complementary regime of intermediate energies and high intensities ($\gamma \simeq a_0 \simeq 10^3$), thus exploring this uncharted region of the standard model for the first time.

The considerations above are valid for an infinite plane wave. This should be a good approximation as long as the pulse duration T is large compared to the laser period, $T \gg 2\pi/\omega$. In this case the electron ‘sees’ sufficiently many cycles to be dragged along with the pulse which effectively increases its mass, $m \rightarrow m_*$. For ultra-short pulses of a few cycles this picture has to be modified [10, 6]. The spectra will then be dominated by finite size effects in both space and time. Qualitatively, the following features can be seen to arise. In an infinite plane wave, the Compton edge becomes red-shifted such that the photon emission signal above $\omega'_1 = 4\gamma^2\omega/a_0^2$ is entirely due to higher harmonics ($n > 1$) and strongly suppressed (see Fig. 13). For a short pulse, the gap between this nonlinear and the linear Compton edge ($\omega' = 4\gamma^2\omega$) gets ‘populated’ with an oscillatory signal (substructure) which, however, remains suppressed compared to the principal maximum at the nonlinear edge [6]. Thus, for large a_0 , one should not expect a substantial yield of frequency up-shifted photons.

This extreme sensitivity to beam characteristics may, nevertheless, be turned into a bonus by using nonlinear Compton/Thomson scattering as a diagnostic tool both for the electron beam [11] and the laser [6]. In particular, it has been suggested to gain information on the carrier phase of the pulse in this way [12].

As pointed out by McDonald [13] the QED (hence *quantum*) analysis of Compton scattering should contain corrections to Thomson scattering due to radiative reaction. The basic reason is energy momentum conservation which in a scattering process equates the total four-momenta of incoming and outgoing asymptotic particles. Recall that in the QED analysis with an infinite plane wave it is the *quasi*-momenta (35) that enter the conservation law. A nice interpretation of radiation reaction and its relation to QED may be given as follows [13]. One writes the force F_{RR} of radiation resistance in an ambient electric field E_0 as

$$F_{\text{RR}} = \frac{2}{3}e^2 F_L \sqrt{\nu_0^2 + \epsilon_0^2}, \quad (37)$$

where F_L is the Lorentz force, while the parameters ν_0 from (33) and $\epsilon_0 \equiv E_0/E_S$ measure photon energy and electric field strength in the electron rest frame³ assuming a head-on collision of laser and electron beam. As usual, $E_S \equiv m^2 c^3 / e \hbar = 1.3 \times 10^{18}$ V/m denotes Sauter’s critical field strength, beyond which the QED vacuum ‘breaks down’ via pair creation. We have temporarily reinstated \hbar to show that radiation resistance can be interpreted as a quantum phenomenon that ‘knows’ about radiative energy-momentum losses or gains which in the classical

³The Lorentz invariant definition of ϵ_0 , often denoted χ , is $\epsilon_0 = e\sqrt{(F^{\mu\nu}p_\nu)^2}/m^3$ where $F^{\mu\nu}$ is the laser field strength tensor.

picture correspond to (proper) time integrals of the force terms⁴. This point has recently been corroborated through a QED derivation of a modified Lorentz-Abraham-Dirac equation [14, 1] based on the original QED analysis [2].

Continuing with our analysis of (37) we note that backreaction becomes important when either ν_0 or ϵ_0 become of order unity. Let us discuss both parameters one after the other. We have already seen (in Footnote 1) that $\nu_0 \ll 1$ implies that we are in the Thomson rather than Compton regime. For ELI parameters one finds $\nu_0 = \gamma(1 + \beta)\nu \simeq 10^{-2}$ so quantum corrections associated with electron recoil should be at the percent level. On the other hand, one calculates $\epsilon_0 = \gamma(1 + \beta)E/E_S = O(1)$ upon assuming an r.m.s. lab field of magnitude $E \simeq 10^{-3}E_S$. Thus, when radiative reaction is large due to large ϵ_0 , then, in its own rest frame, the electron sees an electric field of the order of Sauter's critical field! Accordingly, with the present ELI parameter values we are right at the pair production threshold E_S or, for optimal values, even slightly above. One may thus expect to see positrons generated by the particular combination of high intensity for the laser photons and sufficiently high energy for the electrons ($\gamma \simeq a_0 \gg 1$). This may even lead to prolific pair creation via cascading processes 'maintained' by subsequent repeated laser acceleration of the produced pairs [15, 16, 17].

There is, however, a caveat here: the SLAC experiment has shown that the energy threshold for pair creation becomes intensity dependent, $s > 4m_*^2$, where s is the usual invariant defining the total energy in the centre-of-mass frame, \sqrt{s} . This increase is due to the fact that pairs with *effective* mass m_* need to be produced which, in turn, suggests that the critical field increases as well, $E_S \rightarrow E_S^* \equiv m_*^2/e$. Again, this may depend on pulse duration and possible other finite size effects which makes it all the more important to actually *probe* the details of the mass shift experimentally.

After all, it is this very mass shift which determines the size of the radiative reaction. Upon rewriting (37) as

$$F_{\text{RR}}/F_L = \frac{2}{3}e^2\nu_0\sqrt{1 + a_0^2}, \quad (38)$$

it becomes manifestly proportional to the mass scaling factor, cf. (34), and, reassuringly, yields the same numerical value as (37). We thus can conclude that it is indeed the appearance of a_0 in (38), as well as in the quasi-momenta q and q' and the associated conservation law, which signals backreaction. That's why the analysis of Thomson scattering in [18] using the purely classical language of radiation reaction is nothing but a reinterpretation of the intensity dependent centre-of-mass dynamics characterised by (36) and depicted in Fig. 14. The connection is provided by (38), the right-hand side of which is just the radiation reaction parameter R defined in [18], multiplied by a_0 .

The scattering between laser photons and relativistic electrons is governed by three dimensionless, Lorentz invariant parameters, which can be conveniently written as

$$\nu_0 = \omega_0/m = 10^{-5} E_{\text{el}}/\text{MeV}, \quad (39)$$

$$a_0 = \frac{eE_0}{\omega_0 m} = 6 \times 10^2 \sqrt{I/I_{24}} \lambda/\mu\text{m}, \quad (40)$$

⁴In principle, there may be additional contributions to what classically is radiative reaction stemming from higher-order radiative corrections (final state interactions and loop diagrams). These are obviously not included in the lowest order diagrams of Fig. 12. Not much is known about such corrections and we do not include them in this discussion.

$$\epsilon_0 = \frac{E_0}{E_S} = 6 \times 10^{-3} \sqrt{I/I_{24}} E_{el}/\text{MeV} . \quad (41)$$

The last identity, adapted from [1], is plotted in Fig. 15. The subscripts “0” refer to the electron rest frame with the lab frame electric field being given by $E = \gamma(1 - \beta)E_0$ and likewise for the laser frequency ω .

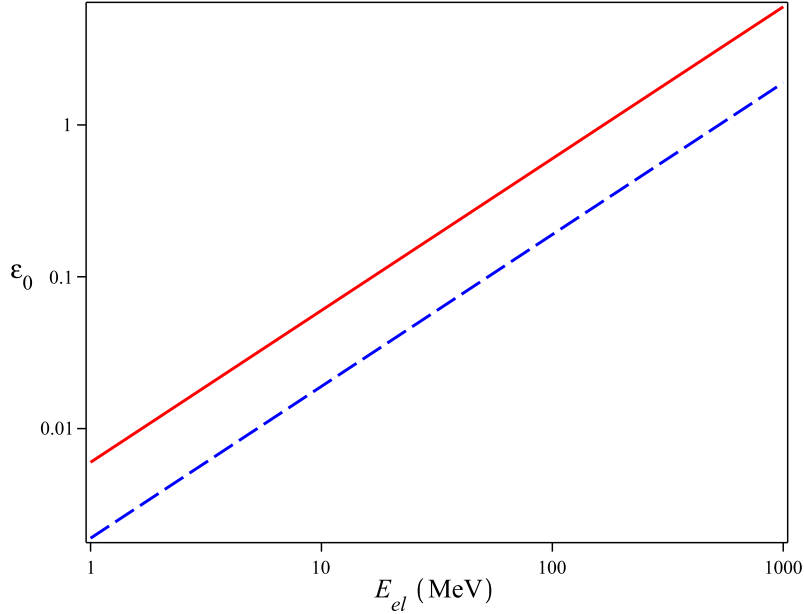


Figure 15: Dependence of the parameter ϵ_0 from (41) on the electron energy E_{el} and the intensity I of the counter-propagating laser beam. Full line: $I = I_{24} = 10^{24}$ W/cm². Dashed line: $I = 10^{23}$ W/cm².

It is important to note that the parameters (39–41) are not independent as $\epsilon_0 = a_0\nu_0$. However, all three are useful as they characterise different physics. When $\nu_0 = O(1)$ we are in the genuine quantum (Compton rather than Thomson) regime. As also stated there, $a_0 = O(1)$ implies that the electron quiver motion in the laser becomes relativistic. Finally, when $\epsilon_0 = O(1)$ the electron ‘sees’ an electric field of the order of the critical one in its rest frame which implies the onset of pair creation. The authors of [1] have fittingly dubbed the electric fields in the last two cases as “relativistically strong” and “QED strong”, respectively.

According to a recent paper by Sokolov et al., [1], for $I = 10^{24}$ W/cm² and a 1 GeV electron beam, photons of $\approx 15\%$ of electron beam energy can be generated efficiently for values of ϵ_0 in the range between 1 and 10. It means that ≈ 150 MeV photons are expected for a 1 GeV electron beam. It is necessary to note that ≈ 100 MeV electrons are easily generated during the interaction of such intense laser pulses with plasmas, what leads to the production of ≈ 15 MeV photons.

References

- [1] I.V. Sokolov, J.A. Nees, V.P. Yanovsky, N.M. Naumova, and G.A. Mourou, *Emission and its back-reaction accompanying electron motion in relativistically strong and QED-strong pulsed laser fields*, Phys. Rev. **E 81** (2010);arXiv:1003.0806v1.
- [2] A. I. Nikishov and V. I. Ritus, *Zh. Eksp. Teor. Fiz.* **46** (1963) 776–796. [Sov. Phys. JETP **19**, 529 (1964)]; A. I. Nikishov and V. I. Ritus, *Zh. Eksp. Teor. Fiz.* **46** (1964) 1768–1781. [Sov. Phys. JETP **19**, 1191 (1964)].
- [3] N. B. Narozhnyi, A. Nikishov, and V. Ritus, *Zh. Eksp. Teor. Fiz.* **47** (1964) 930. [Sov. Phys. JETP **20**, 622 (1965)];
- [4] I. I. Goldman, Phys. Lett. **8**, 103 (1964).
- [5] L. S. Brown and T. W. B. Kibble, Phys. Rev. **133**, A705 (1964).
- [6] T. Heinzl, D. Seipt and B. Kämpfer, Phys. Rev. A **81**, 022125 (2010).
- [7] C. Harvey, T. Heinzl and A. Ilderton, Phys. Rev. A **79**, 063407 (2009) [arXiv:0903.4151 [hep-ph]].
- [8] N. Sengupta, Bull. Math. Soc. (Calcutta) **44** (1952) 175–180.
- [9] C. Bamber *et al.*, Phys. Rev. D **60**, 092004 (1999).
- [10] G. Krafft, Phys. Rev. Lett. **92**, 204802 (2004).
- [11] W. Leemans *et al.*, Phys. Rev. Lett. **77**, 4182 (1996).
- [12] F. Mackenroth, A. Di Piazza and C. H. Keitel, arXiv:1001.3614 [Unknown].
- [13] K.T. McDonald, *Limits on the Applicability of Classical Electromagnetic Fields as Inferred from the Radiation Reaction*, unpublished preprint, available from <http://www.hep.princeton.edu/~mcdonald/examples/radreact.pdf>.
- [14] I.V. Sokolov *et al.*, arxiv:0910.4268 [physics.plasm-ph].
- [15] A. R. Bell and J. G. Kirk, Phys. Rev. Lett. **101**, 200403 (2008).
- [16] J. G. Kirk, A. R. Bell and I. Arka, PPCF **51**, 085008 (2009), arXiv:0905.0987 [hep-ph].
- [17] A. Fedotov, N. Narozhny and G. Mourou, Report on the ELI Grand Challenges Meeting, ed.s G. Korn and P. Antici, Paris 2009.
- [18] A. Di Piazza, K. Z. Hatsagortsyan and C. H. Keitel, Phys. Rev. Lett. **102**, 254802 (2009) [arXiv:0810.1703 DOC-TYPE = PREPRINT [Unknown]].
- [19] T. Heinzl., Journ. of Phys.: Conference Series **198** 012005 (2009).
- [20] T. Heinzl et al., arXiv:0911.1622v2[hep-ph] 14 Dec 2009

5.4 Nuclear Lifetime Measurements by Streaking Conversion Electrons with a Laser Field.

D. Habs¹, M. Gross¹ and P.G. Thirolf¹

³*Ludwig Maximilians University, Munich (Germany)*

Nuclear levels have lifetimes down to the zeptosecond range once one reaches excitation energies beyond the particle emission threshold, while nuclear levels have lifetimes longer than typically 10 fs below the particle threshold [1]. We plan to study this drastic change in lifetime and predicted changes in decay laws for the first time. We modulate the energy of emitted conversion electrons in a phase-locked laser field and carry over the technique used to measure *as* lifetimes of atomic levels [2] to nuclear systems. Only for heavier nuclei we will get sufficiently large conversion coefficients. We will follow the modulated energies of the accompanying conversion electrons of the particle decay. We induce the particle decay by the γ beam, which is locked to the APOLLON laser or the γ 's from the relativistic mirror (project 4.4). Since we do not require the maximum laser fields, we may use laser light from an earlier amplifier state, which is delivered with higher repetition rate like 10 Hz. We want to induce the particle decay with very short γ -pulses, where we hopefully reach times below 1 as for the relativistic mirror. The emitted conversion electrons have energies, where the K binding energy is subtracted from the γ beam energy (typically 6-8 MeV). They can be observed in an electron spectrometer under angles where laser accelerated electrons from the target do not contribute.

Fig. 16 shows some nuclear lifetimes as a function of the excitation energy above the ground state for E1 and M1 transitions. In comparison also typical atomic lifetimes as a function of level energy are shown. Until now only time integrated particle spectra have been measured and it was not possible to measure the particle spectra as a function of the emission time. Typical particle emission times in the range of 10^{-20} s are obtained from statistical model calculations for higher excitation energies [?]. If it were possible to follow the emission spectra as a function of time, e.g. a much better understanding of dissipation and damping processes in the energy region of overlapping resonances above ~ 15 MeV excitation energy could be obtained.

Experimental access to these ultrashort sub-attosecond lifetimes can be gained by exploiting the production technique for brilliant photon beams, where laser pulses are Compton-backscattered from a relativistic electron mirror, thus resulting in an energy boost by a factor of $4\gamma^2$, while the corresponding pulse duration is reduced by a factor $1/(4\gamma^2)$. For a single cycle pulse the energy versus time relation would be described by the uncertainty principle. This demonstrates that excitations with $g\gamma$ pulses much shorter than the expected lifetimes are possible. Though many experimental methods have been developed in different time ranges for different decay modes, transferring the well-established streaking technique of atomic physics to the regime of even shorter lifetimes in nuclear physics will enable to disentangle different channels of nuclear decay processes, where complex energy spectra could be followed as a function of time.

Properties of the decay in time of the compound nucleus Ultrashort light pulses offer the possibility to study photonuclear reactions up to 10 or 15 MeV from a different and completely new perspective. The band width $\Delta E = \hbar/\Delta t$ defined by the length (in time) Δt of the pulse may be large compared to the mean spacing d between adjacent levels of the same spin and parity. For medium-weight and heavy nuclei, d is typically 100 keV near the ground state and decreases exponentially with excitation energy, so that typically $d \sim 10eV$ at the neutron threshold, i.e. there are about 10^6 levels above the ground state. Below the neutron threshold,

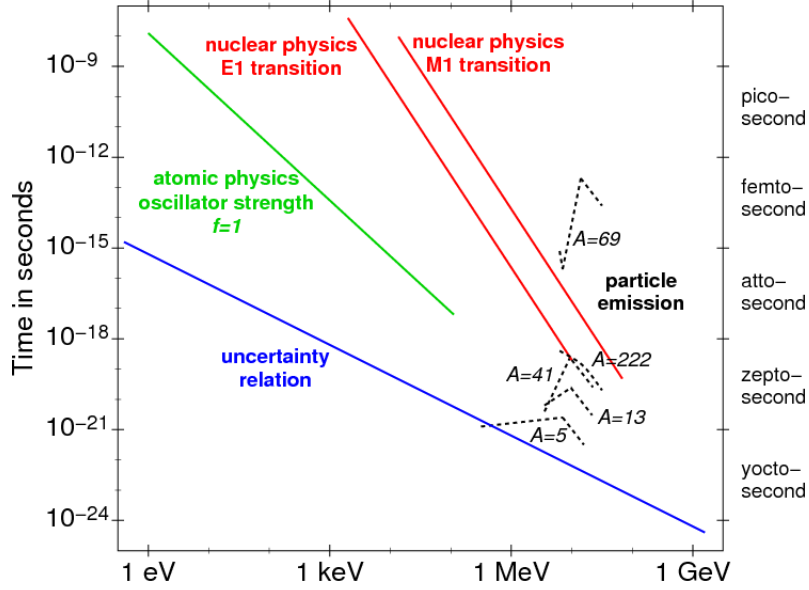


Figure 16: Correlation between nuclear lifetime and energy. The curve in green corresponds to atomic levels with oscillator strength $f=1$, the red curves represent single particle estimates for nuclear E1 and M1 γ transitions, while the blue line denotes the limit given by the uncertainty relation for a single-cycle laser pulse. The dashed black lines indicate lifetimes of nuclear levels after particle emission for different mass numbers A .

the average decay width Γ of nuclear levels is due to γ emission and has typical values of 10 meV. Right above the neutron threshold, particle decay increases Γ to typical values of about 1 eV. From here on Γ increases monotonically with excitation energy, until it reaches typical values of 50 or 100 keV (corresponding to a lifetime of 10^{-21} s) at the upper end of the energy interval here considered. Until now, photonuclear reactions were investigated with continuous beams of fairly poor energy resolution (measured in terms of the values of Γ and d discussed above) and have yielded only gross features of nuclear excitation functions, with the exception of the study of individual levels in the ground state domain. In particular spectroscopic properties of levels in the energy range between several 100 keV of excitation energy and the neutron threshold are unknown. Neutron time-of-flight spectroscopy has offered a window to study spacing distributions and other statistical properties of levels (i.e. neutron resonances) right above the neutron threshold. The outstanding feature of that gross structure is the emergence of giant resonances, especially the giant dipole resonance, that were investigated in considerable detail.

With a band width $\Delta E > d$, several or even many nuclear states will be simultaneously excited. In that case, meaningful theoretical statements can be made only if $\Delta E \gg d$ or, if $\Gamma \gg d$, for $\Delta E \gg \Gamma$. Then the decay in time of the excited nucleus is determined by the Fourier transform of the photonuclear autocorrelation function. With $S_{ab}(E)$ being the scattering amplitude leading from the incident photon channel to the final channel b , that function is defined as

$$S_{ab} = \int |g(E)|^2 S_{ab}(E + 1/2\epsilon) \cdot S_{ab}^*(E - 1/2\epsilon). \quad (42)$$

Here $|g(E)|^2$ describes the distribution in energy of the photon intensity and is centered at

energy E_0 with width ΔE . The autocorrelation function is a running average over energy of the two scattering amplitudes with arguments separated by the energy ϵ . For the energy average to be representative, we must have $\Delta E \gg d, \Gamma$. At the same time, ΔE should be small in comparison with the characteristic energy scale of gross features of photonuclear excitations. For the giant dipole resonance that is the resonance width with typical values around several MeV. The numbers given above for d and Γ then define the desirable band width for short light pulses. It is given by $\Delta E = N \max(d, \Gamma)$, where N determines the relative statistical accuracy $1/\sqrt{N}$ of the energy average. The spectroscopic data taken with neutron time-of-flight spectroscopy are consistent with a random matrix description and suggest that the compound nucleus is chaotic. It is probable that this feature prevails at lower excitation energies. The hallmark of that description is a non-exponential decay in time of the compound nucleus when few channels are open. Only for many open channels is the expected exponential decay attained (mean lifetimes are always defined in terms of the values of Γ that pertains to the energy interval of interest). Measurements on the decay in time of nuclei excited by short light pulses could confirm this theoretical expectation. In particular such data could cast light on hitherto unexplored properties of excited nuclear states below the neutron threshold.

H.A. Weidenmüller et al., [5] are studying the decay of such compound nuclear resonances within random-matrix theory [3] and find an exponential decay below the particle threshold, while they predict an exponential decay folded by a power law above the particle threshold. Weidenmüller et al. state that such measurements “comprise information on amplitude correlations in compound nucleus resonances, which cannot be obtained from other observables and that they would establish a new unambiguous test of random-matrix theory for nuclear physics”.

Streaking of electrons Experimental access to sub-attosecond nuclear lifetimes can be expected from an adaptation of the well-established streaking technique of atomic physics [5, 6] to decay processes in excited nuclei. Nuclear levels below the particle emission threshold (~ 6 -8 MeV) not only decay by γ emission but also are accompanied by prompt conversion electrons with a fraction given by the conversion coefficient. The dominant peaks in the conversion electron spectrum are the K-conversion lines. Now we excite a level of a stable nucleus with a γ beam of suitable energy. In parallel we superimpose a laser field to the nucleus with a tunable delay between the photonuclear excitation and the streaking field for the conversion electron. The energy modulation of the conversion electron should be in the range of 5 keV, requiring only moderate laser intensities of about $10^{14} W/cm^2$. With a magnetic transport and filter system ('Mini-Orange' spectrometer [7]) for conversion electrons we can choose the transmission curve to select a narrow range of the conversion electron spectrum with high efficiency, while fully suppressing all electrons being directly accelerated from atomic shells. By varying the delay of the streaking field, lifetimes in the range of 1-100 fs can be measured. For the release of the conversion electrons we need γ beams of 10 keV - 5 MeV. Metallized tapes with stable target nuclei would be ideal targets. The measurements would allow to determine the spins and parities of the excited levels. From the transition matrix elements many properties of their wave functions could be deduced.

References

- [1] D. Habs et al., Eur. Phys. J. **D 55**, 279 (2009).

- [2] E. Goulielmakis et al., *Science* **317**, 769 (2007).
- [3] H.A. Weidenmüller and R. Dietz; *Photonuclear Reactions induced by Intense Short Laser Pulses*, to be published (2010).
- [4] H.A. Weidenmüller and G.E. Mitchell, *Rev. Mod. Phys.* **81**, 539 (2009).
- [5] J. Itatani et al., *Phys. Rev. Lett.* **88** (2002) 173903.
- [6] R. Kienberger et al., *Nature* **427** (2004) 817.
- [7] J. v. Klinken and K. Wisshak, *Nucl. Instr. Meth.* **98** (1972) 1.

6 Stand-alone γ/e^- Facility for Nuclear Spectroscopy

6.1 Measuring Narrow Doorway States, embedded in Regions of High Level Density in the First Nuclear Minimum, which are identified by specific (γ, f) , (γ, α) , (γ, p) , (γ, n) Reactions and allow to map out the Nuclear Potential Landscape

D. Habs¹, M. Gross¹ and P.G. Thirolf¹

¹ *Ludwig Maximilians University, Munich (Germany),*

We want to make use of the unique high resolution of the γ beam to selectively identify doorway states with a small damping width via the (γ, x) reaction. A prototype example are states in the second or third potential minimum of actinide nuclei, which due to their tunneling through the inner barrier show a small damping width. These transmission resonances can be uniquely identified by their fission decay. Due to the high level density in the first minimum, there are always states in the first minimum which completely mix with the states in the 2. and 3. minimum and can be nicely excited via the γ beam. This concept of weakly coupled doorway states in fission can be carried over to p,n or α decays, where strongly deformed halo states again are particle unstable and we can identify them as rather sharp resonances in photonuclear reactions. We prefer to use odd target nuclei, because then we can populate several members of a rotational band with E1,M1 or E2 transitions.

The present photon energy resolution of the HI γ S facility at 6-8 MeV with 300 keV does not allow to identify these resonances, while a few keV are equivalent to the the resolution of particle-induced reactions, where we identified such resonances [1]. In this way vibrational and rotational bands in the second and third minimum can be identified [2]. From the rotational bands the moments of inertia can be determined for the states in the different minima.

We plan to employ multi-layer actinide targets, which allow to measure the fission fragment angular distributions for rather thick overall targets. From the rotational and vibrational states the potential landscape of the nuclei can be deduced. At higher excitation energies a reasonable transmission through the barrier exists and good yields can be expected. The spin and parity selectivity of the γ excitation is important. Also the damping width is an important parameter.

References

[1] P.G. Thirolf and D. Habs; Prog. in Part. and Nucl. Phys. **49**, 325 (2002).

[2] M. Hunyadi et al., Phys. Lett. **B 505** (2001) 27.

6.2 Precision Tests of Fluctuating Quantities in Nuclear Physics of Highly Excited Nuclear Levels in Comparison to Random-Matrix-Theory and Quantum Chaos

D. Habs¹, P. G. Thirolf¹, H.A. Weidenmüller², B. Dietz³ and N. Pietralla²

¹ *Ludwig Maximilians University, Munich (Germany),*

² *Max-Planck Institut für Kernphysik, Heidelberg (Germany),*

³ *Institut für Kernphysik, TU Darmstadt, Darmstadt (Germany)*

A very detailed theory of highly excited compound nuclear states has been developed over the last 70 years. It started with the compound nucleus picture of Bohr [1], where a nucleon collides with a nucleus and shares its energy with many nucleons and after many collisions the energy is concentrated again in a nucleon, which then is reemitted. This started the random-matrix theory by Wigner and Dyson [2] and finally led to the recent reviews on random matrices and chaos in nuclear physics [3, 4]. The theory represents a prototype for quantum chaos and leads to many generic predictions for fluctuating quantities, like Porter-Thomas distributions for decay widths or nearest-neighbor-spacing (NNS) level distributions of the Gaussian Orthogonal Ensemble (GOE).

Until now only smaller ensembles of quantities have been studied experimentally and seem to confirm this theory. Here we want to perform precision measurements for levels above the particle threshold with the new intense, brilliant γ facility. One example are precise measurements of the energy levels and their strength of (γ, n) resonances via a longer neutron flight path setup ($\approx 100\text{m}$). Here the high intensity of the γ beam, the very precise start signal (3 ps), the larger Breit-Wigner cross section and the good band width of the γ beam allow precision measurements with several orders of magnitude larger ensembles than obtained in earlier measurements.

Thus we can test the generic predictions and perhaps additional refinements become necessary. E.g. deviations from the GOE description are expected when the spreading time or equilibration time becomes comparable to the compound nucleus decay time [4]. At the same time many new predictions are being developed in much more detail within random-matrix theory and they can be tested in high resolution experiments in the energy or time domain.

The former studies of the double excitation of the giant dipole resonance [6, 7] can be regarded as a first prototype of new pump-probe experiments with γ beams, exploring the interference of different amplitudes of states, populated by damping into other compound states and then excited a second time. If the expected higher flux for γ beams can be realized with the relativistic mirror approach, such pump-probe experiments become possible for the given Breit-Wigner resonance cross sections and more detailed time dependent studies of developments in quantum chaos.

Also the decay of these compound nuclear states in time frequently are not simple exponentials, but show power law components [8, 5]. Here new precision measurements in the as and zs time range (see Project 5.4) will allow to test a rich new world of predictable decay patterns.

A fourth class of experiments may explore the violation of symmetries and invariances [4]. An example are parity violating amplitudes in E1/M1 mixing (see also project 6.4), where close lying parity doublets will increase these amplitudes with increasing excitation energy, because more levels of opposite parity move closer and closer together.

Thus these precision experiments will lead to a deeper understanding of higher-lying nuclear levels and quantum chaos. We will be able to predict the strong component of the many very weak, unobservable transitions of the pygmy dipole resonance more accurately via the random

matrix theory of this fluctation strength and obtain better predictions for the element production in astrophysics.

The measurement of the (γ, n) resonances also can have a large impact on the improved operation of the γ beam facility. Here we can measure the γ beam energy above ≈ 7 MeV with an accuracy of better than 10^{-7} by measuring the Time Of Flight (TOF) of the neutrons. By subtracting the large fixed neutron binding energy, by obtaining rather slow neutrons and having a very good start signal for the TOF, we get a very high resolution. The development of keV neutron TOF systems with good efficiency and resolution here are a major task. Thus we can measure the average γ energy and the width of the γ beam within $\approx 100\mu s$ without perturbing the γ facility. This signal can be used in a feedback loop to stabilize the electron beam energy very accurately in the last cavity. In several measurements one wants to perform a controlled variation of the γ beam energy, which again becomes very easy.

For an improved γ beam band width other quantities have to be adjusted: One probably has to reduce the bunch charge to 1 pC and increase the repetition rate. It should not be a problem to improve the band width of the super cavity, as we know from LIGO cavities. Thus the photons have more periods N and smaller angular divergence. It is clear that the emittance of the γ beam is a convolution of the emittance of the electron beam and the photon beam. Thus we need the best normalized emittance from the photo cathode of the electrons. One will use a larger spot size within the diffraction limit to get the best γ beam band width. Presently the high voltage ripple of the clystrons limits the achievable stability to $2 \cdot 10^{-5}$ of the cavities and this is the area where further improvements have to focus on [9].

By using different photon energies in the super cavities for γ energy stabilization and for the γ experiments in parallel the high resolution energy range can be extended significantly in γ energy.

This will open up a complete spectroscopy of 1^- and 1^+ levels up to 8 MeV excitation energy. In this way the vision in nuclear physics becomes possible, to study the transition from regular nuclear motion to chaotic motion for many nuclear species in detail. The change in nearest neighbour spacing of levels or changes in the γ strength distribution and its fluctuations can be studied with high accuracy.

References

- [1] N. Bohr, Nature **137**, 344 (1936).
- [2] C.E. Porter, *Statistical Theories of Spectra: Fluctuations*, Academic Press, New York (1965).
- [3] H.A. Weidenmüller and G.T. Mitchell, *Random matrices and chaos in nuclear Physics: Nuclear structure*, Rev. Mod. Phys. **81**, 539 (2009).
- [4] G.E. Michell, A. Richter and H.A. Weidenmüller, *Random Matrices and Chaos in Nuclear Physics: Nuclear Reactions*, arXiv:1001.2411v1[nucl-th]14 jan 2010.
- [5] H.A. Weidenmüller and B. Dietz, *Photonuclear Reactions induced by Intense Short Laser pulses*, to be published (2010).
- [6] J.Z. Gu and H.A. Weidenmüller, Nucl. Phys. **A 690**, 382 (2001).

- [7] H.A. Weidenmüller and G.T. Mitchell, *Random matrices and chaos in nuclear Physics:Nuclear structure*, Rev. Mod. Phys. **81**, 539 (2009); chapter IV.C2 .
- [8] G.E. Michell, A. Richter and H.A. Weidenmüller, *Random Matrices and Chaos in Nuclear Physics: Nuclear Reactions*, arXiv:1001.2411v1[nucl-th]14 jan 2010; Chapter V.C, *Decay in Time of the Compound Nucleus*.
- [9] M. Liepe et al., ERL-09 workshop, p. 49-52 (2009).

6.3 High Resolution Inelastic Electron Scattering (e,e')

D. Habs¹, M. Gross¹, P. G. Thirolf¹ and N. Pietralla²

¹*Ludwig Maximilians University, Munich (Germany)*, ²*Institut für Kernphysik, TU Darmstadt, Darmstadt (Germany)*

We want to use the high quality, high energy electron beam for inelastic scattering experiments. Here the transfer of larger spins compared to the γ beam is possible. An interesting case is the study of transmission resonances in the (e,e'f) reaction for ^{238}U . Here we want to determine the depth of the third minimum in ^{238}U . For ^{236}U , ^{234}U and ^{232}U we observed a third minimum with a depth comparable to the second potential minimum and theoretically a similarly deep second minimum is expected for ^{238}U [1]. Due to the lack of targets this isotope could not be studied by e.g. (d,p) reactions in the same way as the lighter uranium isotopes. Starting from the 0^+ ground state we want to identify by inelastic scattering rotational bands in the second and third minimum of ^{238}U . We aim at identifying several members of the band to determine the moment of inertia.

References

- [1] P.G. Thirolf and D. Habs; Prog. Part. Nucl. Phys. **49**, 325 (2002).

6.4 Nuclear Transitions and Parity-violating Meson-Nucleon Coupling

D. Habs¹, M. Gross¹, P. G. Thirolf¹, K. Sonnabend², N. Pietralla² and D. Savran²

¹*Ludwig Maximilians University, Munich (Germany)*, ¹*Institut für Kernphysik, TU Darmstadt, Darmstadt (Germany)*

In Ref. [1] light nuclei with known highly excited parity doublets in ¹⁴C, ¹⁴N, ¹⁵O, ¹⁶O, ¹⁸F and ²⁰Ne are investigated theoretically for the enhancement of parity mixing amplitudes of E1/M1 or E2/M2 transitions. According to first order perturbation theory calculations, the mixing is strongly enhanced, because the parity violating matrix element is divided by the small energy difference of the two levels of opposite parity. The doublet levels are at excitation energies between 5 MeV and 12 MeV and can be nicely reached with the high resolution γ beam facility, where $\Delta E_\gamma/E_\gamma \leq 10^{-3}$ is expected to be realized, but even extensions to 10^{-5} appear possible. Until now many nuclei with a possible E1/M1 mixing have been investigated like ¹⁹F (1080keV); ¹⁹F (109.9 keV); ²¹Ne (2789 keV); ¹⁷⁵Lu (396 keV); however, experimental accuracies were insufficient. With the ultra brilliant, tunable, polarized and monochromatic γ beams the effect of parity non-conservation (PNC) will be studied at higher excitation energies. For circularly polarized γ beams a forward-backward asymmetry can be used to measure mixed parity transitions, where a high sensitivity is reached by switching the sign of the circular polarisation. The experiments will allow to understand the fundamental role of the exchange processes of weakly interacting bosons in the nucleon-nucleon interaction [3, 4, 5]. Fig.17 illustrates this exchange process.

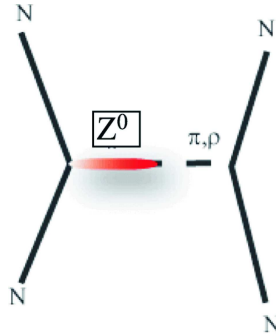


Figure 17: Parity-violating nucleon-nucleon interaction.

The results can also be compared with chiral perturbation theory, furthering the development of effective couplings between Z_0 and π , ρ and ω mesons.

²⁰Ne seems to be most interesting case with largest enhancement. The two highly excited parity doublet levels were observed in particle-induced reactions and not in a (γ, γ') reaction. Their energies are quoted in the Nuclear Data Sheets as 11262.3(19) keV for the 1^+ state and 11270(5) keV for the 1^- state. Both states are assigned to be T=1 states and thus the isospin quantum number does not prevent their mixing. Their excitation energy difference is thus $\Delta E = 7.7(5.7)$ keV. If their total widths are comparable to their energy difference, then mixing due to the effects of the maximum parity-violating weak interaction must be expected. Observation of such a mixing effect would represent a rare precision test of the weak interaction on nuclear structure. Unfortunately, the current accuracy of the energy difference is insufficient for an estimate of the

Table 3: Candidate for PNC asymmetry in light nuclei

Nucleus	Transition	E_{f1}	E_{f2}	Amplif. fac.
^{14}C	$(0^+, 1) \rightarrow (2^-, 1)$	7340 keV	7010 keV	31 ± 6
^{14}N	$(1^+, 0) \rightarrow (1^+, 0)$	6203 keV	5691 keV	7.0 ± 2.0
	$(1^+, 0) \rightarrow (0^+, 1)$	8624 keV	8776 keV	40 ± 5
	$(1^+, 0) \rightarrow (2^-, 1)$	9509 keV	9172 keV	45 ± 5
	$(1/2^-, 1/2) \rightarrow (1/2^-, 1/2)$	11025 keV	10938 keV	37 ± 7
^{15}O	$(0^+, 0) \rightarrow (2^-, 0)$	8879 keV	6917 keV	18 ± 2
^{18}F	$(1^+, 0) \rightarrow (1^-, 0 + 1)$	5605 keV	5603 keV	590 ± 110
^{20}Ne	$(0^+, 0) \rightarrow ((1^-, 0)$	11270 keV	11262 keV	670 ± 7000

amount of parity mixing. The width of the 1^- is known to be smaller than 0.3 keV. The total width of the 1^+ state is unknown. Its ground state $M1$ decay width is $\Gamma_0 = 11 \pm 2$ eV. Direct investigations in high-resolution ($\gamma\gamma'$) reactions with large-volume Germanium detectors are highly desirable.

References

- [1] A.I. Titov et al., J. Phys. G: Nucl. Part. Phys. **32**, 1097 (2006).
- [2] U.E.G. Berg et al., Phys. Rev. **C 27**, 2981 (1983).
- [3] E. Adelberger et al., Nucl. Phys. **A 396**, 221c (1983).
- [4] E. Adelberger et al., Ann. Rev. Nucl. Sci. **35**, 501 (85).
- [5] B. Desplanques., Phys. Rep. **297**, 1 (1998).
- [6] R. Hajima et al., Nucl. Instr. and Meth. **A 608**, 557 (2009).

6.5 The Pygmy Dipole Resonance (PDR) of deformed nuclei

D. Savran¹, N. Pietralla¹, K. Sonnabend¹

¹ *Institut für Kernphysik, TU Darmstadt, Darmstadt (Germany)*

Phenomena in nuclear physics which have recently attracted great interest of experimentalists as well as theoreticians are collective electric dipole modes below the Giant Dipole Resonance, frequently denoted as Pygmy Dipole Resonances (PDR) [1, 2]. Evidence for such excitation modes has been found in many stable spherical nuclei below the particle separation energies [3, 4, 5, 4, 5]. In addition above threshold energies a similar observation has been made recently in exotic nuclei with a large neutron excess [8, 9]. The experiments are accompanied by intense theoretical investigations to explain the nature of this nuclear phenomenon, see e.g. [10] and references therein. Understanding the nature of the low-lying E1 strength will, e.g., help to constrain the symmetry energy in atomic nuclei [11] and has an impact on reaction rates of astrophysical interest [12, 13] as well as on the photodisintegration of ultra-high-energy cosmic rays [14]. However, the experimental database is still scarce, especially for non-magic nuclei. Consequently the influence of deformation on the PDR strength has yet not been investigated experimentally, while recently first relativistic Random Phase Approximation (RPA) calculations of low-lying E1 strength in deformed nuclei became available [15, 16]. It is thus of mandatory importance to extend the experimental investigations towards deformed nuclei in order to provide the necessary test grounds for these modern calculations.

The method of choice for the investigation of low-lying E1 strength below the particle threshold in stable nuclei is the method of real photon scattering [17, 1]. It assures a clean excitation mechanism and allows a model independent extraction of quantum numbers such as multipolarities, absolute strengths, decay branching ratios, and parities. Up to now, nearly exclusively bremsstrahlung has been used as high energy photon source. However, the investigation of the E1 strength close to the particle thresholds in deformed nuclei has been hindered by the extremely high level densities. In addition, the determination of parities is mandatory for the clean identification of E1 strength in deformed nuclei, which is difficult to achieve with unpolarized bremsstrahlung. These drawbacks can be overcome by using Linear Compton Backscattered (LCB) photons, as has partly been shown in [18, 5]. The benefits of using a monoenergetic polarized LCB source is two-fold:

- The monoenergetic character of the beam will allow a energy dependent determination of the photon absorption cross sections even in the vicinity of very high level densities.
- The polarized character of the beam will allow for an unambiguous disentanglement of E1, M1 and E2 contributions to the photon absorption cross section.

Compared to the experiments using LCB photons performed in [18, 5], the superior properties of ELI will improve the sensitivity of the experiments by at least one order of magnitude and thus will allow the investigation of the PDR also in deformed nuclei.

References

- [1] G. A. Bartholomew, E. D. Earl, A. J. Ferguson, J. W. Knowles, M. A. Lone, *Adv. Nucl. Phys.* **7** (1973) 229.

- [2] U. Kneissl, N. Pietralla, A. Zilges, J. Phys. G **32** (2006) R217.
- [3] K. Govaert, F. Bauwens, J. Bryssinck, D. De Frenne, E. Jacobs, W. Mondelaers, L. Govor, V. Y. Ponomarev, Phys. Rev. C **57** (1998) 2229.
- [4] S. Volz, N. Tsoneva, M. Babilon, M. Elvers, J. Hasper, R.-D. Herzberg, H. Lenske, K. Lindenberg, D. Savran, A. Zilges, Nucl. Phys. **A779** (2006) 1.
- [5] R. Schwengner, G. Rusev, N. Benouaret, R. Beyer, M. Erhard, E. Grosse, A. R. Junghans, J. Klug, K. Kosev, L. Kostov, C. Nair, N. Nankov, K. D. Schilling, A. Wagner, Phys. Rev. C **76** (2007) 034321.
- [6] D. Savran, M. Fritzsche, J. Hasper, K. Lindenberg, S. Müller, V. Y. Ponomarev, K. Sonnabend, A. Zilges, Phys. Rev. Lett. **100** (2008) 232501.
- [7] A. P. Tonchev, S. L. Hammond, J. H. Kelley, E. Kwan, H. Lenske, G. Rusev, W. Tornow, N. Tsoneva, Phys. Rev. Lett. **104** (2010) 072501.
- [8] P. Adrich, A. Klimkiewicz, M. Fallot, K. Boretzky, T. Aumann, D. Cortina-Gil, U. Datta Pramanik, Th. W. Elze, H. Emling, H. Geissel, M. Hellström, K. L. Jones, J. V. Kratz, R. Kulesa, Y. Leifels, C. Nociforo, R. Palit, H. Simon, G. Surowka, K. Sümmerer, W. Walus, Phys. Rev. Lett. **95** (2005) 132501.
- [9] A. Klimkiewicz, P. Adrich, K. Boretzky, M. Fallot, T. Aumann, D. Cortina-Gil, U. D. Pramanik, T. W. Elze, H. Emling, H. Geissel, M. Hellstroem, K. L. Jones, J. V. Kratz, R. Kulesa, Y. Leifels, C. Nociforo, R. Palit, H. Simon, G. Surowka, K. Suemmerer, S. Typel, W. Walus, Nucl. Phys. **788** (2007) 145.
- [10] N. Paar, T. Niksic, D. Vretenar, P. Ring, Phys. Lett. B **606** (2005) 288.
- [11] J. Piekarewicz, Phys. Rev. C **73** (2006) 044325.
- [12] S. Goriely, Phys. Lett. B **436** (1998) 10.
- [13] S. Goriely, E. Khan, M. Samyn, Nucl. Phys. **A739** (2004) 331.
- [14] E. Khan, S. Goriely, D. Allard, E. Parizot, T. Suomijärvi, A. J. Koning, S. Hilaire, M. C. Duijvestijn, Astro. Phys. **23** (2005) 191.
- [15] D. Pena Arteaga, P. Ring, Phys. Rev. C **77** (2008) 034317.
- [16] D. Pena Arteaga, E. K. P. Ring, Phys. Rev. C **79** (2009) 034311.
- [17] U. Kneissl, H. H. Pitz, A. Zilges, Prog. Part. Nucl. Phys. **37** (1996) 349.
- [18] N. Pietralla, Z. B. V. N. Litvinenko, S. Hartman, F. F. Mikhailov, I. V. Pinayev, G. S. M. W. Ahmed, J. H. Kelley, S. O. Nelson, R. Prior, K. Sabourov, A. P. Tonchev, H. R. Weller, Phys. Rev. Lett. **88** (2001) 012502.

6.6 Fine-structure of Photo-response above the Particle Threshold

N. Pietralla¹, D. Savran¹, K. Sonnabend¹

¹ *Institut für Kernphysik, TU Darmstadt, Darmstadt (Germany)*

The excitation energy region around the particle separation threshold is of particular importance for nuclear physics. On one hand side this energy region is of interest for theoretical reasons because the coupling of bound quantum states to the continuum of unbound states requires an extended formalism, the mastering of which becomes extremely important for exotic nuclei near the drip-lines where all structures are weakly bound [1]. Examples are the famous halo-nuclei like e.g. ¹¹Li [2]. On the other hand this energy region covers the Gamow-window of thermally driven reactions of nucleons with heavy nuclei. Its understanding is a prerequisite for the modelling of nuclear reaction cascades in hot cosmic objects and thus for nucleosynthesis.

Below the threshold all excited resonances must decay by γ emission. They can be studied with the typical high energy resolution of semiconductor-detector technology (e.g., 5 keV at 8 MeV). The photo-response below the particle separation energy is currently investigated in nuclear resonance fluorescence experiments [1] at existing γ -beam facilities such as the bremsstrahlung facilities at the S-DALINAC electron accelerator in Darmstadt, Germany, [4] or at the High Intensity γ -ray Source (HI γ S) at Duke Univ., Durham, NC, U.S.A [5].

Above the threshold the particle-decay channel opens up. Either no γ rays can be observed at all or their intensity cannot be used as a measure for the total electromagnetic excitation strength to the resonance due to the unknown particle-decay branching ratio. Neutrons cannot be measured with a competitive energy resolution at acceptable solid-angle coverage.

An intense and high-energy resolving γ -ray beam from ELI-NP will open up new horizons for the investigation of the nuclear photo-response at and above the separation threshold. Alternatively to nuclear fluorescence, a photo-transmission experiment could be performed. A reduction in the photo transmission is directly proportional to the photo-excitation cross section. A measurement of the transmitted intensity is sensitive to the fine-structure in the energy window of the photon beam. A high-resolution γ -ray beam with energy width $dE/E \leq 10^{-3}$ will allow for the performance of transmission experiments with semiconductor-detector resolution even in the regime of unbound resonances. We expect a tremendous increase of insight into nuclear structure in the continuum and a deepened understanding of the structure of the nuclear Gamow-window.

References

- [1] B. Jonson, Phys. Rep. **389** (2004) 1
- [2] J. Dobaczewski, I. Hamamoto, W. Nazarewicz, J.A. Sheikh, Phys. Rev. Lett. **72** (1994) 981.
- [3] U. Kneissl, N. Pietralla, A. Zilges, J. Phys. G **32** (2006) R217.
- [4] D. Savran, M. Fritzsche, J. Hasper, K. Lindenberg, S. Müller, V. Y. Ponomarev, K. Sonnabend, A. Zilges, Phys. Rev. Lett. **100** (2008) 232501.
- [5] A. P. Tonchev, S. L. Hammond, J. H. Kelley, E. Kwan, H. Lenske, G. Rusev, W. Tornow, N. Tsoneva, Phys. Rev. Lett. **104** (2010) 072501.

6.7 Nuclear Resonance Fluorescence on Rare Isotopes and Isomers

N. Pietralla¹, D. Savran¹, K. Sonnabend¹

¹ *Institut für Kernphysik, TU Darmstadt, Darmstadt (Germany)*

Nuclear studies with the powerful experimental method of Resonance Fluorescence have been possible up to now only if sufficient amounts of (preferably isotopically enriched) target material on the order of about 1 g has been available. The production of such an amount of target material is not always possible at a reasonable cost (e.g., the worlds rarest naturally occurring isotope ¹⁸⁰Ta costs about \$ 10,000 per mg at an enrichment of 5%). The advances in γ -ray beam brilliance at ELI will increase the sensitivity of NRF experiments by the same factor and thus it offers the opportunity to perform NRF studies on small target samples whose amounts could be reduced with respect to todays NRF experiments by the same factor. This opens up an entire new area of applicability of the NRF method to materials that may be available only in quantities of a few mg.

The dipole response of the long-lived radioactive isotope ¹⁴C, the basis of radio-carbon dating method, will be accessible. These experiments will shed light on the neutron-spectroscopic factors for the *p*- and *sd*-shell orbitals in that mass region that nowadays is accessible to ab initio no-core shell models calculations.

Nuclear high-spin *K* isomers are known to be examples of highly-deformed nuclear structures. Due to their simple Nilsson-model wave function they offer a unique laboratory for the study of very deformed nuclear systems. Nuclear spectroscopy experiments with hadronic probes have previously been performed on the the long-lived *K*-isomer of ¹⁷⁸Hf. An investigation of the *E1* and *M1* response of the highly-deformed isomer using NRF on an enriched isomeric sample of a few mg will enable us to study the phenomenon of quadrupole-octupole coupling (*E1*) or the nuclear scissors mode (*M1*) at a nuclear deformation that has not been accessible for these types of investigations before.

References

- [1] U. Kneissl, N. Pietralla, A. Zilges, J. Phys. G **32** (2006) R217.

6.8 Multiple Nuclear Excitons

R. Schützhold¹, D. Habs² and P. Thirolf²

¹ *University of Duisburg-Essen, Duisburg (Germany),*

² *Ludwig Maximilians University, Munich (Germany),*

The development of the laser based on stimulated emission was a giant breakthrough in quantum optics. It enabled us to create light with unprecedented accuracy, intensity, and control – thereby facilitating many novel applications. However, so far these applications are mostly restricted to the optical regime. The free electron laser (FEL) is a very interesting approach to achieve similar goals at higher energies. However, the free electron laser (in its usual design) is not a laser in the same sense as the optical laser, because the former is not really based on stimulated emission whereas the latter is. Therefore, the free electron laser does not incorporate all the advantages known from the optical laser. Within this project, we study the possibility to build a laser based on stimulated emission working at higher (e.g., keV) energies. To this end, we intend to use nuclear excitonic states known from Mössbauer spectroscopy instead of the electronic excitations of atoms/molecules used in optical lasers. These coherent excitations [1] spread over many nuclei (Dicke states)[3] possess many advantages and are thus perfect candidates for our purpose. As a result, we expect such a "nuclear exciton laser" to be able (in principle) to outperform a conventional FEL/XFEL facility in terms of energy and momentum accuracy and possibly even intensity.

For nuclear transitions up to 100 keV the recoilless Mössbauer γ resonance absorption [5, 6] has been observed and is widely used as spectroscopic technique, where for bound nuclei the photon recoil may be taken up by the crystal without lattice excitation. A prototype nucleus is ^{57}Fe with its 14.4 keV Mössbauer M1 transition, which has a mean lifetime of 141 ns, a line width of 4.7 neV, a relative line width of $\Delta E/E = 3 \cdot 10^{-13}$ and a K-conversion coefficient $\alpha_K = 10$. At synchrotron facilities the non-resonant radiation could be suppressed sufficiently by nuclear Bragg reflection. Here the delocalized excitation of a nuclear ensemble - called nuclear exciton [9] - was studied in detail. Its delayed propagation through a crystal, showing quantum beats due to the interference of different transitions between hyperfine components was observed. This coherent γ -ray optics shows many new phenomena [14]. Although the brilliance of synchrotron γ beams much increased over the years, the chance to excite several nuclear excitons in a single bunch was negligible.

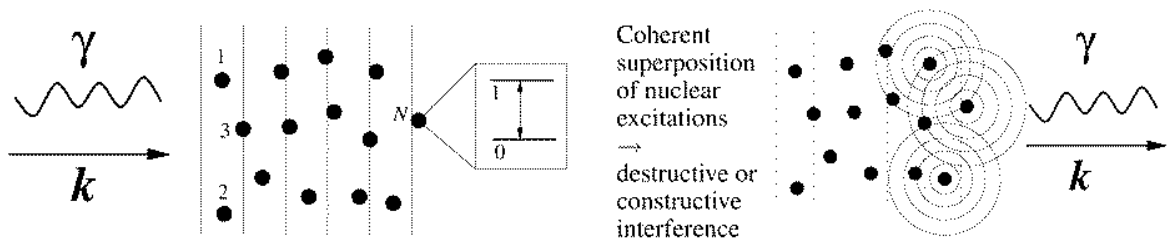


Figure 18: Excitation (left) and deexcitation (right) of a coherent nuclear ensemble, leading to directed X ray emission ('polariton laser') when the delocalized coherent nuclear ensemble is destroyed 'on demand'.

Fig. 18 schematically displays the excitation process of a nuclear polariton in an ensemble of

nuclei (left) by X ray photons with wave number k . On the right-hand side it is depicted how a coherent superposition of nuclear excitations will result in a constructive or destructive interference during the deexcitation process, leading to a directed coherent emission exclusively in forward direction if the coherent multi-exciton state is destroyed. Thus a potential application of such multi-exciton states could lead to an 'exciton laser' with coherent X ray emission 'on demand'. Studying the collective properties of these bosonic condensates opens up a new and exciting perspective of coherent nuclear physics.

For an incoherent pulse of γ 's the exciton number N_p grows linear with intensity. If one calculates within the Weisskopf-Wigner approach [7], the exciton decay rate (or γ width) increases with the number of nuclei in the wave length volume and soon exceeds the width due to conversion. Then an avalanche-like growth of the linewidth occurs and more and more photons of the much broader driving X-ray beam may join the multiple exciton condensate. Due to the required recoilless Mössbauer-like absorption we here will use rather low energy γ rays in the 100 keV range. While we get multiple excitons with the γ beam, the exciton laser should be excited with coherent γ photons from the relativistic mirror. In this scenario a quadratic growth of the exciton number could be expected for coherent pumping with X rays produced by the ELI-NP laser and a relativistic mirror.

References

- [1] D. Habs et al., Eur. Phys. J. **D 55**, 279 (2009).
- [2] G.V. Smirnov et al., *Propagation of nuclear polaritons through a two-target system: Effect of inversion targets*, Ohys. Rev. **a 71**, 023804 (2005).
- [3] R.H. Dicke; *Coherence in spontaneous radiation processes*, Phys. Rev. **93**, 99 (1954).
- [4] T. Holstein and H. Primakoff, Phys. Rev. **58**, 1098 (1940).
- [5] R.L. Mössbauer, Z. Physik **151**, 124 (1958), Naturw. **45**, 538 (1958).
- [6] R.L. Mössbauer, Z. Naturforsch. **14a**, 211 (1959).
- [7] M.O. Scully and M.S. Zubairy, *Quantum Optics*, Cambridge University Press, Cambridge, England (1997).
- [8] H.J. Lipkin; *Coherent effects in the transitions between states containing several nuclear excitons* p. 128; in "Multiple Facets of Quatization and Supersymmetry, Michael Marinov Memorial Volume; edt.: M. Olshanetsky and A. Vainstein, World Scientific (2000).
- [9] G.V. Smirnov et al., *Propagation of nuclear polaritons through a two-target system: Effect of inversion targets*, Ohys. Rev. **a 71**, 023804 (2005).
- [10] U.v. Bürck; Hyp. Int. **123/124**, 483 (1999)
- [11] M.O. Scully et al., Phys. Rev. Lett. **96**, 010501 (2006).
- [12] D.C. Burnham and R.Y. Chao; Phys. Rev. **188**, 667 (1p69).
- [13] D. Fröhlich et al., Phys. Rev. Lett. **67**, 2343 (1991).

- [14] J.P. Hannon and G.T. Trammell; *Coherent γ -optics*, Hyp. Int. **123/124**, 127 (1999).
- [15] N.E. Rehler and J.H. Eberly; *Superradiance*, Phys. Rev. **A 3**, 1735 (1971).
- [16] Y.Y. Shuydku et al., Phys. Rev. Lett. **77**, 3232 (1996).

7 Stand-alone γ/e^- Facility for Astrophysics

The production of heavy elements in the Universe, a central question of astrophysics, will be studied within ELI-NP in several experiments. While we want to address the s-process and p-process with the γ beam, we also plan to study the r-process at the N=126 waiting point by producing these neutron-rich nuclei via fission-fusion reactions with the APOLLON laser. This close interaction between nuclear physics and astrophysics will be very productive.

7.1 Neutron Capture Cross Section of s-Process Branching Nuclei with Inverse Reactions

K. Sonnabend¹, N. Pietralla¹, D. Savran¹

¹ *Institut für Kernphysik, TU Darmstadt, Darmstadt (Germany)*

The heavy elements above the so-called iron peak are mainly produced in neutron capture processes: the *r* process (*r*: rapid neutron capture) deals with high neutron densities well above 10^{20} cm^{-3} and temperatures in the order of $2 - 3 \cdot 10^9 \text{ K}$. It is thought to occur in explosive scenarios like *e.g.* supernovae [1, 2]. In contrast, the average neutron densities during *s*-process nucleosynthesis (*s*: slow neutron capture) are rather small ($n_n \approx 10^8 \text{ cm}^{-3}$), *i.e.* the neutron capture rate λ_n is normally well below the β -decay rate λ_β and the reaction path is close to the valley of β stability [3, 4, 5]. However, during the peak neutron densities branchings occur at unstable isotopes with half-lives as low as several days. While the half-lives of these branching points are normally known with high accuracy at least under laboratory conditions and rely only on theory for the extrapolation to stellar temperatures [6], the neutron capture cross sections are only in special cases accessible to direct experiments. Besides the production of a sufficient amount of target material, the intrinsic activity of the target mainly hinders the experimental access especially in the case of the short-lived branching points.

However, the predictions in the Hauser-Feshbach model yield different results due to the underlying parameter sets. Additionally, the single studies on long-lived branching points (*e.g.* ^{147}Pm [7], ^{151}Sm [8, 9], ^{155}Eu [10]) showed that the recommended values of neutron capture cross sections in the Hauser-Feshbach statistical model [11] differ by up to 50% from the experimentally determined values. Thus, any experimental constraints on the theoretical predictions of these crucial values are welcome. Therefore, the inverse (γ, n) reaction could be used to decide for the most suitable parameter set and to predict a more reliable neutron capture cross section using these input values. This method has been applied to the branching nuclei ^{185}W and ^{95}Zr using a continuous-energy bremsstrahlung spectrum [12] and Laser-Compton backscattered photons [13].

In addition, data of the inverse (γ, n) reaction is also supposed to yield information for the calculation of Stellar Enhancement Factors (SEF) in some special cases like *e.g.* ^{151}Sm [14]. The inverse $^{152}\text{Sm}(\gamma, n)$ reaction only populates excited states in ^{151}Sm for energies close to the reaction threshold. Using the high resolution of ELI would allow measuring the matrix elements of the transitions to the particular states and, hence, measure the SEF which is the main source of uncertainty for the stellar cross section of $^{151}\text{Sm}(n, \gamma)$.

References

- [1] K.-L. Kratz *et al.*, *Astrophys. J.* **403** (1993) 216.
- [2] G. Wallerstein *et al.*, *Rev. Mod. Phys.* **69** (1997) 995.
- [3] F. Käppeler, *Prog. Part. Nucl. Phys.* **43** (1999) 419.
- [4] F. Käppeler, A. Mengoni, *Nucl. Phys.* **A777** (2006) 291.
- [5] I. Dillmann, C. Domingo Pardo, F. Käppeler, A. Mengoni, K. Sonnabend, *Publications of the Astronomical Society of Australia* **25** (2008) 18.
- [6] K. Takahashi, K. Yokoi, *Nucl. Phys.* **A404** (1983) 578.
- [7] R. Reifarth *et al.*, *Astrophys. J.* **582** (2003) 1251.
- [8] U. Abbondanno *et al.*, The N Tof Collaboration, *Phys. Rev. Lett.* **93** (2004) 161103.
- [9] K. Wisshak *et al.*, *Phys. Rev. C* **73** (2006) 015802.
- [10] S. Jaag, F. Käppeler, *Phys. Rev. C* **51** (1995) 3465.
- [11] Z. Y. Bao *et al.*, *At. Data Nucl. Data Tables* **76** (2000) 70.
- [12] K. Sonnabend *et al.*, *Astrophys. J.* **583** (2003) 506.
- [13] K. Sonnabend *et al.*, *AIP*, 2009, Volume 1090, (p. 481–485).
- [14] A. Mengoni, *AIP*, 2005, Volume 769, (p. 1209–1212).

7.2 Measurements of (γ, p) and (γ, α) Reaction Cross Sections for p -Process Nucleosynthesis

K. Sonnabend¹, N. Pietralla¹, D. Savran¹

¹ *Institut für Kernphysik, TU Darmstadt, Darmstadt (Germany)*

Photodesintegration rates – like (γ, n) , (γ, p) , and (γ, α) – play an important role in the nucleosynthesis of the so-called p nuclei. These proton-rich, in general very low-abundant isotopes cannot be produced by neutron capture reactions. Complete network calculations on p -process nucleosynthesis include several hundred isotopes and the corresponding reaction rates. Therefore, theoretical predictions of the rates, normally in the framework of the Hauser-Feshbach theory, are necessary for the modelling. The reliability of these calculations should be tested experimentally for selected isotopes.

Different approaches are available and necessary to improve the experimental data base for the p process. While the (γ, n) cross sections in the energy regime of the Giant Dipole Resonance around 15 MeV have already been measured extensively several decades ago (see *e.g.* [1]), many efforts using continuous bremsstrahlung spectra have been made at the S-DALINAC at Darmstadt [2, 3] and the ELBE setup at Forschungszentrum Dresden [4] to determine the reaction rates without any assumptions on the shape of the cross section's energy dependence in the astrophysically relevant energy region close above the reaction threshold. A determination of the reaction rates by an absolute cross section measurement is also possible using monoenergetic photon beams produced by Laser Compton Backscattering [5].

In contrast, the experimental knowledge about the (γ, p) and (γ, α) reactions in the corresponding Gamow window is worse. In fact, the experimental data is based on the observation of the time reversal (p, γ) and (α, γ) cross sections, respectively [6, 7, 8, 9, 10] for the proton-rich nuclei with mass numbers around 100. Due to the difficulties concerning the experimental accessibility of the (γ, α) reaction rates a method using elastic α scattering has been established [11, 12].

Therefore, it would be a tremendous advance to measure these rates directly. However, the impact on the understanding of p -process nucleosynthesis would not be the measurement of one or two selected reactions but the development of a broad database. This is only possible if the time needed for one experiment is kept very short as it will be provided by the high intense γ beam of ELI.

References

- [1] B. L. Berman, S. C. Fultz, *Rev. Mod. Phys.* **47** (1975) 713.
- [2] K. Vogt, P. Mohr, M. Babilon, J. Enders, T. Hartmann, C. Hutter, T. Rauscher, S. Volz, A. Zilges, *Phys. Rev. C* **63** (2001) 055802.
- [3] K. Sonnabend, K. Vogt, D. Galaviz, S. Müller, A. Zilges, *Phys. Rev. C* **70** (2004) 035802.
- [4] M. Erhard, A.R. Junghans, R. Beyer, E. Grosse, J. Klug, K. Kosev, C. Nair, N. Nankov, G. Rusev, K.D. Schilling, R. Schwengner, A. Wagner, *Eur. Phys. J. A* **27** (2006) s01.135.
- [5] H. Utsunomiya, H. Akimune, S. Goko, M. Ohta, H. Ueda, T. Yamagata, K. Yamasaki, H. Ohgaki, H. Toyokawa, Y.-W. Lui, T. Hayakawa, T. Shizuma, S. Goriely, *Phys. Rev. C* **67** (2003) 015807.

- [6] T. Sauter, F. Käppeler, Phys. Rev. C **55** (1997) 3127.
- [7] J. Bork, H. Schatz, F. Käppeler, T. Rauscher, Phys. Rev. C **58** (1998) 524.
- [8] N. Özkan, A. S. J. Murphy, R. N. Boyd, A. L. Cole, M. Famiano, R. T. Güray, M. Howard, L. Şahin, J. J. Zach, R. deHaan, J. Görres, M. C. Wiescher, M. S. Islam, T. Rauscher, Nucl. Phys. **A710** (2002) 469.
- [9] W. Rapp, M. Heil, D. Hentschel, F. Käppeler, R. Reifarth, H. J. Brede, H. Klein, T. Rauscher, Phys. Rev. C **66** (2002) 015803.
- [10] G. Gyürky, Z. Fülöp, G. Kiss, Z. Máté, E. Somorjai, J. Görres, A. Palumbo, M. Wiescher, D. Galaviz, A. Kretschmer, K. Sonnabend, A. Zilges, T. Rauscher, Nucl. Phys. **A758** (2005) 517.
- [11] Z. Fülöp, G. Gyürky, Z. Máté, E. Somorjai, L. Zolnai, D. Galaviz, M. Babilon, P. Mohr, A. Zilges, T. Rauscher, H. Oberhummer, G. Staudt, Phys. Rev. C **64** (2001) 065805.
- [12] D. Galaviz, Z. Fülöp, G. Gyürky, Z. Máté, P. Mohr, T. Rauscher, E. Somorjai, A. Zilges, Phys. Rev. C (2005) in press.

8 Stand-alone γ Facility for Applications

Having at ELI-NP at the same place a brilliant γ beam, a brilliant X-ray beam, a brilliant micro neutron source and a brilliant micro positron source will be very advantageous in material science and life sciences because the same target can be studied with the different techniques which complement each other.

8.1 Industrial Applications for the Management of Nuclear Materials

T. Hayakawa¹, T. Shizuma¹, and R. Hajima²

¹ *Advanced Photon Research Center, JAEA, Kizugawa, Kyoto (Japan),*

² *Advanced Photon Research Center, JAEA, Tokai, Ibaraki (Japan),*

The non-destructive detection of materials hidden by heavy shields such as iron with a thickness of several centimeters is difficult. Such detection of clandestine materials is of importance e.g. for applications for nuclear engineering: the management of nuclear materials produced by nuclear power plants, the detection for nuclear fissile materials in the recycling process, and the detection of explosive materials hidden in packages or a cargo containers. A nondestructive assay has been proposed with the extremely high-flux LCS γ source based on an energy recovery linac. The elemental and isotopic composition is measured using nuclear resonance fluorescence (NRF) with LCS γ -rays.

Here one has to stress the political importance of this project. Measuring remotely and precisely isotopes like ^{239}Pu , ^{235}U or dominant fission products is very important for the radioactive waste management. The handling of radioactive waste and its long term storage are partially unsolved problems not only in Europe but worldwide.

References

- [1] T. Hayakawa et al., *Nondestructive assay of plutonium and minor actinoid in spent fuel using nuclear resonance fluorescence with laser Compton scattered γ -rays*; subm to NIM (2010).

8.2 High Resolution, high Intensity X-Ray Beam

D. Habs¹ and P. Thirolf¹

¹*Ludwig Maximilians University, Munich (Germany)*

High resolution X-ray beams are available at high energy synchrotron light sources using monochromators. There is a large interest in small compact devices for many applications like protein crystalline structure analysis [4] or Extended X-ray Absorption Fine Structure (EXAFS) for studying the structures of local neighbouring shells [1]. Here new developments with small storage rings and super-cavities are underway [2, 3]. However, for many applications the 10%-3% energy resolution of the 50 keV X-rays from compact storage rings is rather marginal and machines which would offer a direct bandwidth of 10^{-3} or better would be ideal. The diffraction patterns at several wavelength around absorption edges can be measured. This technique of Multi-wavelength Anomalous Diffraction (MAD) is used to determine complex protein structures [1]. Thus technological developments for better bandwidth – as required for ELI-NP – would be very decisive to serve a much larger community. Thus the ELI-NP γ facility could serve as a demonstrator for such technologies and applications. Here the low energy beamline for Mössbauer transitions and multiple nuclear excitons could be used.

References

- [1] J. Als-Nielsen and D. McMorrow; *Elements of Modern X-ray Physics*, WILEY (2009).
- [2] C. Bruni et al., *THOMX, Conceptual Design Report*, LAL/RT 09-28; SOLEIL/SOU-RA-2678 , (2009).
- [3] M. Bech et al., *Journ. of Synchr. Rad.* **16**, 43 (2009)
- [4] PSI-whitepaper; *Opportunities for Structural Genomics Beyond 2010, Creating Partnerships for the future*, (2008).

8.3 Extremely BRilliant Neutron-Source produced via the (γ, n) Reaction without Moderation (BRIN)

D. Habs¹, M. Gross¹, P. G. Thirolf¹ and P. Böni²

¹ *Ludwig Maximilians University, Munich (Germany),*

² *Physik-Department E21, Technische Universität München, D-85747 Garching, (Germany)*

Presently, thermal and cold neutron beams are produced at large-scale facilities like reactors or spallation neutron sources via moderation of MeV neutrons down to 1/40 eV. Moderators and shielding result in very large sources with ≈ 10 m diameter and accordingly reduced flux density. We propose to produce a brilliant pulsed neutron source directly without moderation by generating it with brilliant γ beams of 5–8 MeV via the (γ, n) reaction with energies up to 1000 meV above the neutron threshold [1]. This development became possible because very brilliant γ sources are being developed with spectral densities of $7 \cdot 10^8$ /[s eV] at 100mA electron current, where the γ rays will be produced by incoherent Compton back-scattering of laser light from brilliant high-energy electron bunches. The γ energy spread is presently limited to 10^{-3} by the energy spread of $4 \cdot 10^{-4}$ of the electron beam due to the stability of the accelerator voltage. Presently, in the most advanced control system (for example at the Euro-XFEL) a stability of the amplitude of 0.01% and for the phase of 0.01^0 can be achieved. These numbers are corresponding to 10^{-4} energy stability. This is the limitation of the present technology, but hopefully the feedback system can be improved in the near future and so a few times 10^{-5} may be achievable. Such an improvement in γ -energy spread is very essential and will result in large gains of brilliance. Very small beam size γ beams with 20 μm diameter can be produced, which due to the strong collimation of the γ beam can be transferred to the place of neutron production. Thus we can obtain $7 \cdot 10^8$ neutrons with energies below 1 eV, which may be pulsed by macro-pulsing the electron beam. It emerges from a source with a diameter of 20 μm . We prefer to select states which neutron-decay by p waves, resulting in an angular distribution peaked normal to the orbital angular distribution. Since the spin of the polarized γ beam is transferred to the neutron-emitting nuclei and if the excitation starts from a 0^+ ground state, we can choose the projection of the orbital angular momentum of the neutrons with respect to the recoil direction of the emitting nucleus. Due to this \sin^2 -like neutron distribution, the neutron brilliance in the detector region is increased by a factor of about 10 compared to an isotropic distribution. Selecting the right spin direction is very important. Furthermore the neutron energy spectrum becomes strongly angular dependent due to the recoil and within the 10% solid angle of the neutron guide system will have a narrow energy bandwidth. In this way a rather high brilliance neutron beam with $10^5 \text{n}/[\text{s} (\text{mm mrad})^2 0.1\% \text{ BW}]$ is obtained, which is roughly 2 orders of magnitude larger than the one at existing high-flux reactors and comparable to spallation sources. The highly divergent neutron beams can be extracted over a wide band of wavelengths (100-0.1Å) by means of elliptic guides using the latest supermirror technology and transported to the instruments for neutron scattering and imaging.

In neutron scattering there is a large development ongoing towards cold and thermal micro-neutron-beams for studying the structure and dynamics of small samples under ambient extreme conditions, for example in the area of solid state and soft matter physics. The large field of reflectometry and small-angle neutron scattering will also profit from highly brilliant and small beams. A large research field in fundamental physics as well as in applied physics can be opened up by such a new facility with a large user community with long-term experience in thermal neutron scattering. The investment costs and running costs of such a facility are 1 - 2 orders

of magnitude smaller compared with present large-scale neutron facilities and may be installed even at universities. Moreover the large amounts of radioactive waste and the efforts for safety and security are minimized. The photon recoil of the γ rays causes a recoil momentum of the neutron emitting nucleus, which corresponds to a neutron energy of about 200 meV. Depending on the neutron emission this neutron momentum has to be added vectorially to the momentum of the emitted neutrons, resulting in strongly angle dependent neutron spectra with narrow band width, reaching down to rather low energies.

Here several neutron beamlines with elliptical or parabolic neutron guides [3, 4, ?] are foreseen for neutron scattering and imaging. Experiments with Small Angle Neutron Scattering (SANS), Time Of Flight (TOF) measurements with choppers or Triple Axis Spectrometers (TAS) are foreseen.

References

- [1] D. Habs et al., Eur. Phys. J. **D 55**, 279 (2009).
- [2] Guide to Neutron Research facilities at the ILL, The Yellow Book, Grenoble, (1988).
- [3] R. Valicu and P. Böni, *Focusing Neutron Beams to Sub-Millimeter Size*, subm. to NIM , (2010).
- [4] M. Schneider, J. Stahn and P. Böni., Nucl. Instr. and Meth. **A 610**, 530 (2009).
- [5] P. Böni, Nucl. Instr. and Meth. **A586**, 1 (2008).
- [6] C. Grünzweig et al., Appl. Phys. Lett. **91**, 203504 (2007).
- [7] Ch. Schanzer et al., Nucl. Instr. and Meth. **A 529**, 63 (2004).
- [8] M. Janoschek et al., Nucl. Instr. Meth. A **613**, 119 (2010).

8.4 An Intense BRILLIANT Positron-Source produced via the (γ, e^+e^-) Reaction (BRIP)

D. Habs¹, M. Gross¹, P. G. Thirolf¹, K. Schreckenbach² and C. Hugenschmidt²

¹ *Ludwig-Maximilians University, Munich, Germany*

² *Physik-Department E21, Technische Universität München, D-85747 Garching, Germany*

Using an intense γ beam of $5 \cdot 10^{15}$ photons/s with (2.5 ± 0.5) MeV we propose to realize an intense moderated positron beam of about $5 \cdot 10^9 e^+/s$ via the (γ, e^+e^-) reaction. Using a Ne moderator we expect an about tenfold increased moderation efficiency compared to W or Pt moderators [1]. The intensity of this novel source is comparable to the presently most intense moderated positron source NEPOMUC at the Munich neutron source FRM 2 with about $9 \cdot 10^8 e^+/s$ [2], where about $10^{16} \gamma/s$ from neutron capture hit the inner converter volume. Due to the small diameter and well-directed γ beam we expect for the new source a brilliance of $10^9 e^+/[s(\text{mm mrad})^2 0.1\% \text{BW}]$, which is about 6 orders of magnitude more brilliant than the NEPOMUC source. Using fully polarized γ beams for the first time we will obtain an intense, fully polarized positron beam, which can be transported through beamlines via solenoidal fields to different detector systems [3]. Introducing a macro-time structure in the γ beam via the initial electron beam, this time structure can be transferred to the positron beam. Frequently pulsed positron beams are requested and one can improve the energy resolution of the positron beam by using a time dependent acceleration field. The brilliance of this positron beam can be improved by remoderation by a factor of 10^3 , while at the same time the intensity is reduced by a factor of 10–15 [4]. Low-energy positron beams are used in fundamental physics studies of the properties of positronium (Ps), Ps^- or more complex electron-positron systems. In applied physics studies with positron beams of Fermi-surfaces, defects, interfaces etc. offer excellent diagnostics tools. The new brilliant source is best suited for micro-positron beams, e.g. in positron microscopy. Polarized positron beams open up a totally unexplored research area, where polarized electrons in e.g. magnetic structures can be studied.

References

- [1] A. P. Mills and E. M. Gullikson, *Appl. Phys. Lett.* **49**, 1121 (1986).
- [2] C. Hugenschmidt et al., *NIMA* **593**, 616 (2008).
- [3] C. Hugenschmidt et al., *NIM A* **554**, 384 (2005).
- [4] C. Piochacz et al., *Appl. Surf. Sci.* **255**, 98 (2008).

9 Industry Relevant Developments at ELI-NP

The unique source of ELI-NP will be the high-flux, high-brilliance γ -beam, which shows a very fast improvement of the parameters over the last years (s.section 2.2). The combination of most recent laser technology and classical superconducting electron accelerator promise a further fast development. The efficient recycling of the electron beam and the photon beam in the super cavity allow to compensate for the small Compton scattering cross section. Laser repetition rates will increase to kHz with diode pumped systems. Efficient high surface harmonics from intense lasers may be used in Compton backscattering with shorter wavelength and high peak brilliance. We see many fields of industrial applications of brilliant γ -rays with large socio-economical relevance:

1) Radioactive waste management

- study of $^{238}\text{U}/^{235}\text{U}$ and dominant fission fragments in radioactive waste barrels.
- isotope-specific identification of location and quantity ($^{235}\text{U}, ^{239}\text{Pu}$) by remote detection with destruction of the sample.

2) isotope material detection (homeland security)

- scan containers in harbors for nuclear materials and explosives
- detect specific small isotopic amounts (like ^{210}Po)

3) Burn-up of nuclear fuel rods (clean energy)

- fuel elements are frequently changed in position to obtain a homogeneous burn-up
- measuring the final $^{235}\text{U}, ^{238}\text{U}$ content may allow to use the fuel elements 10% longer
- one obtains more nuclear energy without additional radioactive waste.

4) Medical diagnostics without radioactivities (medicine)

- NRF does not appear to become very important compared to PET

5) protein structure determination (life science)

Very monochromatic X-ray beams are very essential to determine complex protein structures. MAD and EXAFS are used to localize more heavy atoms like iron or selenium in the complexes and thus resolve the complete structure.

6) brilliant low energy neutron and positron sources

With the improved bandwidth of the high intensity γ -rays and X-rays scanning and detection will be drastically improved, allowing for more sensitive detection techniques. Even sorting inhomogeneously distributed isotopes with remote inspection, allows for new applications. For industry more compact versions of the γ -beam facility with dedicated applications promise the delivery of many units. New techniques can be patented like the brilliant X-rays production from relativistic electron mirrors. Possible industry partners are Siemens or Areva.

10 Layout, Principles of Panning and Performance Goals of the Complete ELI-NP Facility

shielding, we will get 10^{11} neutrons of several MeV for one shot of Apollon on a solid target. how many meters of dense concrete are required for shielding?

we could copy the gamma beam dump from HI γ S and also the precollimator – collimator system.

for the storage ring or recycling arc of the ERL 0.5 M concrete similar to the BESSY ring should be sufficient.

perhaps one should preserve space for a fourth APOLLON laser in case one needs somewhere higher intensities.

state-of-the-art equipment for experiments.

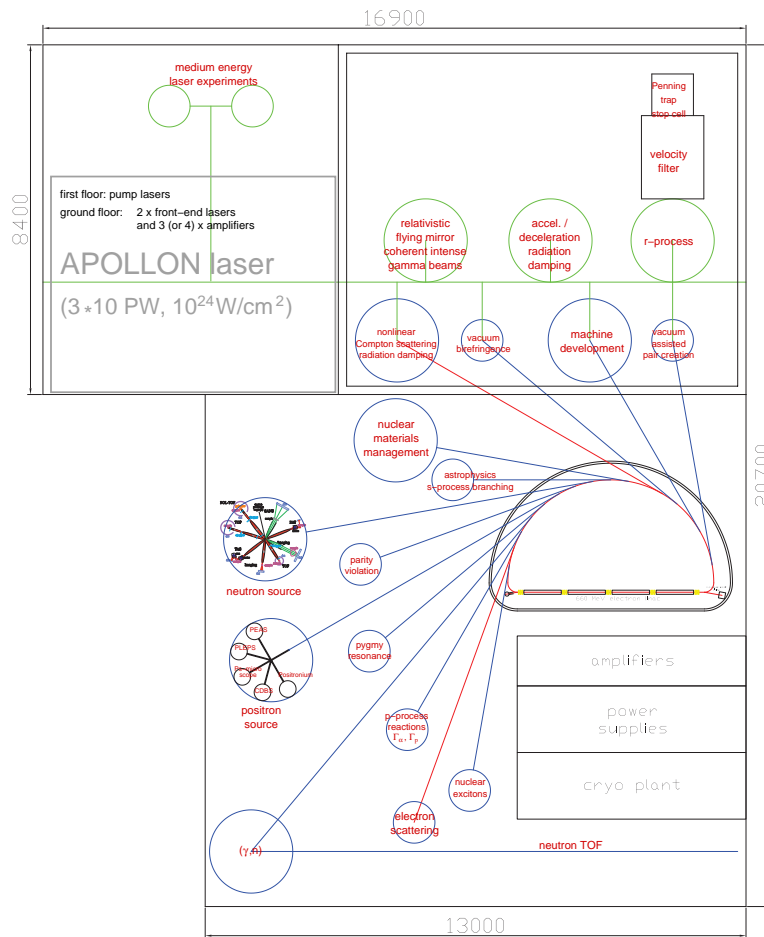


Figure 19: Layout of the ELI-NP facility.

Table 4: Cost of Experiments APOLLON stand-alone

Project	Item	cost [kEURO]	cost [kEURO]
		Period:2010-2015	Period:2015-2020
4.1	beam line	200	
4.1	target chamber	500	
4.1	reaction prod. ident.	400	
4.1	two-stage Wien filter		5000
4.1	buffer gas cell		200
4.1	quad. mass filter		100
4.1	Multi-Reflection-TOF		350
4.1	Multi-Passage Spect A/q		200
4.1	charge breeder		400
4.1	double Penning Trap		800
4.1	electr./data acquis.		150
4.1	Total	900	7100
4.2	beam line	200	
4.2	target chamber	500	
4.2	Thomson Par.	200	
4.3	Target production	300	
4.4	Beam line	200	
4.4	Electron spectrometers	100	
4.4	CCD detector	50	
4.4	Target chamber	500	
4.5	nn	nn	
4.1-4.5	grand total	3150	7100

Table 5: Cost of Experiments APOLLON + γ Beam

Project	Item	cost [kEURO]	cost [kEURO]
		Period:2010-2015	Period:2015-2020
5.1	Beam line	400	
5.1	Beam dump	100	
5.1	e^+e^- Spectr.	200	
5.1	chamber	500	
5.2			
5.3	beam line (laser)	200	
5.3	beam line (electron)	200	
5.3	chamber	500	
5.3	detectors	200	
5.4			
5.1-5.4	grand total	2300	

Table 6: Cost of γ Beam stand-alone Nuclear + Astrophysics

Project	Item	cost [kEURO]	cost [kEURO]
		Period:2010-2015	Period:2015-2020
6.1	beam line	200	
6.1	Ionis. chambers	100	
6.1	chamber	200	
6.2	beam line	200	
6.2	chamber	200	
6.2	keV neutron TOF	100	
6.3	chamber		300
6.3	e-spectrometer		300
6.3	beam line		200
6.4-6.7	4 Clover Det.	600	
6.4-6.7	4 Clover Electr.	100	
6.4-6.7	4 Clover Det.		600
6.4-6.7	4 Clover Electr.		100
6.4-6.7	Liquid. Scint.	300	
6.4-6.7	2 LEPS-Det.	200	
6.4-6.7	Time P.Ch.	100	
6.4-6.7	target lab.	100	
6.4-6.7	isotope material	100	
6.4-6.7	γ -beam dump	50	
6.8			
7.1-7.2			
6.1-7.2	grand total	2550	1500

Table 7: Cost of γ Beam stand-alone Applications

Project	Item	cost [kEURO]	cost [kEURO]
		Period:2010-2015	Period:2015-2020
8.1	chamber	200	
8.1	4 Ge. Detec.	600	
8.1	4 Ge. Detec. Electr.	100	
8.1	4 Ge. Detec.	600	
8.1	4 Ge. Detec. Electr.	100	
8.2	beam line	200	
8.2	target chamber	200	
8.2	rot. target	200	
8.3	POL. TOF interm. foc.		7000
8.3	TOF + Chop.+ iner.foc		6000
8.3	TAS + monoch.+ anal.		2000
8.3	Imag + foc.+ spin ana.		800
8.3	TOF + chop.		5000
8.3	Imag. with parall. b.		700
8.3	Diffract. + monochr.		1500
8.3	SANS		4000
8.3	Reflect. + chopper		3000
8.3	Reflect. + monochr.		1500
8.3	Irrad. station canc.		1000
8.3	large. mag. fields		1500
8.3	high-pressure cell		200
8.3	biomed. cell setup		100
8.3	gas handl. system		200
8.3	in-situ reflectomet.		600
8.3	cryogenics		2000
8.3	ellip. multilayer	200	
b.3	supermirror		300
8.3	total	100	37500
8.4	positron source	84	
8.4	beam line	100	
8.4	remoderator		300
8.4	coinc. Doppler Broad. Spect(CDB)		400
8.4	pulsed Low-e Pos. Syst(PLEPS)		400
8.4	Pos. Annih. Aug. Elect. Spec.(PAES)		600
8.4	Pos. Microscopy		1500

Table 8: Cost of all Experiments at ELI-NP

Project	Item	cost [kEURO]	cost [kEURO]
4.1-4.5	total	3150	7100
5.1-5.4	total	2300	
6.1-7.2	total	2550	1500
8.1-8.4	total	2800	40100
all	grand total	10700	48700

11 Questions and Comments

- does one expect a similar splitting of the pgymy dipole resonance as for the GDR, that one has a more low energy component along the long axis and a high energy component (which is twice as intense) for the transeverse oscillation ? (project 5,3)
- How to discriminate E1 and M1 absorpion above perticle threshold? γ decay?
- improve understanding of damping width etc. Weidenmüller?
- New insight into M1 physics at higher excitation energies?? if there is bunched M1 strength above 5 MeV one probably could not see it until now because the strong E1 resonance and the bad resolution have prevented identifying these states. major shell transitions??
- show γ spectrum from naumova and sokolov
- heinzl a_0 scaling of mass for static E-field (λ gets infinite)?
- is there astrophysics beyond nucleosynthesis like e^-e^- cascades in γ -ray bursters?
- in each proposal of nuclear physics we should state the new expected theoretical developments.
- for photonuclear reaction studies with α paricles or protons the maximum γ energy of 14 MeV should be sufficent because we have e.g. for 56 Fe an S(p)=10 MeV and the energy of 4 MeV above threshold should be sufficent. Furthermore for astrophysics the region right at the threshold is most important.
- pump-probe experiments with nuclei. let us assume we have a coherent gamma beam from the relativistic mirror at 5 MeV or a wavelength of 200fm and a pulse with 10 cycles and $10^6\gamma$ -photons. For the very small nucleus with less than 10 fm diameter the clasical laser γ field looks like individual peaks of field strength where the nucleus can absorb two separate photons from different maxima. The nucleus is that small and the nuclei move that fast within the nucleus that the absorptions can be visualized as independent processes. With 10% energy uncertainty of the gamma quanta and indiviual level spacings of the nucleus are below 1 eV the photon energies always match to levels of the nucleus. It now makes a large difference if we have a chaotic level or a regular level with a few periodic orbits. thus we could get a measure of the randomness of the level.
- is the giant dipole more like a plasma excitation proportional to the fieldstrength, so that a coherent excitations has a much ;larger cross section. ir the only effect of a coherent gamma beam has a much larger flux better focused better directed?? what is the gain by coherently reflected gamma pulses. dipole excitation Breit-Wigner $4\pi\lambda^2$.
- shouldn't one use λ^2/π as a cross section and not the nuclear radius². one needs more than 10^{12} per shot. double excitation becomes possible
- second state may be chaotic stae state or regular state interference between amplitudes.
- flight time of protons and energy loss in the target.

- horizontal neutron flight tune, starting at pygmy experimental area.
- 20 GeV/u onto 20GeV/u: one will have 100 colliding nuclei per event, but in BNL they want only one hit per collision. The probability of three nuclei colliding is still negligible. For a gamma beam ion collider the gamma boost of 10 results in 150 MeV gammas, which are studied at HI γ S. However, the very small repetition rate of APOLLON is not competitive compared to MHz of other facilities.